

# **Biosensor Based Detection of Tuberculosis Biomarkers**

Saurabh Kumar Srivastava

## **Thesis committee**

### **Promotor**

Prof. Dr C.J.M. van Rijn

Professor of Microsystem and NanoTechnology for Agro, Food and Health  
Wageningen University

### **Co-promotor**

Dr M.A. Jongsma

Senior Scientist, Plant Research International  
Wageningen University and Research Center

### **Other members**

Prof. Dr A.H. Velders, Wageningen University

Dr A. van Amerongen, Wageningen University

Prof. Dr E.J.R. Sudhölter, Delft University of Technology

Dr A.H.J. Kolk, University of Amsterdam

This research was conducted under the auspices of the Graduate School VLAG (Advanced studies in Food Technology, Agrobiotechnology, Nutrition and Health Sciences).

# **Biosensor Based Detection of Tuberculosis Biomarkers**

Saurabh Kumar Srivastava

## **Thesis**

submitted in fulfillment of the requirements for the degree of doctor  
at Wageningen University  
by the authority of the Rector Magnificus  
Prof. Dr M.J. Kropff,  
in the presence of the  
Thesis Committee appointed by the Academic Board  
to be defended in public  
on Wednesday 10 December 2014  
at 4 p.m. in the Aula.

Saurabh Kumar Srivastava

Biosensor based detection of tuberculosis biomarkers

156 pages.

PhD thesis, Wageningen University, Wageningen, NL (2014)

With references, with summaries in English and Dutch

ISBN: 978-94-6257-158-7

*Dedicated to my son Shauryansh, family .....  
and friends...*



# *Table of Contents*

<b>Abbreviations</b>		<i>ix</i>
<b>Chapter 1</b>	General introduction	<i>1</i>
<b>Chapter 2</b>	Biosensor-based detection of tuberculosis	<i>15</i>
<b>Chapter 3</b>	16 kDa heat shock protein from heat-inactivated <i>Mycobacterium tuberculosis</i> is a homodimer – suitability for diagnostic applications with specific llama VHH monoclonals	<i>35</i>
<b>Chapter 4</b>	Upconcentration and fluorescence based detection of <i>Mycobacterium tuberculosis</i> bacteria and proteins with microsieves	<i>53</i>
<b>Chapter 5</b>	A lateral flow immunoassay for <i>Mycobacterium tuberculosis</i> detection	<i>65</i>
<b>Chapter 6</b>	A generic microfluidic biosensing module for nanowire-based FET measurements	<i>81</i>
<b>Chapter 7</b>	A generic microfluidic biosensor of G protein-coupled receptor activation – impedance measurements of reversible morphological changes of reverse transfected HEK293 cells on microelectrodes	<i>97</i>

<b>Chapter 8</b>	General discussion	<i>115</i>
<b>Appendix A</b>	Supporting Information: Chapter 3	<i>127</i>
<b>Summary</b>		<i>129</i>
<b>Samenvatting</b>		<i>133</i>
<b>Overview of completed training activities</b>		<i>137</i>
<b>Acknowledgement</b>		<i>139</i>
<b>List of Publications</b>		<i>143</i>
<b>About the Author</b>		<i>145</i>

# Abbreviations

AC	Alternating current
AIDS	Acquired immunodeficiency syndrome
BB	Borate buffer
BCG	<i>Bacille-Calmette-Guerin</i>
BSA	Bovine serum albumin
CFU	Colony forming units
CNPs	Carbon nanoparticles
CXR	Chest X-ray
DC	Direct current
DNA	Deoxyribonucleic acid
DOT	Directly observed therapy
ELISA	Enzyme-linked immunosorbent assay
ESI-TOF	Electrospray ionisation-time of flight
FET	Field effect transistor
GC-MS	Gas chromatography-mass spectroscopy
GFP	Green fluorescent protein
GPCR	G protein-coupled receptor
h	hours
HIV	Human immunodeficiency virus
HPLC	High performance liquid chromatography
HSP	Heat Shock Protein
HTS	High-throughput screening
IUPAC	International Union of Pure and Applied Chemistry
kDa	Kilodalton
LAM	Lipoarabinomannan
LFIA	Lateral flow immunoassay
LPS	Lipopolysaccharide
LSP	Localized surface plasmons
<i>M.tb.</i>	<i>Mycobacterium tuberculosis</i>
<i>MAC</i>	<i>Mycobacterium avium complex</i>
MDG	Millennium Development Goal
MDR TB	Multi-drug resistant Tuberculosis
mg	milligram
min	minutes
ml	millilitre
mM	millimolar
MNP	Magnetic nanoparticle
MSPQC	Multi-channel series piezoelectric quartz crystal
NA	NeutraAvidin
nA	Nanoampere
NAAT	Nucleic acid amplification test
NC	Nitrocellulose
ng	nanogram
nm	nanomolar
NMR	Nuclear magnetic resonance

## Abbreviations

---

ORR	Optical ring resonance
PBS	Phosphate buffered saline
PCB	Printed circuit board
PGV	Pixel gray volumes
PolyDADMAC	poly(diallyldimethylammonium chloride)
PPB	Protein printing buffer
PSA	Prostate-specific antigen
QCM	Quartz crystal microbalance
RB	Running buffer
RT-PCR	Real time polymerase chain reaction
SA	Streptavidin
SB	Storage buffer
Sec	Seconds
SEC	Size exclusion chromatography
SiNW	Silicon nanowire
SMU	Source measure unit
SPR	Surface plasmon resonance
TB	Tuberculosis
TIR	Total internal reflection
TMB	Tetramethylbenzidine
VHH	Variable heavy chain
WB	Washing buffer
WHO	World Health Organization
Wt.	Weight

# *Chapter 1*

## *General Introduction*

## *Abstract*

Tuberculosis (TB) is one of the most important infectious diseases worldwide; about 9 million people developed TB in 2013. The disease is however poorly controlled for a variety of reasons, a major hurdle being the lack of proper diagnostic-tools available in resource poor countries. In this thesis, research was conducted in order to investigate the potential of novel biosensing platforms utilizing optical or electrical transducer systems with known/potential biomarkers of TB. For optical biosensors, fluorescence and lateral flow based techniques were employed for the detection of a specific 16 kDa cell internal antigen protein HSP from *Mycobacterium tuberculosis*. For electrical biosensors, silicon nanowire (SiNW) field effect transistor (FET) biosensors and cellular impedance biosensors were explored. On the SiNW platform real-time and label-free detection of HSP protein was tested, while on the cellular impedance platform real-time and label-free detection of a model analyte was done using a *G protein-coupled receptor (GPCR)*. The cell-based system could be used to detect biomarkers induced in the human host and can be further developed to detect TB. The detection platforms described in this thesis can be applied broadly for the detection of other biomarkers as well. This thesis may therefore hopefully contribute to other future developments of diagnostics in general.

## 1.1 Introduction

Tuberculosis (TB) is a globally prevalent disease that is caused by the gram-positive *Mycobacterium tuberculosis* (*M.tb.*) [1-3]. For many decades now, TB has continued to pose a significant threat to human health and despite the availability of broad-spectrum antibiotics, which are effective against the bacterium, the social and financial burden for sufferers from the disease continues to be huge. Especially, in developing countries, like India and sub-Saharan Africa, it is one of the most dreadful and prevalent diseases affecting members from all age groups [4]. Therefore, the national and international health agencies, governments and policy makers have rightly diverted a very large amount of funding towards research and management of TB. Unfortunately, despite declining global numbers of patients, it still remains a major health problem to be tackled [4, 5].

Clinically, TB is typically manifested with clinical symptoms of chronic fever (mainly at night), cough, anorexia, general malnutrition, weakness and significant weight loss. It occurs due to infection and colonization of human lung tissues and respiratory tract epithelium with *M.tb.* The bacterium spreads through aerosols produced by sneezing and coughing of a patient. Till date, no animal vector has been identified [4,6]. There are some reports that suggest passage of *M.tb.* from pregnant mothers to the fetuses. The *M.tb.* bacterium has a cell wall comprising lipopolysaccharides (LPS) and glycoproteins [7]. It has been postulated that these two components of the bacterial cell wall can both act as an antigen and initiate inflammatory reactions. Additionally, there are other constituent proteins in the bacterium, like 16 kDa Heat Shock Protein (HSP), that are also claimed to be antigenic in nature, although much debate exists on their structures and antigenicities [8-11]. As a pathogenic bacterium, *M.tb.* initiates inflammatory conditions resulting in fever, neutrophilia (in peripheral blood), weight loss, anorexia and other health conditions. Hence, TB is more debilitating in patients with low nutritional status or immunocompromised (like AIDS patients) [12, 13]. The *M.tb.* bacterium causes granuloma formation, often with a necrotic core surrounded with inflammatory tissues rich in leucocytes, which causes the typical cough and breathlessness [14]. In advanced stages, these necrotic granuloma tissues may be expelled while coughing along with blood.

Apart from the conventional pulmonary TB as described above, *M.tb.* can also cause TB in other parts of the body (extrapulmonary TB), like in intestines and bones. In certain cases, TB can spread throughout the body causing infections at multiple sites, known as miliary TB [15]. These conditions can be more grave and life threatening at advanced conditions warranting early diagnosis and chemotherapy. Unfortunately, the availability of diagnostics for TB is still daunted by methods that are too expensive, require logistic support and highly trained personnel. Additionally, once diagnosed the need for highly expensive antibiotics, essential in the therapy especially in cases of multidrug resistance, represents a huge financial burden. As a result it is a frustrating fact that in spite of billions of Euros of investments by different agencies, a satisfactory level of control of TB at the international level remains elusive [4].

## 1.2 Multidrug Resistant TB

The emergence of Multidrug resistant (MDR) TB cases which cannot be treated by multiple or entire groups of antibiotics have severely complicated the management scenarios. The antibiotic resistance is caused by mutations in the genome of the bacterium. It is known that usually 1 out of  $10^6$  bacteria is inherently resistant to anyone of the first line anti-TB drugs, like isoniazid, rifampicin, ethambutol etc. As a result cases emerge which are resistant to an entire regime of such antibiotics [4]. Globally in 2013, an estimated 480 000 people developed MDR-TB.

The MDR TB sets a major challenge in the management of TB worldwide. Especially, in countries like India, Vietnam and African countries, MDR cases are a prevalent and dominant cause for mortality. To treat MDR cases, usually a regime consisting of multiple first line drugs is used, which however at the same time selects for even more complex MDR TB strains. Research is necessary to discover and develop new antibiotics, but the few new drugs that are under clinical trial still require more evaluation before they can be introduced [16-18].

## 1.3 Epidemiology and statistics

The WHO TB Report 2012 collected reports from 204 countries and territories under its jurisdiction, totally representing >99% of the global TB cases [4]. The report successfully compiled the existing burden of the disease and the remaining challenges in TB management. India and China together accounts for >40% of the total TB cases in the World although the overall infection rate within the population is highest in African countries where sometimes >80% of the population is infected with *M.tb*. In 2011, there were 8.7 million new cases and about 1.4 million people have died. Furthermore, 13% of all newly reported cases were also immuno-compromised with HIV. As per the WHO 2012 report, resistance to more than one first line anti-TB drugs is reported amongst 3.7% of new cases and 20% previously treated cases [4]. The good news is that the goal to halt the progression and reverse the global TB pandemic, as described in the Millennium Development Goal (MDG) is showing good promise. There was a 2.2% reduction in new cases between 2010 and 2011 and relative to 1990 there has been even been a 41% reduction in annual new cases. This has triggered hopes that the MDG of reducing the number of new cases by 50% by 2015 is achievable. Since the initiation of the Global TB program in the 1990s, an estimated 51 million people have been successfully treated thanks to very large funding schemes that went into the program (US\$ 8 billion projected for 2013-2015) [4].

## 1.4 The current TB diagnostic methods and their drawbacks

The most commonly used technique for the clinical diagnosis of TB is the chest X-ray (CXR) [19]. Usually, with the posterior-anterior (PA) view, the chest region is imaged to demonstrate the pulmonary structures. Granuloma of the TB [20] is quickly recognized with

areas of necrosis and distribution of nodules in the lung parenchyma. The chest X-ray findings are further supported with clinical findings and patient histories.

The available diagnostic test alternatives are:

- (1) *Tuberculin skin test (TST)*: this TST or *Mantoux test* was one of the first tests to be used for diagnosis in TB since 1907 and has undergone several improvements [21]. Usually this test comprises subcutaneous injection of a protein purified derivative (PPD) obtained from a sub culture of *M.tb.* bacteria. The immunogenic response as the diameter of the inflammation found in skin after 48-72 h is used to diagnose positive cases. It requires trained healthcare personnel to perform it. Subjects with immuno-deficiencies generally fail to generate sufficient responses and therefore add to the false negative cases, and patients with *Bacille Calmette-Guérin* (BCG) vaccination show an 8.5% incidence of false positive cases [22-24].
- (2) *Bacterial culture from sputum samples*: A bacterial culture from sputum collected in the morning remains popular in detection of TB. Unfortunately, the sensitivity of these tests for TB varies between 34-80% and requires a bacteria-concentration of at least 5.000-10.000 CFU/ml. The test does not differentiate TB from other mycobacterial infections, and it is also very time consuming, as 2-3 weeks are needed to obtain the outcome. Recently, detection of bacterium using fluorescent labels in combination from bacterial culture has been advocated and this definitely increases the sensitivity of the technique [25]. A downside is that the methodology requires at least two independent samples taken at two different days making it harder to implement as a point-of-care diagnostic. One of the challenges of such sputum-based detection of *M.tb.* through microscopy of the smear is the fact that *M.tb.* is quite hard to differentiate from other prevalent *Mycobacterium sp.*, like *Mycobacterium kansasii*, *Mycobacterium marinum* and *Mycobacterium Avium Complex (MAC)* [26].
- (3) *Interferon gamma (IFN- $\gamma$ )-based assays*: In these assays, the amount of IFN- $\gamma$  released from the human immune T-cells upon exposure to *M.tb.*-specific antigens, like ESAT-6 and CFP-10, is quantified. Usually, these kits are either ELISA (QuantiFERON) or enzyme linked immunospot (ELISPOT) assays (T-spot TB test) [27]. Unfortunately, these assays offer no better sensitivities or specificities compared to the TST tests and cannot differentiate between active and latent TB infections. These tests are also highly expensive and therefore, WHO has stopped endorsing these tests especially for lower and middle-income countries [28].
- (4) *Urine-based assays*: In these assays, a simple commercially available kit detects an antigen, lipoarabinomannan (LAM), as part of the cell wall of *M.tb.* Although this test is cheap (~\$3.5/test) and simple to perform, the accuracy is low (28.2%). This test also fails to differentiate between active and latent cases. Interestingly, the accuracy of the test increases to ~66% with if a CD4 cell count is included (<50 cells/ $\mu$ l) and has a better potential to diagnose TB cases with HIV and can be useful in African countries where TB is the leading cause of mortality in AIDS cases [29].

- (5) *Nucleic acid amplification-based assays*: In these types of assays, certain parts of the bacterial DNA are amplified, either by RT-PCR or by line probe assays before detection. For RT-PCR usually either of two kits is used: Amplicor *M.tb.* From Roche Diagnostics or Amplifier *Mycobacterium tuberculosis* Direct Test from Gen Probe Inc., and for line probe assays, Inno-LiPA *Mycobacteria* assay and GenoType *Mycobacterium* assay. The advantages of the line probe assays are that they are simpler to execute. They usually detect the 16S and 23S genes by amplification of the nucleic acid sequences on a nitrocellulose membrane. The advantage of these assays is that they can differentiate between *M.tb.* and other *Mycobacterium sp.* more precisely, and can also detect MDR *M.tb.* resistant against drugs like rifampicin, ethambutol, isoniazid and fluoroquinolones [30].
- (6) *Immune response-based detection assays*: One of the most popular assays for detection of TB is latex agglutination based antibody binding assays with the *M.tb.* antibodies present in the blood of *M.tb.* infected persons. Due to the antigen-antibody reactions, there are significant aggregations of particles that can later be quantified. Unfortunately, this technique has a low sensitivity of only 53% with inability to differentiate between active, latent and carrier stages. However, the specificity (~98%) of the technique is acceptable [31].
- (7) As a new diagnostic technique in December 2010 the WHO endorsed the use of a cartridge based automated diagnosis test called Xpert *M.tb./RIF* which detects DNA sequences specific for *M.tb.* as well as rifampicin resistance utilizing polymerase chain reaction by Nucleic acid amplification test (NAAT) within 100 min. It is estimated that by June 2012, 1.1 million units were purchased with South Africa leading the way in implementing it. The initial reports are quite promising. Apart from that, WHO targets to licence at least one vaccine for TB prevention by 2020 [32].

## 1.5 Gaps between current diagnostic techniques and need

At close inspection it can be concluded, that many of the current diagnostic tests in TB fall short of the requirements for an early diagnosis or suitability for resource poor countries. Most of them have inadequate sensitivity and/or specificity or do not differentiate between active and latent cases. The points leading to such problems with TB diagnostics are: (1) *M.tb.* is a very slow growing bacterium taking 2-3 weeks to grow, (2) Pulmonary TB often shows symptoms only at advanced stages making an early diagnosis difficult and (3) even the active cases often exhibit low bacteria content of sputum thus making it difficult to detect with the current diagnostic tests. There is an urgent unmet need, therefore, for innovative TB diagnostic platforms, which are cheap, fast, sensitive, reproducible, can identify and differentiate between active and latent cases, require single visits from patients, cause minimum discomfort, require minimum logistic support and trained personnel, assess

drug susceptibility, can measure non-sputum samples, are user friendly, smart, tailor-made and can be used in resource poor settings.

## 1.6 Biosensors in TB detection

Biosensors offer unique opportunities for the detection of TB. According to the International Union of Pure and Applied Chemistry (IUPAC), “*biosensors are devices that use specific biochemical reactions mediated by isolated enzymes, immunosystems, tissues, organelles or whole cells to detect chemical compounds usually by optical, thermal or electrical signals*”. In addition some would add that biosensors should also allow for real time, preferably reversible and label free measurements of certain analytes [33]. Such biosensors can be broadly classified into mass/piezoelectric, biochemical, optical and electrical based systems. A review on the current state-of-the-art techniques that have been implemented in relation to TB is given in Chapter 2 of this thesis. The main motivation behind using these analytical devices is the simplicity offered by real time monitoring of the target-analyte interaction. To enable this, a biosensor consists of a detection area where essentially an analyte is detected through its coupling to a biological sensing layer. The reaction or interaction and the physico-chemical changes resulting from the reaction or interaction between the analyte and the detection molecule are thereby detected by different transducer systems. The main advantages that biosensing method should ideally possess over conventional techniques are that they are fast in execution, require only small amounts of sample, have the flexibility to be tailor-made for a specific or a group of unique target molecules. It is based on these achievements, that biosensors in some areas like blood glucose measurements are popularly used nowadays. In an effort to also implement biosensing methods towards sensitive and specific detection of tuberculosis infections, this thesis focuses on three different biosensing principles involving optical and electrical transducer systems and protein and cell based functionalizations.

### 1.6.1 Optical biosensors

#### 1.6.1.1 Nanoparticle (NP) based protein biosensors

With the rapid growth of nanotechnology, carbon nanoparticles (CNPs) have experienced an explosive growth both in production and utility [34, 35]. Expectedly, a new range of applications for carbon nanomaterials has emerged in applications such as cancer treatment, medical imaging, disease diagnosis, gene therapy, drug delivery and many other areas. These CNPs could serve as replacement for existing signalling labels such as gold, latex, coloured silica or quantum dots in diagnostic assays. There are three naturally occurring allotropes of carbon i.e. graphite, diamond and amorphous carbon. Relatively poorly defined amorphous CNPs have been used in lateral flow immunoassays (LFIA) as indicators of the presence of a particular protein or nucleic acid ligand in a sample [37]. The sensitivity of these types of assays may in principle be improved by the use of other types of particles which are visible not by the absorption of light but by the emission of fluorescence. These amorphous CNPs are often produced from carbon soot and are an excellent tool in

developing simple, inexpensive but highly sensitive readout assay-based platforms in LFIA [37]. The amorphous CNPs are also quite stable which facilitates their uses in developing stable and reliable nanoprobes for such NP-based sandwich ELISA assays. Such CNPs can also be produced in bulk quantities, which is an added advantage. The assay result can also be presented with an easy readout using simple imaging software.

Also quantum dot type of NPs may exhibit qualities that are suitable for diagnostic applications [34, 35]. Due to their extremely small size (< 20 nm), these particles are able to sensitively detect molecules or chemical species at the nm scale. In a recent development it was shown that carbon quantum dots (similar to silicon or CdSe/ZnS quantum dot) may emit fluorescence after being exposed to bright light [36]. These carbon quantum dots showed adequate quantum yield and were resistant to photo bleaching. Additionally, they provide sufficient scope for surface functionalization (including binding to specific antibodies) to enhance its capability in detecting biomolecules including proteins.

### **1.6.1.2 Fluorescence based protein biosensors**

Optical detection of (changes in) fluorescence is one of the most prominent and mature techniques for the visualization of biomolecules or molecular events in the field of molecular biology. Advancements in these techniques over the past few decades have not only outlined the roles and locations of various biomolecules of interest but also successfully demonstrated extra- and intracellular relationships between those molecules. Attributes such as ease of use, high sensitivity, specificity, selectivity, sufficient temporal and spatial resolution at low costs have placed fluorescence techniques into the lime light as one of the most promising choices for biosensing transducers [38]. Many fluorescence-based biosensors have been utilizing synthetic and biological receptors such as DNA, proteins and aptamers [39]. The design of a fluorescence based biosensor basically involves the selection of an appropriate macromolecular receptor or binding molecule which has affinity and specificity for the target molecule in consideration, followed by the signal transduction unit required to sense the molecular binding event at the surface of the receptor. Usually the receptor or binding molecules are not fluorescent, thus they require coupling to foreign reporter moieties such as green fluorescent protein (GFP) [40] or synthetic fluorophores (Alexa-Fluor) [41] at appropriate positions on the receptor component. Upon binding to ligands, the fluorescence properties change due to change in the biochemical environment. Examples of such biosensing molecules are Molecular Beacon and Cameleon proteins. Fluorescence based biosensors can be very sensitive as the excitation and emission wavelengths are different.

## **1.6.2 Electrical biosensors**

### **1.6.2.1 Silicon nanowire-based biosensors**

Silicon nanowire (SiNW) field effect transistor (FET)-s offer a unique diagnostic tool for real-time and label free detection of molecules. Due to the fact that the nanowires have a diameter in the range of bound charged ligand molecules, each binding molecule may directly

influence the electrical conductivity along these semiconductor wires. As a result much higher sensitivities have been reported than in regular immunoassays [42,43]. In general, SiNW FET-based biosensor systems where the SiNWs are placed between source and drain electrodes, while a gate electrode regulating the conductance and sensitivity [43]. Usually, they are surface functionalized with bio-receptor molecules in order to capture specific target molecules. Upon binding of the target molecules (analytes), the electric current changes due to an altered resistance induced by the field effect of the bound molecule [43]. For example, if the receptor molecules capture negatively charged analyte molecules, the anionic analyte molecules repel the anions close to the surfaces of the SiNWs and thus, decreasing the electric current.

SiNWs of various thickness (20-60 nm) and lengths up to 100 nm have been used in development of such biosensors [44]. These biosensors have been used to detect different protein biomarkers for diseases, like prostate specific antigen (PSA) in prostate cancer, ions, small molecules, viruses, and cells [45]. Considering the availability of highly characterized antibodies [46], these SiNW-based biosensors may possibly also be used effectively in TB-detection.

### 1.6.2.2 Impedance based cell biosensors

Sensing devices utilizing specific receptors and signalling pathways present in living cells are known as cell based biosensors. Cell based sensing can be achieved utilizing a wide variety of transducers such as electrical, optical, mechanical, thermal principles. Impedance spectroscopy is a well-established technique in electrochemical and (bio)chemical sensing, redox reactions, and in studying morphological responses of a wide range of organisms like bacteria, neuromuscular cells, and eukaryotic cells [47, 48]. Eukaryotic cell based biosensors have been used as a model system for a wide range of applications that include drug discovery, single cell analysis, pathogens and toxin detection, taste receptors analysis, cancer detection etc. by exploiting the complex, but advanced bio-recognition elements and signal transduction pathways present on and in eukaryotic cells [49]. Impedance responses are transduced by induced morphological changes in cell shape a result of the activation of receptors such as G protein-coupled receptors (GPCRs) [50]. GPCRs are a family of 800 genes coding for different types of GPCRs, which may be utilized for sensing various analytes/targets depending on the research question [51]. These receptors include recognition of specific extracellular stimulants like photons, glycoproteins, cytokines, hormones, neurotransmitters, growth factors and odorant molecules [52]. Though there are three main GPCR pathways that are mediated by four ( $G_{\alpha s}$ ,  $G_{\alpha i/o}$ ,  $G_{\alpha q/11}$  and  $G_{\alpha 12/13}$ ) subclasses of G-proteins, the pathway that appears most relevant for impedance-based measurements is the  $G_{\alpha 12/13}$  pathways which upon activation triggers a signal transduction pathway causing a change in cell shape [53]. Receptor-cell based studies may enable diagnosis of a specific host response to infection by TB.

## 1.7 Aims and objectives of the thesis

The primary aims of the thesis are: (1) to develop, optimize and validate new diagnostic methods in order to detect biomarkers for TB; (2) to devise tests which exhibit improved sensitivities and specificities compared to the various currently available diagnostic tests.

The secondary aims of the thesis are: (1) to successfully implement nano-microtechnology, such as silicon nanowire sensing, in order to develop advanced biosensing tools for TB biomarker detection; (2) to design biosensing tools with potential as a user-friendly point-of-care diagnostic for TB detection – especially for resource-poor areas; (3) to further extend and explore possibilities of integration and miniaturization of such biosensing platforms in order to develop devices enabling high-throughput screening (HTS) capabilities.

## 1.8 Outline of the thesis

The work presented in this thesis describes the development of a variety of different biosensing methods towards the goal of the detection of TB biomarkers in patients. The diversity of approaches described in this thesis was partly invoked by the fact that the platform at which we aimed originally, based solely on silicon nanowire FETs (Chapter 6), did not materialize until the very end of the project, due to a late supply of sufficient and/or functional nanowire chips.

Chapter 2 gives an overview of the available biosensing techniques that are either already in use or under development for TB detection. This chapter also focuses on newly emerging biosensing approaches while comparing their advantages and disadvantages with conventional techniques.

Chapter 3 focuses on the identification and characterization of the *M.tb.* 16 kDa HSP epitopes in relation to different VHH antibodies along with evaluating the suitable capture-detection probe combinations for detection of tuberculosis on robust protein-based diagnostic platforms using these antibodies. In this chapter it was demonstrated that HSP protein from heat-inactivated *M.tb.* exists as a homodimer.

In chapter 4, fluorescence based biosensing tool was employed for the detection 16 kDa HSP which is a specific cell internal antigen protein of *M.tb.* In order to do so, first the *M.tb.* bacteria were concentrated on microsieves functionalized with PolyDADMAC, which could later be lysed using standard lysis protocols to give the cell internal lysate protein. This lysate protein contains the 16 kDa HSP target protein that was detected in a sandwich assay using microsieves functionalized with specific llama antibodies. It was also shown in this chapter that due to the homodimer nature of the 16 kDa HSP, it is also capable of agglutinating when in contact with specific antibodies coupled to a surface, beads or other protein capable of binding multiple antibodies.

Chapter 5 utilizes the knowledge and methods of chapter 3 and 4 to demonstrate how HSP released from concentrated *M.tb.* bacteria could be implied in an application involving a lateral flow immunoassay (LFIA) technique for the detection of TB. Characterization of various parameters like adequate concentration and VHH combinations for anchoring, capture and detection were carried out to achieve acceptable sensitivity of the LFIA test.

Chapter 6 reports the development of a compact modular biosensing system and an application to carry out SiNW-based electro-physical detections inside a re-sealable glass microfluidic flow cell. It validates the set up by measuring with silicon nanowire FETs developed at DIMES (TU Delft) flow injected iso-ionic pH solutions, and *M.tb.*-specific HSP binding kinetics in real time on the nanowire surface.

In chapter 7, the modular biosensing system of chapter 6 is used to test the efficiency of interdigitated microelectrodes for impedance measurements of live mammalian cells expressing specific GPCRs. Certain biomarkers circulating in patient's serum are specifically induced by TB infections and some are targeting specific GPCRs. Highly sensitive measurements were achieved and approaches are outlined to convert the system into a high throughput assay for the detection of multiple analytes in a single run of 5 min.

Finally, chapter 8 presents an overview of the main findings of this thesis along with pending issues that remain to be solved and aims to provide recommendations for future directions of research.

## References

1. Grange JM, Gandy M, Farmer P, Zumla A; *Int J Tubercul Lung D*, **2001**, 5, 208
2. Gandy M, Zumla A; *Soc Sci Med*, **2002**, 55, 399
3. Kruh NA, Troutt J, Izzo A, Prenni J, Dobos KM; *PLoS One*, **2010**, 5, e13938
4. Global Tuberculosis Report; WHO, **2012**
5. Nahid P, Pai M, Hopewell PC; *Proc Am Thorac Soc*, **2006**, 3, 103
6. Murray JF; *Am J Resp Crit Care Med*, **2004**, 169, 1181
7. Choudry IW, Ormerod LP; *Thorax*, **2007**, 62, A4
8. Bulut Y, Michelsen KS, Hayrapetian L, Naiki Y, Spallek R, *et al.*; *J Biol Chem*, **2005**, 280, 20961
9. Kennaway CK, Benesch JLP, Gohlke U, Wang LC, Robinson CV, *et al.*; *J Biol Chem*, **2005**, 280, 33419
10. Raja A, Devi KRU, Ramalingam B, Brennan PJ; *Clin Diag Lab Immunol*, **2002**, 9, 308
11. Devi KRU, Kumar KSS, Ramalingam B, Alamelu R; *Prot Expres Purif*, **2002**, 24, 188
12. Swaminathan S, Padmapriyadarsini C, Narendran G; *Clin Inf Dis*, **2010**, 50, 1377
13. Kranzer K, Houben RMGJ, Glynn JR, Bekker LG, Wood R, *et al.*; *Lancet Inf Dis*, **2010**, 10, 93
14. Segovia-Juarez JL, Ganguli S, Kirschner D; *J Theoret Biol*, **2004**, 231, 357
15. Sharma SK, Mohan A, Sharma A; *Ind J Med Res*, **2012**, 135, 703
16. Cavalcante SC, Soares ECC, Pacheco AGF, Chaisson RE, Durovni B; *Int J Tubercul Lung D*, **2007**, 11, 544
17. Anuwatnonthakate A, Limsomboon P, Nateniyom S, Wattanaamornkiat W, Komsakorn S, *et al.*; *PLoS One*, **2008**, 3, e3089
18. Harries AD, Jahn A, Zachariah R, Enarson D; *PLoS Med*, **2008**, 5, e124
19. Marais BJ, Pai M; *Arch Dis Child*, **2007**, 92, 446
20. Rubin EJ; *New Eng J Med*, **2009**, 360, 2471
21. Mendel F; *Medizinische Klinik München*, **1908**, 4, 402
22. Pottumarthy S, Wells VC, Morris AJ; *J Clin Microbiol*, **2000**, 38, 2227
23. Gennaro ML; *Clin Inf Dis*, **2000**, 30, S243
24. Chan ED, Heifets L, Iseman RD, *Tuberc Lung Dis*, **2000**, 80, 131
25. Ghodbane R, Raoult D, Drancourt M, *Sci Reports*, **2014**, 4, 4236
26. Khan Z, Miller A, Bachan M, Donath J; *Open Respir Med J*, **2010**, 4, 76
27. Miranda C, Tomford JW, Gordon SM; *Clev Clin J Med*, **2010**, 77, 606
28. Parsons LM, Somoskövi Á, Gutierrez C, Lee E, Paramasivan CN, *et al.*; *Clin Microbiol Rev*, **2011**, 24, 314
29. Kasprowicz VO, Achkar JM, Wilson D; *J Inf Dis*, **2011**, 204, S1099
30. Teo J, Jureen R, Chiang D, Chan D, Lin R; *J Clin Microbiol*, **2011**, 49, 3659
31. Steingart KR, Henry M, Laal S, Hopewell PC, Ramsay A, *et al.*; *PLoS Med*, **2007**, 4, e202
32. Rappuoli R, Aderem A; *Nature*, **2011**, 473, 463
33. Turner APF; *Chem Soc Rev*, **2013**, 42, 3184
34. Liu J, Cao Z, Lu Y; *Chem Rev*, **2009**, 109, 1948
35. Rosi NL, Mirkin CA; *Chem Rev*, **2005**, 105, 1547
36. Sun Y-P, Zhou B, Lin Y, Wang W, Fernando KAS, *et al.*; *J Am Chem Soc*, **2006**, 128, 7756
37. Posthuma-Trumpie G A, Wichers J H, Koets M, Berendsen L B J M, van Amerongen A; *Anal Bioanal Chem*, **2012**, 402,593.
38. Tamura T, Hamachi I; *ACS Chem Biol*, **2014**, Article ASAP (DOI: 10.1021/cb500661v)
39. Wang RE, Zhang Y, Cai J, Cai W, Gao T; *Curr Med Chem*, **2011**, 18, 4175
40. Hellinga HW, Marvin JS; *Trends Biotechnol*, **1998**, 16, 183
41. Nolan EM, Lippard SJ; *Acc Chem Res*, **2009**, 42, 193
42. Patolsky F, Lieber CM; *Mater Today*, **2005**, 8, 20
43. Patolsky F, Zheng GF, Lieber CM; *Anal Chem*, **2006**, 78, 4260

44. Patolsky F, Zheng GF, Lieber CM; *Nat Protoc*, **2006**, *1*, 1711
45. Zhang G-J, Ning Y; *Anal Chim Acta*, **2012**, *749*, 1
46. Trilling AK, de Ronde H, Noteboom L, van Houwelingen A, Roelse M, *et al.*; *PLoS One*, **2011**, *6*, e26754
47. Randviir EP, Banks CE; *Anal Method*, **2013**, *5*, 1098
48. Daniels JS, Pourmand N; *Electroanalysis*, **2007**, *19*, 1239
49. Liu QJ, Zhang DM, Zhang FN, Zhao Y, Hsia KJ, *et al.*; *Sensor Actuat B-Chem*, **2013**, *176*, 497
50. Meshki J, Douglas SD, Hu MY, Leeman SE, Tuluc F; *PLoS One*, **2011**, *6*, e25332
51. Roelse M, de Ruijter NCA, Vrouwe EX, Jongsma MA; *Biosens Bioelectron*, **2013**, *47*, 436
52. Zhang R, Xie X; *Acta Pharmacol Sin*, **2012**, *33*, 372
53. Meshki J, Douglas SD, Lai JP, Schwartz L, Kilpatrick LE, *et al.*; *J Biol Chem*, **2009**, *284*, 9280
54. Rocheville M, Jerman JC; *Curr Opin Pharmacol*, **2009**, *9*, 643



# ***Chapter 2***

## ***Biosensor-based detection of Tuberculosis***

*This chapter is submitted for publication*

## *Abstract*

Tuberculosis (TB), caused by *Mycobacterium tuberculosis* (*M.tb.*), is one of the most prevalent and serious infectious diseases worldwide with an estimated annual global mortality of 1.4 million in 2010. Diagnosis of TB in the developing world is very challenging due to the limited suitability of currently available techniques under tropical field conditions. *M.tb.* is a slowly growing *Mycobacterium* that takes around six to eight weeks to be detected via sensitive culture methods. There is also hardly any clinical symptom at an early stage of infection, thereby causing a delay in diagnosis and treatment, and the complexity of the disease is further increased by the emergence of multiple drug resistance (MDR) strains.

A lot of work has been done over the last few decades to develop effective point of care diagnostic techniques that are cheap, robust and can be performed at high throughput in rural areas. However, despite considerable technical improvements reported from the lab, such economical full proof diagnostic assays are still lacking on the market. The objective of this review is to evaluate currently available biosensing techniques that are either already in use or under development for detection of TB. The focus of the review is on the emerging field of diagnostic biosensors that combine ligand capture and detection in a one-step assay. A comparison will be made with conventional multistep techniques.

## 2.1 Introduction

### 2.1.1 Background

Tuberculosis (TB) is an age-old infectious disease of the human race [1, 2], which recently re-emerged globally as an important health-related issue, especially due to the emergence of multi-drug resistant (MDR) strains [3, 4]. The specific characteristics of the gram-positive bacteria, *Mycobacterium tuberculosis* (*M.tb.*) causing TB [5] makes it currently one of the most prevalent diseases [6]. TB bacteria can remain inactive or in dormant state for years without causing symptoms or spreading to other subjects, but as soon as the immune system of the host becomes weakened the bacteria become active and infect mainly the lungs along with other parts of body. TB cases are further aggravated by other illnesses that affect the immune system, such as HIV, which is very prevalent in resource poor countries. Unfortunately, in spite of sustained efforts at national and global levels, only limited success has been achieved in detection and management of TB worldwide [7, 8].

The main obstacles facing successful field detection and treatment of TB are:

1. The omnipresence of the pathogen and disease across different continents which complicates management and eradication programs [9]. Most of the reported cases (~98 %) are concentrated in developing countries, due to which TB is also known as a disease of poverty, with two-thirds of cases estimated to occur among people aged 15-59, adults in their most productive years [6]. However, also developed Western countries continue to report TB cases [10].
2. The high costs of the first line anti-TB drugs to treat TB (like isoniazid, rifampicin, pyrazinamide, ethambutol) bar their use especially when multiple first line drugs need to be applied to suppress resistance [11-14]. This follow-up is often lacking in several affected countries like India [15-17].
3. Emergence of resistance in *M.tb.* against major first line chemotherapeutic agents has hindered the treatment of TB cases.
4. To date, most diagnostic procedures rely largely on immuno-assays that are not sufficiently specific. *M.tb.* shares antigens to many other *Mycobacterium* species resulting in false positive cases in ~35% of patients with active TB [18-20]. Other techniques that have been employed like flow cytometry, radiometric detection, latex agglutination etc. have their own set of disadvantages which will be discussed in detail in the coming sections.

The objective of this study is to present a succinct review of the available biosensing techniques that are either already in use or under development in detection of TB. The focus of the review will be on emerging biosensor-approaches that are compared to conventional

techniques. Special attention will be given to their potential for deployment under field conditions in resource poor countries.

## 2.1.2 Epidemiology

The WHO Global TB Control Report 2012 reported that the WHO's Millennium Development Goal to halt the growth of the TB epidemic by 2015 is showing some success with a decrease of 2.2% observed between 2010 and 2011 for new TB cases, along with a 41% mortality rate decreases relative to 1990. Between 1995 and 2011, 51 million people were successfully treated for TB, saving 20 million lives. Despite this progress, the global burden of TB remains enormous with 8.7 million new cases of TB were registered in 2011, out of which 13% patients were co-infected with HIV. The mortality in 2011 due to TB was 1.4 million, including almost one million deaths among HIV-negative individuals and 0.4 million among people who were HIV-positive. The distribution of TB cases also shows a gender-dependence with men reporting more cases compared to females in all age groups and from every geographical region of the world. India and China together account for 40% whereas the African region contributes 24% of the world's TB cases. The statistics of the MDR cases in TB are alarming according to the WHO 2012 report. It reported resistance to more than one first line anti-TB drugs among 3.7% of new cases and 20% previously treated cases. In recognition of the problem, 26 nations have already listed MDR-TB as a top priority health programme and founded a global fund to support Directly Observed Therapy (DOT) to ensure the effectiveness of given medications [21-23].

## 2.1.3 Current TB diagnostics

### 2.1.3.1 Immunological and microbiological tests

For the diagnosis of TB, five conventional tests are available:

- 1) *Smear Microscopy*: microscopy based smear tests are rapid, inexpensive, simple and relatively easy to perform methods for the detection of acid-fast bacterium such as *M.tb.* bacterium. Conventionally the Ziehl-Neelsen staining is utilized requiring a minimum of  $1 \times 10^4$  bacterium per ml of sputum [24]. Fluorescence microscopy utilizing auramine-rhodamine staining was found to be more sensitive though expensive, as it requires a fluorescence microscope [25]. The fluorescence-based method is more sensitive as slides can be examined at lower magnification [24]. Results from this method can be obtained within an hour.
- 2) *Immunological assays* like Latex Agglutination, ELISA, and Mantoux tests: in these tests, typically the binding of antibodies in serum to *M.tb.* antigens is tested [26, 27]. For example, in latex agglutination tests, the polystyrene (latex) beads are functionalized with antigens extracted from a pathogenic Mycobacterium that are then reacted with serum samples [28]. In case of a reaction, the latex beads coagulate showing a positive test. The sensitivity of these tests are not high enough [29]. Hence, when the bacterial load is low,

these tests will fail. Also, the serum could contain antibodies (due to vaccinations like Bacille-Calmette–Guérin/BCG) that might interfere with the tests adding further to the shortfalls of these assays.

- 3) *Radiometric detection test*: in this type of test, the metabolic activity of *M.tb.* is detected radiologically [30]. For example, *M.tb.* (and also some other mycobacteria) are known to produce CO<sub>2</sub> from carbon sources like glycerol or acetate. The important selective criterium is that *M.tb.* cannot form CO<sub>2</sub> from glucose. This helps to differentiate *M.tb.* from other *Mycobacterium sp.* and bacteria. Utilizing this selective property, the capability of *M.tb.* in producing <sup>14</sup>CO<sub>2</sub> from 14C-U-glycerol or 14C-U-acetate, but not from 14C-U-glucose is measured. Due to the technical complexity this technique is not suitable for developing countries.
- 4) *Flow cytometry test*: In the last few years, use of flow cytometry has increased rapidly in the detection of TB cases [31-33]. This technique is based on the ability of viable *M.tb.* bacterium to absorb fluorescein diacetate (FDA) and to hydrolyse it into fluorescein, which upon accumulation in metabolically active bacterium could successfully be detected by flow cytometry. The reproducibility is high and it does not require active cell division of mycobacteria [34, 35]. The technique, however, needs logistic support from a specialized laboratory that makes it difficult to implement in developing countries [36].
- 5) *Cultivation detection tests* (like MB/Bact, Bactec MGIT 960 systems): In these techniques, biological samples are selectively cultured on solid media to detect and quantify the presence of *M.tb.* [37-40]. Although quite accurate, this technique is time consuming, as it requires a growth period of 9-42 days. It also requires a laboratory back-up which complicates applications under field conditions in developing countries [40].

### 2.1.3.2 Genotypic tests

DNA-based techniques are becoming increasingly important, especially for the detection of resistant strains of *M.tb.* They need a laboratory setting, however, so that for field use they do not yet represent a suitable method. The most popular techniques are the following:

- 1) *Polymerase chain reaction (PCR)-based techniques*: PCR is one of the most sensitive methods to detect the presence of *M.tb.* strains, also sequencing of PCR amplified DNA fragments is the most direct technique of detecting codons responsible for resistance in *M.tb.* [41-43]. PCR amplified DNA fragments are generally analysed by the following two methods:
  - a) *Electrophoresis*: This method mainly relies on the difference in electrophoretic mobility of mutated DNA fragments of *M.tb.* especially of resistant strains. By electrophoretic techniques, PCR amplified DNA can be compared with the electrophoretic mobility of a wildtype/reference *M.tb.* DNA, and thus caution for any resistance [44]. A heteroduplex

analysis method has also been developed in recent years where strands with a single-base mismatch can easily be identified and separated utilizing conformation-sensitive gel electrophoresis from the strands containing no mismatches [45, 46].

- b) *Hybridization-based techniques*: This type of technique relies on the hybridization of clinical DNA with complementary DNA and the binding is then compared with the results of wild/reference *M.tb.* DNA [47, 48]. In case the complementary strand is sufficiently homologous, the binding of clinical DNA can be detected using ELISA readers. The hybridization can be done user-friendly on strips, microtiterplates as well as microarrays.
- c) *Real-time PCR*: with the help of fluorescently labelled DNA strands, it is possible to visualize the increase of the product in “real time” [49-51]. Different types of fluorescent labels have been applied in a diverse range of real-time PCR techniques, like TaqMan probes [50, 52, 53], Beacons [54, 55] and FRET probes [56, 57].

The main disadvantages of PCR-based tests are the relatively high costs of equipment and reagents. It also requires highly skilled personnel along with dedicated pre- and post- PCR rooms to avoid contamination. Even if it were less expensive, the technological and sample preparation complexities make it largely inappropriate for use in resource poor settings.

## 2.2 Biosensors in TB detection

Considering the fact that 98% of all TB cases occur in areas of developing countries without access to specialized laboratories, there is a strong need to develop alternative, simpler and lower cost techniques for TB diagnosis. Biosensors are analytical devices that transduce biochemical reactions/interactions of isolated enzymes, receptor proteins, antibodies, nucleic acids, organelles, whole cells or tissues with specific chemical compounds into an optical, thermal or electrical signal, which can be more easily measured and quantified. The main advantages of biosensors over conventional diagnostic techniques can be stated as follows:

1. *Technical advantage*: In biosensors often a high level of device and capture/detection integration is achieved allowing single step detection.
2. *Ease of use*: Many of the designed biosensors are tailored with user-friendly interfaces connecting them to advanced instrumentation.
3. *Quick Response*: Response time is typically a few minutes for most biosensors enabling rapid and better control over the measurement.

A general framework of different classes of biosensors that could be used for the detection of TB is given in Fig. 1 to guide the reader through the upcoming sections of the review and will be discussed in more detail within relevant sections.

### 2.2.1 Electrochemical and electrical biosensors

Electrochemical and electrical biosensors are among the most popular biosensors that are used today in detection of not only TB but also a large number of other diseases [60-62]. The mechanism of detection relies on specific changes in electrical signals (conductance, impedance, potential, capacitance) at a surface-functionalized electrode by either chemical reactions or physical interactions. For example, monoclonal antibodies rose against *M.tb.* cell wall components can be immobilized onto an electrode surface exposed to a suspension of *M.tb.* and detect the interaction between the *M.tb.* bacteria and the antibodies by a change of conductance [63]. Similarly, an electrode-based DNA biosensor can also be made where certain probes that specifically bind to specific regions of *M.tb.* DNA are immobilized on the electrode [62]. For electrodes carbon paste, gold or zirconia (ZrO<sub>2</sub>) coated carbon nanotubes have been used [60, 62, 64-66]. These sensors are sensitive, flexible and allow a high degree of multiplexing, but they also present some disadvantages. Firstly, a constant pH and ion concentration of the reaction compartment is very critical, as they directly affect the baseline conductance of the electrodes. Secondly, the obtained electrical signal strictly depends on many molecular factors, like the positive or negative net charge or neutrality of the analyte etc.

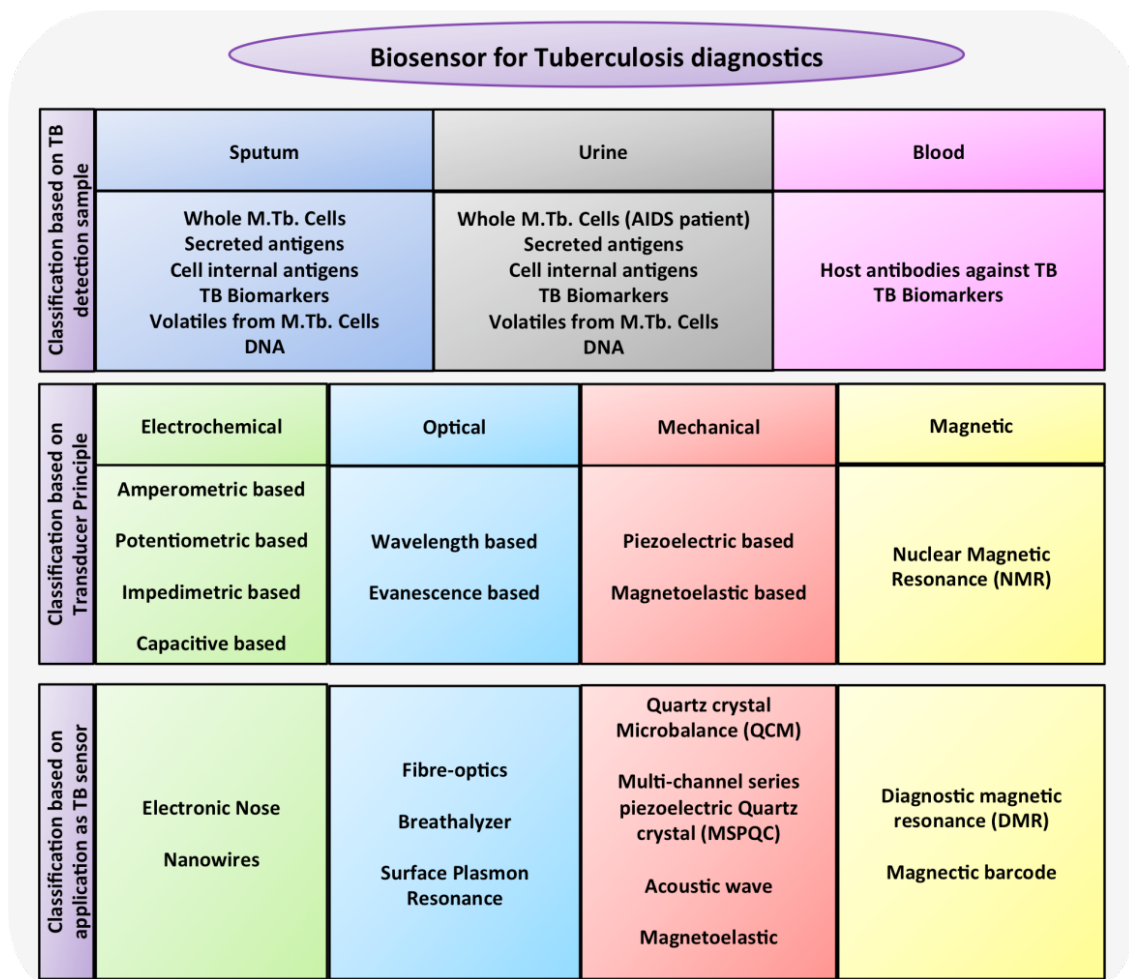
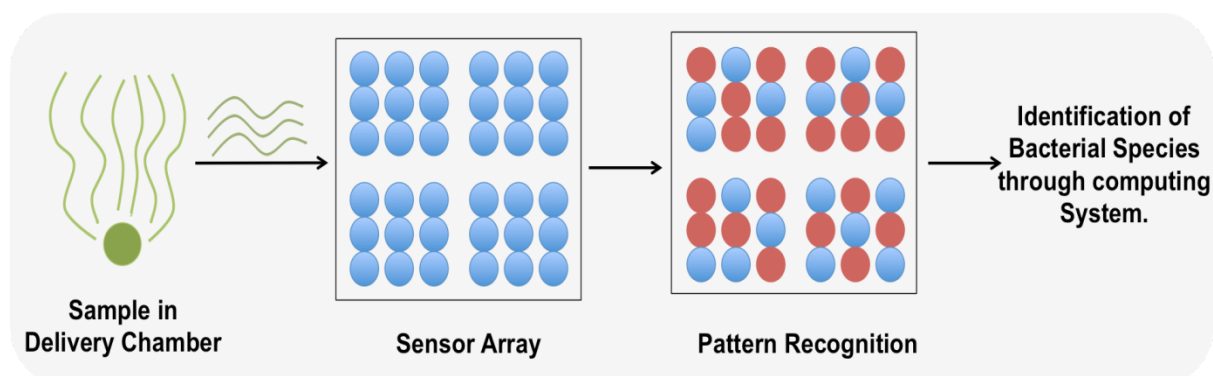


Figure 1: Generic classification of biosensors tested as TB diagnostics [59, 60]

### 2.2.1.1 Electronic nose-based biosensors

Electronic “nose” type biosensors are designed to recognize volatile substances produced by *M.tb.* in liquid medium (Fig. 2) [67-70]. It basically consists of three main building blocks i.e. (i) a volatile gas chamber that passes the volatile molecule products over a sensor array, (ii) a pattern of more or less specific responses by the sensor array and (iii) a data analysis system to interpret the output pattern of the detection system. In an electrochemical transducer based system metal oxide semiconductors (MOS-FETs like ZnO, MnO, TiO<sub>2</sub>, SnO<sub>2</sub>) or conducting polymers (like polypyrroles, polyanilines) coupled to the transducer are used. To obtain reliable signals, the humidity and temperature must be regulated well. The principle is based on the observation that *M.tb.* produces specific volatile organic compounds that are significantly different from the volatiles produced by other gram positive bacteria, like *Mycobacterium avium*, *Mycobacterium scrofulaceum* and *Pseudomonas aeruginosa* [67]. Electronic nose appliances have been used successfully to detect the presence of *M.tb.* [68].



**Figure 2:** An electronic nose based biosensor consisting of three main parts i.e. a sample delivery chamber, a detection array/pattern recognition system and a computing system for data analysis and result interpretation. This is fundamentally a sensor assay where a specific pattern is produced upon interaction with volatile/gaseous by-products from specific bacterial species [71]

### 2.2.1.2. Nanowire-based biosensors

Biosensors built with nano-sized transducing elements are most prominently represented by silicon nanowires that operate as field effect transistors (FETs). A detailed discussion on the design of such FET sensors falls beyond the scope of this review. However, most commonly, a silicon nanowire with a low p-type doping is connected with a higher doped source and drain region, whereas the more heavily doped silicon support wafer is designed to serve as a back gate via an intermediate 100 to 500 nm thick silicon oxide layer. The backgate voltage controls the nanowire channel resistance and in case of a positive voltage (e.g. +2V) a depletion layer is created in the silicon nanowire where the majority charge carriers (positively charged holes) are repelled, herewith creating a lower conductance (Fig. 3). For measurement, when a drain-source voltage is applied, a drain current ( $I_d$ ) is generated between the source and drain regions that can then be measured and plotted against time. Any change in the amount of a (charged) target molecule binding to the surface gets

reflected in a charge displacement in the wire (attraction or repulsion of holes) and results in a variation in the  $I_d$  that can be interpreted against a calibration curve. Usually, silicon nanowires [72, 73] or carbon nanotubes [66, 74-76] are used to obtain the properties of nanowires. The testing system is often made on a microchip-like set up where the nanotubes are fixed along with surface functionalization with antibodies or antigens depending on the samples to be used. For example, boron-doped silicon nanowires were used to detect different bacterial antigens by the change of conductance after binding [77, 78]. Similarly, carbon nanotubes (both single and multi-walled) have been used to detect various antigens [79] including *M.tb.* antigens or ssDNA specific for *M.tb.* [80].

The major advantage offered by this category of biosensors is its higher than normal sensitivity, because of two main factors i.e. (1) The size of the biological species/analyte to be detected is comparable to the size of the nanowire, hence the charge of the incoming species can sensitively control the conductivity of the charge carriers in the semiconductor material within the Debye length [82], (2) The wire represents a serial circuit where interaction at each receptor molecule can control the current flowing through the entire nanowire [83]. The chemical nature of silicon and carbon wires and tubes allow a wide scope of surface functionalizations, which is an advantage compared to metal electrodes. However, the delicate surface functionalization and nature of silicon nanowires, makes it technologically much more challenging to actually design and implement these types of sensors [84].

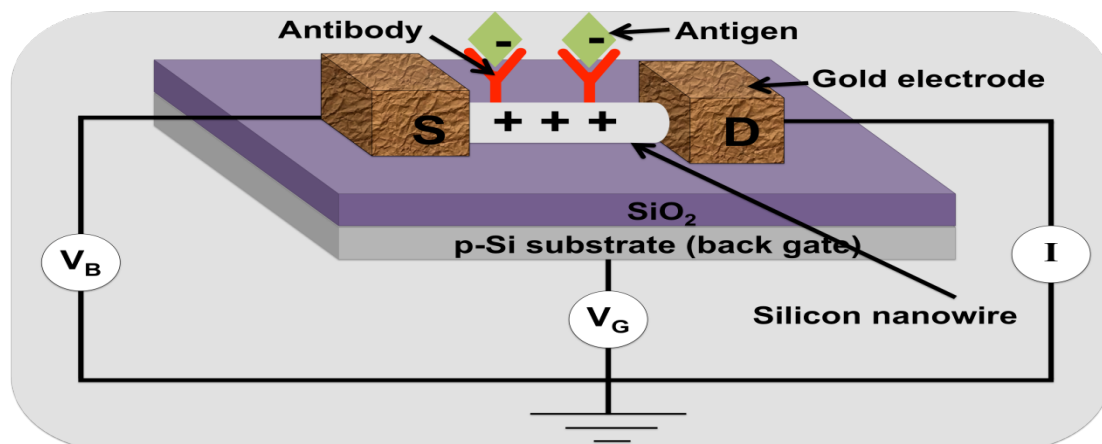


**Figure 3:** A silicon nanowire based biosensor: a change in conductance of an antibody-functionalized nanowire is measured upon binding of the antigen [81]

## 2.2.2 Optical biosensors

### 2.2.2.1 Fibre-optic biosensors

Light propagating through an optical fibre consists of two components i.e. the light propagating through the core of the fibre and the exponentially decaying evanescent field outside the core of the fibre (Fig. 4). In case of total internal reflection (TIR), the intensity of the reflected light does not decay rapidly as only a very small amount of light passes through

the thickness of the tube and hence not able to interact with the fibre's surroundings. The decay of the transmitted light (evanescent wave) is exponentially related to the distance travelled ( $d$ ) outside the core and is typically 100 to 200 nm. This rate of decay of the evanescent wave can be reduced by decreasing the thickness of the cladding layer (walls) of the tube, making the method suitable for sensing applications. In this situation, the evanescent wave interacts with the fibre's surrounding causing an energy flow that could activate fluorophores bound to the outer surface of the fibre tube. The emitted light from the fluorophores can then also be detected using a spectrophotometer. These sensors can be tailor-made to detect specific pathogens. For example, *M.tb.* produces niacin which after reaction with cyanogen bromide and aniline produces a compound of yellow colour [72]. Hence, a *M.tb.*-rich sputum sample will contain high levels of niacin which after reaction with cyanogen bromide and aniline will produce a colour which can be detected by fibre-optics. Similar types of sensitive fibre-optics-based biosensors for TB detection have also been reported elsewhere [85-88]. Multiplexing is required to render such detection platforms more reliable.

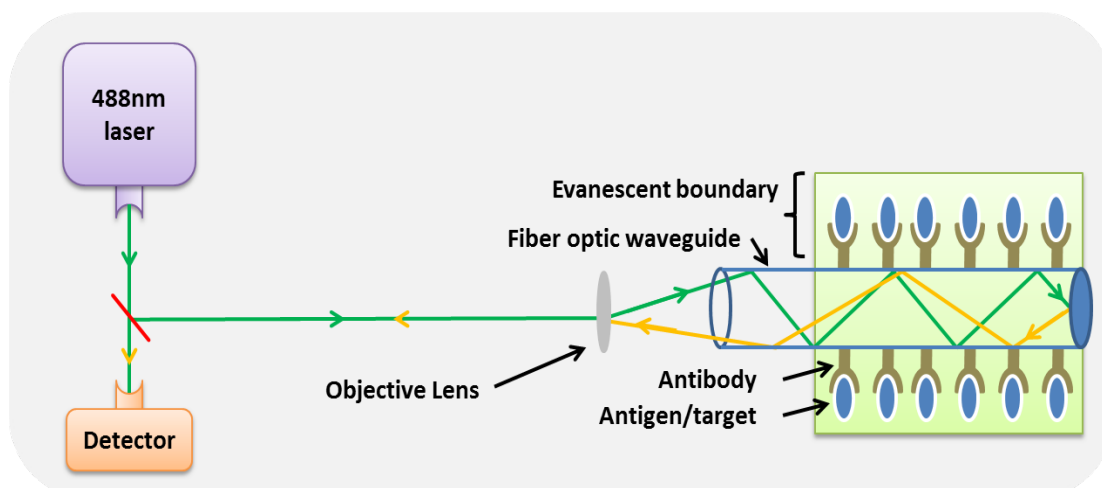


**Figure 4.** A fibre optics based biosensor where specific binding at the exterior of fibre optic waveguide via specific antibodies is measured by determining the change in the angle of reflection of the incident light. The system works using the principle of evanescence [89].

Another interesting class of biosensors with good potential for TB detection is the so-called optical ring resonance (ORR) detectors. The principles of optical ring resonance are complex and fall beyond the scope of this review. In summary, these ORR systems are based on total internal reflection and constructive interference [90]. Recently, such ORR detectors could be designed on lab-on-a-chip platforms [91, 92] with multiple parallel channels with one channel coated with specific antibody (test channel) and others coated with non-specific antibodies (reference channel). With binding of the antigens with their specific antibodies, there are changes observed in total internal reflection and simultaneous interference patterns which are recorded by a CCD camera and compared to the data obtained from reference channels. Pending the availability of highly specific antibodies to *M.tb.* antigens, these ORR detectors may be of potential in early detection of TB although the surface functionalization has the same challenges as in case of nanowire functionalization, because the core material of the fibre is mostly silicon based.

### 2.2.2.2 Surface plasmon resonance (SPR)-based biosensors

Surface plasmon resonance (SPR) is an optical principle frequently used in biosensors. Surface plasmons (evanescent waves) are produced when a polarized light is incident at the back of a thin film of noble metals like gold and silver. The angle of reflection changes depending on mass bound to the surface on the other side. The other side of these noble metals are therefore coated with bio-recognition elements or receptor molecules that interact with an analyte molecule present in a liquid sample. A light wave can excite surface plasmons at metal-dielectric interface only when the component of the light wave vector parallel to the interface matches with that of the surface plasmon. For this, the light wave vector needs to be enhanced so that it matches the surface plasmons, as the real part of the propagation constant is always larger than that provided by the light wave vector in the dielectric. Usually attenuated total reflection methods with a prism are employed for excitation of the surface plasmons. A light wave passing through an optical prism is allowed to fall on the metal film of about 50 nm thick at an angle of incidence that is larger than the critical angle for the prism-dielectric system. Now this light is totally reflected producing evanescent waves propagating along the metal film. A portion of the light energy is transferred into energy of these surface plasmons and is dissipated in the metal field resulting in a drop of intensity of reflected light. The coupling conditions can be fulfilled for multiple combinations of angle of reflection and the wavelength. Therefore, a characteristic dip associated with the excitation of surface plasmons can be observed both in angular and spectral domains. The instrumentation of SPR consists of a convergent monochromatic beam source directed onto the prism coupler, over which the sample containing the metal layer modified with receptor molecule is passed (Fig. 5).

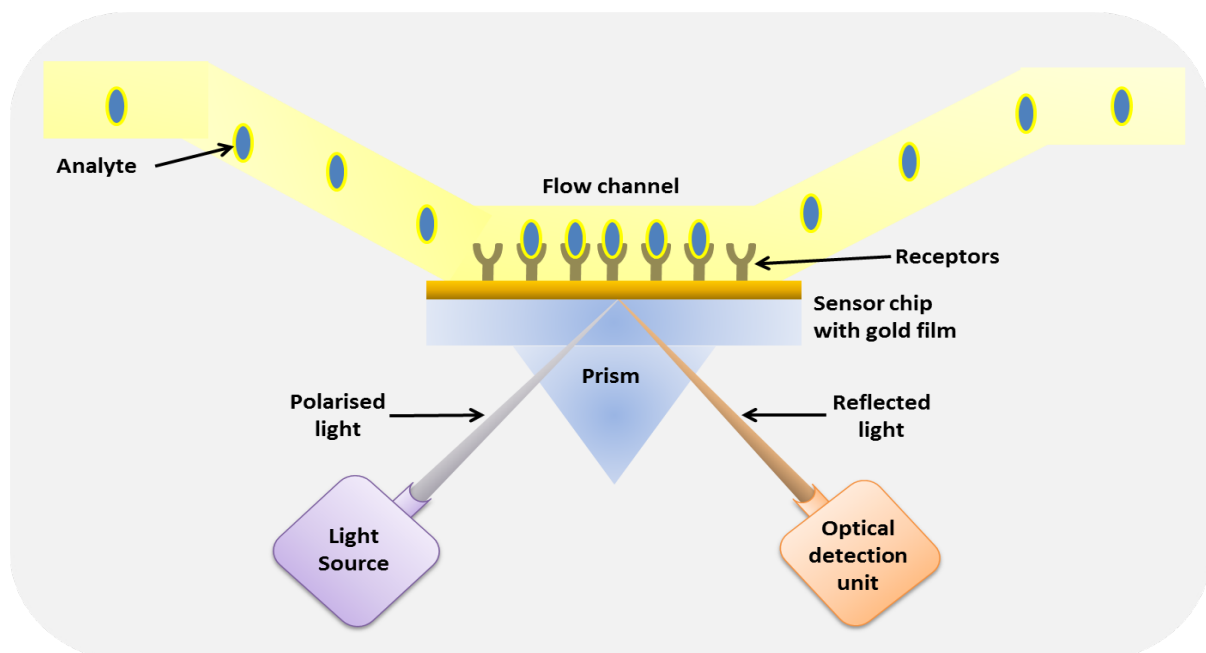


**Figure 5.** A surface plasmon resonance based biosensor. In this type of biosensor, a thin gold plate is functionalized with antibodies that upon binding to the antigen cause a change in the angle of reflection of the polarised light incident at the other side of the gold film [93]

### 2.2.2.3 Breathalyzer biosensors

Breathalyzer sensors have specifically been developed to diagnose pulmonary TB in patients. Typically, in these types of sensors the patients are asked to cough in a masked bag-like structure containing a collection tube (usually 10 cm in length and 3.5 cm in width) after administration of a nebulized dose of saline [104,105]. The samples thus collected are distributed across the surface of a coated prism at the bottom of the glass tube. This prism surface is coated with a *M.tb.* specific antibody and fluorescent peptide epitopes [104]. The peptide analogue comprises artificially modified peptide sub-sequences of the T-cell epitope from *M.Tb* Ag85B [106]. The antibody has a higher affinity for TB bacterium compared to the fluorescent peptide analogues, which enables a competition assay on such platforms [104]. In the presence of TB bacterium, the fluorescent-coated analogues are displaced by TB bacterium and this biochemical process is interrogated by the diode laser of the measuring device. The sensitivity of the system for detection of *M.Tb* cells was 50-75 CFU/ml [104]. The biosensors are portable, rapid and sensitive encouraging their use in outdoor clinics in the developing World. The collection tube is cheap and easy to dispose after one use per patient [104].

### 2.2.3 Mechanical Biosensors

#### 2.2.3.1 Piezoelectric quartz crystal biosensor

Piezoelectric quartz crystal biosensors are based on the Sauerbray equation ( $\Delta F = -2.3 \times 10^6 F^2 \Delta M / A$ , where  $\Delta F$  is change in frequency,  $F$  is resonant frequency,  $\Delta M$  is change in deposited mass and  $A$  is area of electrode), which shows that change in frequency of the crystal is directly related to the change in deposited mass over the electrodes. Due to this unique resonant frequency property of quartz crystals, any changes in resonating mass by the binding of specific biomolecules or microbes and bacteria like *M.tb.* can be sensitively detected (Fig. 6) [107-109]. Piezoelectric biosensors of three types have been described: quartz crystal microbalance (QCM), multi-channel series piezoelectric quartz crystal sensor (MSPQC) and acoustic wave biosensor.

##### 2.2.3.1.1. Quartz crystal Microbalance (QCM)

In QCM systems applied to TB, the crystal electrode was first coated with protein A followed by binding of an anti-TB-cells antibody (rabbit IgG against *M.tb.*) and then incubated with weakened TB cells. Binding of *M.tb.* cells on the crystal electrodes was monitored in real time and the frequency shift was calculated. The sensitivity using this system was  $10^5$  CFU/ml [110]. The main advantage of QCM lies in the fact that it is fast, reusable (after washing), label-free, requires minimal sample preparation and is easily operated. The major disadvantage lies in the fact that the density, temperature, viscosity and electrical conductivity of the sample may affect the results and require calibration correction and that it is relatively insensitive.

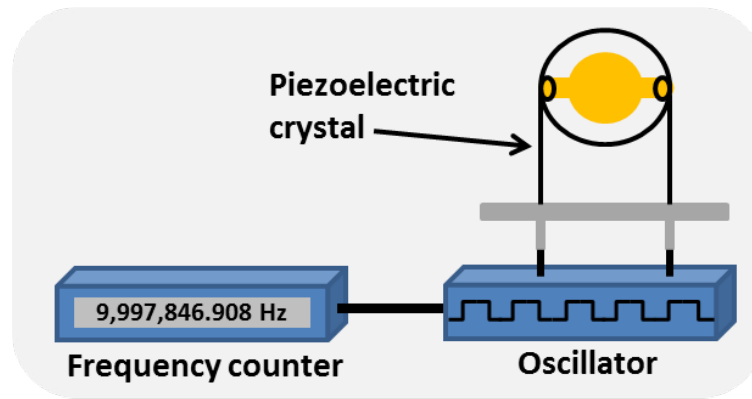


**Figure 6.** A piezoelectric quartz crystal based biosensor where the change in resonating frequency of a piezoelectric crystal is measured. The resonance frequency of the crystal shows a change after binding of antigens with specific antibodies immobilised on the crystal [110]

### 2.2.3.1.2. Multi-channel series piezoelectric quartz crystal sensor (MSPQC)

In the MSPQC system, there are eight sample detectors along with a microprocessor and a data output system. The system relies on detection of volatiles produced by the growth of *M.tb.* such as  $\text{NH}_3$  and  $\text{CO}_2$ . These volatiles cause an impedance change when they are absorbed by a KOH absorbing solution, which in turn will change the oscillating frequency. The limit of detection with this system is  $10^7$  CFU/ml at the time of detection [111]. Apart from being time consuming involving a laborious *M.tb.* culture process (eight days in case of a low *M.tb.* burden), another major drawback of this system is the sample pre-treatment required to remove contamination with other bacteria.

### 2.2.3.1.3. Acoustic wave biosensor

Acoustic wave biosensors rely upon acoustic waves propagating near the surface of a piezoelectric crystal. The sensor electrically produces a mechanical wave that is sensitive to any change or binding at the piezoelectric crystal and then transduces the mechanical output waves back into an electrical signal, which is compared with the input electrical signal for changes in amplitude, phase, and frequency [112]. In one application apart from the acoustic signal also the conductivity change (impedance) of the medium over the crystal was measured. Here the conductivity change due to growth of *M.tb.* cells and by-product production was studied [113, 114]. The limit of detection with this bulk acoustic wave impedance biosensor was  $2 \times 10^3$  CFU/ml. The disadvantage of the system is the time consuming and laborious *M.tb.* culture process that reduced the applicability for field uses.

### 2.2.3.2 Magnetoelastic biosensors

Magnetoelastic biosensors possess a magneto-elastic strip, often made up of ferromagnetic alloys comprising iron, boron, nickel and molybdenum. Capture molecules (like antibodies) that can bind target molecules, microbes or viruses are immobilized on the strip (Fig. 7) [115-117]. Exposure of the magnetoelastic strip to a varying external magnetic field causes the magnetoelastic strip to resonate at a specific (fundamental) frequency. The

fundamental resonant frequency for longitudinal vibration of a thin ribbon like strip vibrating in its basal plane is given by the equation

$$f = \sqrt{\frac{E}{\rho(1 - \sigma^2)2L}}$$

where E denotes modulus of elasticity,  $\sigma$  is the Poisson's ratio,  $\rho$  is the mass density of the sensor material, and L is the longitudinal dimension of the sensor. The change in resonant frequency also depends on mass change when the initial mass, temperature and humidity are constant and is given by the equation.

$$\Delta f = -\frac{f}{2} \left( \frac{\Delta m}{M} \right)$$

where f is the initial resonance frequency, M is the initial mass,  $\Delta m$  is the mass change, and  $\Delta f$  is the shift in the resonant frequency of the sensor [118]. It is due to this dependence on mass change, that upon binding of antigens or *M.tb.* bacteria to the antibody, there is a shift in fundamental resonant frequency, which is often monitored wirelessly on a frequency counter.

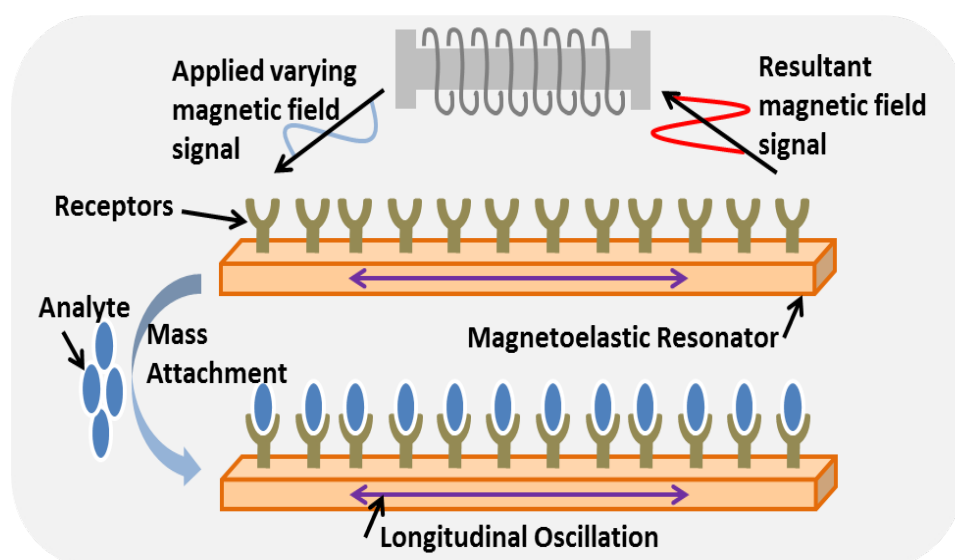


**Figure 7:** A magnetoelastic biosensor where the change in basal resonating frequency of a magnetoelastic strip as a result of binding of antigens with specific antibodies under varying magnetic fields is measured in order to detect analyte [119]

The advantages of these types of sensors over SPR-based sensors are their ease of use as the sensors are (i) freely hanging inside a sample solution, (ii) do not require complicated integration with microfluidics pumps and (iii) do not produce a complex signal. The fundamental resonating frequency of the strip immersed in liquid (culture media) can also be altered due to the consumption of nutrients. *M.tb.* in the liquid media, upon proliferation decomposes macromolecule into by products (such as ammonia, carbon dioxide, organic acid) thereby causing a change in the physical properties of the culture that can then be

detected with the help of such biosensors. A suitable calibration curve must be made to detect a specific *M.tb.* signature [117]. The sensor resonant frequency shift upon immersion in liquid is given by the equation

$$f = - \frac{\sqrt{\pi f_0}}{2\pi \rho_s d} (\eta \rho_l)^{1/2}$$

where  $f_0$  is the resonant frequency of the sensor in air,  $\rho_s$  and  $d$  are the density and thickness of the sensor,  $\eta$  and  $\rho_l$  are the density and viscosity of the liquid, respectively. Under liquid medium, the shear wave created due to the sensor vibration reduces the oscillation of the sensor. The detection limit of this biosensor can be as low as  $10^4$  *M.tb.* cells/ml [117].

## 2.2.4 Magnetic Biosensors

### 2.2.4.1 Diagnostic Magnetic Resonance (DMR)

DMR system is an automated, high-throughput miniaturized lab-on-a-chip scale adaptation of conventional nuclear magnetic resonance (NMR). Its principle is based on detection of changes in the spin relaxation time of surrounding water molecules i.e. when antibodies coated on mono-dispersed nanoparticle binds to target (*M.tb.* cells) forming a cluster or aggregate and thus becomes more efficient in dephasing the nuclear spin of surrounding water molecules, thereby causing a decrease in spin-spin relaxation time. It consists of four miniaturized modules i.e. a microcoil array for applying the magnetic field, a small permanent magnet, feedback based read out electronics for temperature compensation and a microfluidic network for automated sample injection [120, 121]. Capture antibody functionalized magnetic nanoparticles are used which can specifically detect the mycobacterium cells. By virtue of its operating principle, highly sensitive (20 CFU/ml) magnetic measurements can be done on easier to handle turbid and unprocessed sputum samples without pre-treatment or false positives as biological samples show virtually no magnetic background [122, 123]. The decreased assay time, small sample volumes, versatility and multiplicity make it suitable for point of care diagnostics. The low cost of the setup and disposable chip could be an advantage for use in remote clinics and hospitals in the developing world. In 2013, the DMR was further miniaturized for very small volume sample detection (2 ml) and rapid, high throughput operations in point of care settings [124]. This approach has been used to analyse varied bacterial mixtures with specific probes. Another improvement is the amplification of 16S rRNA from total RNA extracted from whole bacterial cells by asymmetric RT-PCR. Single-strand DNA amplified from 16S rRNA is then captured by magnetic beads conjugated with capture probe. After which hybridization with magnetic NPs (MNPs) coated with detection probe is done to form a magnetic sandwich complex detectable using  $\mu$ NMR system. Though the magneto-genetic assay has not been utilized yet for tuberculosis detection, it has a strong potential to be applied for clinical and point of care settings [124].

### 2.2.4.2 Magnetic barcode platform

A novel platform for the detection of nucleic acids is based on a magnetic bar coding strategy. PCR-amplified mycobacterial genes can be sequence-specifically captured on microspheres, labelled by magnetic nanoprobe and detected by nuclear magnetic resonance. This significant improvement of  $\mu$ NMR in terms of size and design has resulted in glass slide sized magnetic barcode platform detection. The sample volume to be analysed passes through a microfluidics channel enclosed by an electromagnetic coil. This sensing component eliminates the use of permanent magnets [125]. The coil functions as a sensing element where a shift in relaxation time is measured using a feedback of the readout electronics [120, 121]. The platform also integrates lab on a chip PCR for assay optimization. For TB detection the total RNA is extracted from the tuberculosis cells and the 16S rRNA is amplified by asymmetric Real Time-PCR to single-strand DNA which is then immobilised on conjugated beads, followed by hybridizing with magnetic nanoparticles (MNPs) and coated with a detection probe to form a magnetic sandwich complex. The complex thus formed is allowed to pass through microfluidic channels, where it is detected [125]. In an example using 92-nt fadE15 amplicons, they showed that magnetic bar coding assays had a strong magnetic signal within 1 min of labelling at 37°C. The costs of the device can potentially be scaled down to <\$200 in contrast with existing diagnosis instruments that cost over \$10,000 [125].

## 2.3 Challenges and outlook

TB remains one of the major unresolved global health problems, especially in the developing parts of the world, predominantly due to the complexity of a proper and economic affordable diagnosis and treatment in time along with recently arising issues like multiple drug resistance and other allied infections that decrease body immunity, like HIV. Current technologies for diagnosis are either too insensitive, too laboratory intensive or utilize expensive detection modules, which are all a challenge in resource poor settings. An overview comparing the analyzed sample and detection limits of different biosensors are shown in Table 1. With WHO's aim to completely eliminate TB by 2050, development of techniques for early and accurate detection of tuberculosis is crucial. To build an effective biosensor for TB detection, criteria that need to be fulfilled are: (1) cost-effectiveness (2) high sensitivity (3) reliability (no false positives) (4) portability and (5) disposability. Unfortunately, designing a biosensor with all these advantages has not yet been completely successful, as each attempt has specific drawbacks. It is a challenge to satisfy all these needs in a single biosensing device. Nevertheless, the advances in nanosensors and other upcoming technologies reviewed here, suggest that biosensors to detect TB can be expected to play a larger role in the near future. Such platforms will also need to solve issues around sample collection and preparation. Currently most diagnosis techniques available utilize sputum samples as test sample, which due to its high viscosity and sticky nature is very difficult to work with. Hence other sources like blood or urine should also be considered as test samples. Lack of reliable and tested biomarkers in those samples is, however, an issue that needs attention.

**Table 1:** Comparison of different biosensors for *M.tb.* detection

#	Transducer	Sensing technique	Sample analysed	Detection limit	References
2.1	Electrochemical	Electronic Nose Sensor	<i>M.tb.</i> produced volatiles compounds	N.A.	Pavlou <i>et.al.</i> [67]
		Nanowire/nanotube based biosensor	<i>M.tb</i> specific ssDNA	N.A.	Das <i>et.al.</i> [80]
2.2	Optical	Fibre-optics	<i>M.tb.</i> produced organic compounds	N.A.	Lee <i>et.al.</i> [72]
		SPR	CFP 10 <i>M.tb.</i> antigen or Protein complex	100 ng/ml 30 ng/μl	Hong <i>et.al.</i> [102] Duman <i>et.al.</i> [97]
		Breathalyzer	<i>M.tb.</i> cells	50-75 CFU/ml	McNerney <i>et.al.</i> [104]
2.3	Mechanical	QCM	<i>M.tb.</i> cells	10 <sup>5</sup> cells/ml	He <i>et.al.</i> [108]
		MSQC	Volatiles produced by the growth of <i>M.tb.</i> such as NH <sub>3</sub> and CO <sub>2</sub>	10 <sup>7</sup> CFU/ml	Ren <i>et.al.</i> [111]
		Acoustic Wave	<i>M.tb.</i> cells	2×10 <sup>3</sup> CFU/ml	He <i>et.al.</i> [114]
		Magnetoelastic	<i>M.tb.</i> cells by-products	10,000 cells/ml	Pang <i>et.al.</i> [117]
2.4	Magnetic	DMR	<i>M.tb.</i> cells	20 CFU/ml	Lee <i>et.al.</i> [123,126]
		Magnetic Barcode	RNA from <i>M.tb.</i> cells	100 CFU/ml	Liong <i>et.al.</i> [125]

## References

1. Gandy M, Zumla A; *Soc Sci Med*, **2002**, *55*, 385
2. Grange JM, Gandy M, Farmer P, Zumla A; *Int J Tubercul Lung D*, **2001**, *5*, 208
3. Shah NS, Wright A, Bai GH, Barrera L, Boulahbal F, *et al.*; *Emerg Inf Dis*, **2007**, *13*, 380
4. Palomino JC, Martin A, Camacho M, Guerra H, Swings J, *et al.*; *Antimicrob Agent Chemo*, **2002**, *46*, 2720
5. Kruh NA, Troutd J, Izzo A, Prenni J, Dobos KM; *PLoS One*, **2010**, *5*, e13938
6. Murray JF; *Am J Resp Crit Care Med*, **2004**, *169*, 1181
7. Nahid P, Pai M, Hopewell PC; *Proc Am Thorac Soc*, **2006**, *3*, 103
8. Expert Group Meeting Report; *WHO*, **2014**, *1*
9. Murray S; *Can Med Assoc J*, **2006**, *174*, 33
10. Ormerod LP; *Br Med Bull*, **2005**, *73-74*, 17
11. Mitnick C, Bayona J, Palacios E, Shin S, Furin J, *et al.*; *New Eng J Med*, **2003**, *348*, 119
12. Caminero JA; *Int J Tubercul Lung D*, **2006**, *10*, 829
13. Isaakidis P, Cox HS, Varghese B, Montaldo C, Da Silva E, *et al.*; *PLoS One*, **2011**, *6*, e28066
14. Colijn C, Cohen T, Ganesh A, Murray M; *PLoS One*, **2011**, *6*, e18327
15. Shin SS, Furin JJ, Alcantara F, Bayona J, Sanchez E, *et al.*; *Emerg Inf Dis*, **2006**, *12*, 687
16. Lee C-H, Lee M-C, Lin H-H, Shu C-C, Wang J-Y, *et al.*; *PLoS One*, **2012**, *7*, e37978
17. Mulenga C, Mwakazanga D, Vereecken K, Khondowe S, Kapata N, *et al.*; *BNC Pub Heal*, **2010**, *10*, 756
18. Bekmurzayeva A, Sypabekova M, Kanayeva D; *J Tubercul* **2013**, *93*, 381
19. Somoskovi A, Hotaling JE, Fitzgerald M, Jonas V, Stasik D, *et al.*; *J Clin, Microbiol*, **2000**, *38*, 2743
20. Singh S, Singh J, Kumar S, Gopinath K, Balooni V, *et al.*; *PLoS One*, **2012**, *7*(7), r40213
21. Cavalcante SC, Soares ECC, Pacheco AGF, Chaisson RE, Durovni B; *Int J Tubercul Lung D*, **2007**, *11*, 544
22. Anuwatnonthakate A, Limsomboon P, Nateniyom S, Wattanaamornkiat W, Komsakorn S, *et al.*; *PLoS One*, **2008**, *3*, e3089
23. Harries AD, Jahn A, Zachariah R, Enarson D; *PLoS Med*, **2008**, *5*, e124
24. Palomino JC; *Eur Res J*, **2005**, *26*, 339
25. Steingart KR, Henry M, Ng V, Hopewell PC, Ramsay A, *et al.*; *Lancet Infect Dis*, **2006**, *6*, 570
26. Minton K; *Nat Rev Immunol*, **2003**, *3*, 355
27. Fernández JG, Fernández-de-Mera I, Reyes LE, Ferreras MC, Pérez V, *et al.*; *J Vet Diag Inv*, **2009**, *21*, 102
28. Bhaskar S, Banavaliker JN, Hanif M; *FEMS Immunol Med Microbiol*, **2003**, *39*, 235
29. Bhaskar S, Banavaliker JN, Bhardwaj K, Upadhyay P; *J Immunol Met*, **2002**, *262*, 181
30. Satana D, Coban AY, Uzun M; *J Clin Microbiol*, **2010**, *48*, 4291
31. Dinser R, Fousse M, Sester U, Albrecht K, Singh M, *et al.*; *Rheumatology*, **2008**, *47*, 212
32. Cosmi L, Maggi L, Santarasci V, Liotta F, Frosali F, *et al.*; *Int J Allergy Immunol*, **2007**, *143*, 1
33. Li L, Qiao D, Fu X, Lao S, Zhang X, *et al.*; *PLoS One*, **2011**, *6*, e20165
34. Bonecini-Almeida MD; *Mem Inst Oswaldo Cruz*, **2000**, *95*, 491
35. Piuri M, Jacobs WR, Jr., Hatfull GF; *PLoS One*, **2009**, *4*, e4870
36. Pina-Vaz C, Costa-de-Oliveira S, Rodrigues AG; *J Med Microbiol*, **2005**, *54*, 77
37. Yan J-J, Huang A-H, Tsai S-H, Ko W-C, Jin Y-T, *et al.*; *Diag Microbiol Infect Dis*, **2000**, *37*, 25
38. Saitoh H, Yamane N; *Rinsho Biseibutshu Jinsoku Shindan Kenkyukai Shi*, **2000**, *11*, 19
39. Alcaide F, Benítez MA, Escribà JM, Martín R; *J Clin Microbiol*, **2000**, *38*, 398
40. Garrigo M, Aragon LM, Alcaide F, Borrell S, Cardenosa E, *et al.*; *J Clin Microbiol*, **2007**, *45*, 1766

41. Itani LY, Cherry MA, Araj GF; *J Med Liban*, **2005**, *53*, 208
42. Kobayashi N, Fraser TG, Bauer TW, Joyce MJ, Hall GS, *et al.*; *Arch Pathol Lab Med*, **2006**, *130*, 1053
43. Cousins DV, Wilton SD, Francis BR, Gow BL; *J Clin Microbiol*, **1992**, *30*, 255
44. Shawar RM, el-Zaatari FA, Nataraj A, Clarridge JE; *J Clin Microbiol*, **1993**, *31*, 61
45. Thomas GA, Williams DL, Soper SA; *Clin Chem*, **2001**, *47*, 1195
46. Mohamed AM, Bastola DR, Morlock GP, Cooksey RC, Hinrichs SH; *J Clin Microbiol*, **2004**, *42*, 1016
47. Tevere VJ, Hewitt PL, Dare A, Keen A, Spadaro JP, *et al.*; *J Clin Microbiol*, **1996**, *34*, 918
48. Michelon CT, Rosso F, Schmid KB, Sperhacke RD, Oliveira MM, *et al.*; *Mem Inst Oswaldo Cruz*, **2011**, *106*, 194
49. Drosten C, Panning M, Kramme S; *Clin Chem*, **2003**, *49*, 1659
50. Broccolo F, Scarpellini P, Locatelli G, Zingale A, Brambilla AM, *et al.*; *J Clin Microbiol*, **2003**, *41*, 4565
51. Baba K, Pathak S, Sviland L, Langeland N, Hoosen AA, *et al.*; *Diag Mol Pathol*, **2008**, *17*, 112
52. Kim JH, Kim YJ, Ki C-S, Kim J-Y, Lee NY; *J Clin Microbiol*, **2011**, *49*, 173
53. Bustin SA; *J Mol Endocrin*, **2002**, *29*, 23
54. Papaparaskevas J, Houhoula DP, Siatelis A, Tsakris A; *J Clin Microbiol*, **2008**, *46*, 3177
55. Kumar P, Nath K, Rath B, Sen MK, Vishalakshi P, *et al.*; *J Mol Diag*, **2009**, *11*, 430
56. Taylor MJ, Hughes MS, Skuce RA, Neill SD; *J Clin Microbiol*, **2001**, *39*, 1272
57. Luo T, Jiang LL, Sun WM, Fu G, Mei J, *et al.*; *J Clin Microbiol*, **2011**, *49*, 3132
58. Sang S, Zhang W, Zhao Y; *Review on the Design Art of Biosensors*, **2013**
59. Thusu R; *Sensors Online (Strong Growth Predicted for Biosensors Market)*, **2010**
60. Dai Z, Yan F, Chen J, Ju H; *Anal Chem*, **2003**, *75*, 5429
61. Drummond TG, Hill MG, Barton JK; *Nat Biotechnol*, **2003**, *21*, 1192
62. Das M, Sumana G, Nagarajan R, Malhotra BD; *Appl Phys Lett*, **2010**, *96*, 133703
63. Diaz-Gonzalez M, Gonzalez-Garcia MB, Costa-Garcia A; *Biosens Bioelectron*, **2005**, *20*, 2035
64. Fernandez-Sanchez C, Gonzalez-Garcia MB, Costa-Garcia A; *Biosens Bioelectron*, **2000**, *14*, 917
65. Ouerghi O, Senillou A, Jaffrezic-Renault N, Martelet C, Ben Ouada H, *et al.*; *J Electroanal Chem*, **2001**, *501*, 62
66. Das M, Dhand C, Sumana G, Srivastava AK, Vijayan N, *et al.*; *Appl Phys Lett*, **2011**, *99*, 143702
67. Pavlou AK, Magan N, Jones JM, Brown J, Klatser P, *et al.*; *Biosens Bioelectron*, **2004**, *20*, 538
68. Wilson AD, Baietto M; *Sensors*, **2011**, *11*, 1105
69. Freeman R, Goodacre R, Sisson PR, Magee JG, Ward AC, *et al.*; *J Med Microbiol*, **1994**, *40*, 170
70. Keshri G, Magan N; *J Appl Microbiol*, **2000**, *89*, 825
71. Turner AP, Magan N; *Nat Rev Microbiol*, **2004**, *2*, 161
72. Lee TMH; *Sensors*, **2008**, *8*, 5535
73. Shen F, Tan M, Wang Z, Yao M, Xu Z, *et al.*; *Environ Sci Technol*, **2011**, *45*, 7473
74. Jeykumari DRS, Narayanan SS; *J Neurosci Nanotechnol*, **2009**, *9*, 5411
75. Zhou LX, He XX, He DG, Wang KM, Qin DL; *Clin Dev Immunol*, **2011**, *193963*
76. Pumera M; *Methods Mol Bio*, **2010**, *625*, 205
77. Zheng G, Gao XPA, Lieber CM; *Nano Lett*, **2010**, *10*, 3179
78. Lund J, Mehta R, Parviz BA; *Nanomedicine*, **2006**, *2*, 230
79. Kim SN, Rusling JF, Papadimitrakopoulos F; *Adv Mater*, **2007**, *19*, 3214
80. Chatterjee S, Castro M, Feller JF; *J Mater Chem B*, **2013**, *36*, 4563
81. Chen K-I, Li B-R, Chen Y-T; *Nano Today*, **2011**, *6*, 131
82. Gregersen MM, Andersen MB, Soni G, Meinhart C, Bruus H; *Phys Rev*, **2009**, *E79*
83. Zheng GF, Patolsky F, Cui Y, Wang WU, Lieber CM; *Nature Biotechnol*, **2005**, *23*, 1294

84. Kazemi-Zanjani N, Kergrene E, Liu LJ, Sham TK, Lagugne-Labarthet F; *Sensors*, **2013**, *13*, 12744
85. Denton KA, Kramer MF, Lim DV; *J Rapid Method Automat Microbiol*, **2009**, *17*, 17
86. Hewitt BM, Singhal N, Elliot RG, Chen AYH, Kuo JYC, *et al.*; *Environ Sci Technol*, **2012**, *46*, 5414
87. Yan RJ, Lynn NS, Kingry LC, Yi ZJ, Slayden RA, *et al.*; *Appl Phys Lett*, 2011, **98**, 13702
88. Leung A, Shankar PM, Mutharasan R; *Sensor Actuat B-Chem*, **2007**, *125*, 688
89. Gouveia CAJ, Baptista JM, Jorge PAS; *Refractometric Optical Fiber Platforms for Label Free Sensing*, **2013**
90. Zhu H, White IM, Suter JD, Dale PS, Fan X; *Opt Exp*, **2007**, *15*, 9139
91. White IM, Gohring J, Fan X; *Opt Exp*, **2007**, *15*, 17433
92. Baaske M, Vollmer F; *ChemPhysChem*, **2012**, *13*, 427
93. Cooper MA; *Nat Rev Drug Discov*, **2002**, *1*, 515
94. Rachkov A, Patskovsky S, Soldatkin A, Meunier M; *Talanta*, **2011**, *85*, 2094
95. Hsieh SC, Chang CC, Lu CC, Wei CF, Lin CS, *et al.*; *Nanoscale Res Lett*, **2012**, *7*, 180
96. Prabhakar N, Arora K, Arya SK, Solanki PR, Iwamoto M, *et al.*; *Analyst*, **2008**, *133*, 1587
97. Duman M, Piskin E; *Biosens Bioelectron*, **2010**, *26*, 908
98. Huang JG, Hung CCK, Lai HC, Lee CK, Lin SM, *et al.*; *IEEE Engg Med Biol Soc*, **2004**, *26*, 2553
99. Duman M, Ilayhan, Demirel G, Khan, Pi, *et al.*; *Sensor Lett*, **2009**, *7*, 535
100. Trilling AK, de Ronde H, Noteboom L, van Houwelingen A, Roelse M, *et al.*; *PLoS One*, **2011**, *6*, e26754
101. Srivastava SK, Ruigrok VJB, Thompson NJ, Trilling AK, Heck AJR, *et al.*; *PloS One*, **2013**, *8*, e64040
102. Hong SC, Chen H, Lee J, Park H-K, Kim YS, *et al.*; *Sensor Actuate B-Chem*, **2011**, *156*, 271
103. Homola J, Yee SS, Gauglitz G; *Sensors Actuat B-Chem*, **1999**, *54*, 3
104. McNerney R, Wondafrash BA, Amena K, Tesfaye A, McCash EM, *et al.*; *BMC Infect Dis*, **2010**, *10*, 161
105. Begg TB, Hill ID, Nickolls LC; *Br Med J*, **1964**, *1*, 9
106. Mustafa AS, Shaban FA, Abal AT, Al-Attiyah R, Wiker HG, *et al.*; *Infect Immun*, **2000**, *68*, 3933
107. Mi X, He F, Xiang M, Lian Y, Yi S; *Anal Chem*, **2011**, *84*, 939
108. He FJ, Zhang LD; *Anal Sci*, **2002**, *18*, 397
109. He FJ, Zhang LD, Zhao JW, Hu BL, Lei JT; *Sensors Actuat B-Chem*, **2002**, *85*, 284
110. Kumar A; *J Miner Metal Mater Soc*, **2000**, 52
111. Ren JL, He FJ, Yi SL, Cui XY; *Biosens Bioelectron*, **2008**, *24*, 403
112. Gronewold TM; *Anal Chim Acta*, 2007, *603*, 119
113. Ferreira GN, da-Silva AC, Tome B; *Trends Biotechnol*, 2009, *27*, 689
114. He FJ, Zhao JW, Zhang LD, Su XN; *Talanta*, 2003, *59*, 935
115. Ruan C, Zeng K, Varghese OK, Grimes CA; *Anal Chem*, **2003**, *75*, 6494
116. Zhang R, Tejedor-Tejedor MI, Grimes CA, Anderson MA; *Anal Chem*, **2007**, *79*, 7078
117. Pang P, Cai Q, Yao S, Grimes CA; *Talanta*, **2008**, *76*, 360
118. Cai QY, Cammers-Goodwin A, Grimes CA; *J Environ Engg*, **2000**, *2*, 556
119. Shen W, Li S, Park M-K, Zhang Z, Cheng Z, *et al.*; *J Electrochem Soc*, **2012**, *159*, B818
120. Issadore D, Min C, Liong M, Chung J, Weissleder R, *et al.*; *Lab Chip*, **2011**, *11*, 1182
121. Haun JB, Castro CM, Wang R, Peterson VM, Marinelli BS, *et al.*; *Sci Trans Med*, **2011**, *3*, 71
122. Chun AL; *Nat Nano*, **2009**, *4*, 698
123. Lee H, Sun E, Ham D, Weissleder R; *Nat Med*, **2008**, *14*, 869
124. Chung HJ, Castro CM, Im H, Lee H, Weissleder R; *Nat Nano*, **2013**, *8*, 369
125. Liong M, Hoang AN, Chung J, Gural N, Ford CB, *et al.*; *Nat Comm*, **2013**, *4*, 1752
126. Lee H, Yoon T-J, Weissleder R; *Angew Chem Int Ed*, **2009**, *48*, 5657

# *Chapter 3*

*16 kDa heat shock protein from heat-inactivated Mycobacterium tuberculosis is a homodimer – suitability for diagnostic applications with specific llama VHH monoclonals*

This chapter was published as:

Srivastava SK, Ruigrok VJB, Thompson NJ *et al.*; *PLoS One*, **2013**, *8*, e64040

## *Abstract*

The 16 kDa heat shock protein (HSP) is an immuno-dominant antigen, used in diagnosis of infectious *Mycobacterium tuberculosis* (*M.tb.*) causing tuberculosis (TB). Its use in serum-based diagnostics is limited, but for the direct identification of *M.tb.* bacteria in sputum or cultures it may represent a useful tool. Recently, a broad set of twelve 16 kDa specific heavy chain llama antibodies (VHH) has been isolated, and their utility for diagnostic applications was explored. To identify the epitopes recognized by the nine (randomly selected from a set of twelve 16 kDa specific VHH antibodies), distinct VHH antibodies 14 overlapping linear epitopes (each 20 amino acid long) were characterized using direct and sandwich ELISA techniques. Eight out of 9 VHH antibodies recognized 7 out of 14 epitopes. The two highest affinity binders B-F10 and A-23 were found to bind distinct epitopes. Sandwich ELISA and SPR experiments showed that only B-F10 was suitable as secondary antibody with both B-F10 and A-23 as anchoring antibodies. To explain this behaviour, the epitopes were matched to the putative 3D structure model. Electrospray ionization time-of-flight mass spectrometry and size exclusion chromatography were used to determine the higher order conformation. A homodimer model best explained the differential immunological reactivity of A-23 and B-F10 against heat-treated *M.tb.* lysates. The concentrations of secreted antigens of *M.tb.* in sputum are too low for immunological detection and existing kits are only used for identifying *M.tb.* in cultures. Here we describe how specific combinations of VHH domains could be used to detect the intracellular HSP antigen. Linked to methods of pre-concentrating *M.tb.* cells prior to lysis, HSP detection may enable the development of protein-based diagnostics of sputum samples and earlier diagnosis of diseases.

### 3.1 Introduction

Tuberculosis (TB), caused by *Mycobacterium tuberculosis* (*M.tb.*), is one of the most prevalent and serious infectious diseases worldwide [1]. Each year ~9.4 million new cases are reported with an estimated global mortality in 2010 of 1.4 million people [2]. With problems like multiple drug resistance (MDR), treatment of diagnosed TB cases is becoming more and more difficult and challenging [3]. TB cases are often intensified due to malnutrition and other allied infections that decrease body immunity, like HIV, especially in the developing parts of the world [4, 5]. Early detection of TB guarantees fast treatment and can offer much better prognosis. Therefore, development of techniques for early and accurate detection is called for [6, 7].

There are many different types of diagnostic assays available for detection of tuberculosis. Bacterial cultures are sensitive, but too time consuming, taking 2-3 weeks for detection under optimal conditions [8]. Microscopic identification of acid-fast bacilli in sputum smears is a fast technique but less sensitive than culture techniques, laboratory intensive and dependent on high concentrations of bacteria [8]. Nucleic acid amplification methods are fast, highly specific and sensitive, but they are technically complex, expensive and require skilled personnel with high quality standards for accurate performance [9]. Other immunological methods tend to detect secreted antigen protein from *M.tb.* Sensitivity and specificity of these methods is also too low to detect the antigens in sputum. As a result they are mainly used on cultures that take a long time to grow, i.e. around 2-6 weeks [9-12].

TB is most prevalent in poor, remote areas of the world, where reliable DNA-based diagnostic procedures that need costly, advanced laboratory infrastructure and personnel are not available. This contrasts with antibody-dependent assays that are more easily implemented. The development of better target antigens are, therefore, a high priority, especially if they are less subject to generating false positives [13, 14] from cross reactivity with similar antigens of non-pathogenic *Mycobacterium sp.*

Monoclonal VHH antibodies have recently gained considerable attention due to their unique physico-chemical stability [15] as well as low molecular weight of ~15 kDa. Considering the limitations of existing diagnostics of TB, VHH antibodies can be utilized as tools for improvement of the existing immunological tests in detection of TB. They are 3-4 times smaller (4 nm) in volume than conventional antibodies due to lack of light chains and removal of conserved domains. Furthermore, they can be produced at low cost in yeast or bacteria, and are easy to handle with long shelf life [16, 17].

Previously, we described the selection and preliminary characterization of a panel of 12 VHH antibodies against *M.tb.* [18]. Using ELISA and SPR techniques it was demonstrated that these VHH antibodies were specific for TB-causing mycobacteria and exclusively recognized the 16 kDa heat shock protein (HSP) [18], which is known to be a major contributor to the pathogenicity of the *M.tb.* bacterium [19]. During latent phase, *M.tb.* persists inside macrophages due to the presence of the 16 kDa HSP protein, and it is also the

most dominant protein in the extract of *M.tb.* [20]. The best VHH antibody showed a high affinity for HSP, with a dissociation constant ( $K_d$ ) of  $4 \times 10^{-10}$  M [18]. HSP is a cell-internal protein, which is peripherally associated with the membrane [21]. For diagnostics purposes, it can be isolated in higher concentrations than secreted proteins by pre-concentrating the bacteria [18].

The main objective of this study was to characterize the binding of *M.tb.* HSP epitopes, protein and lysates to different VHH antibodies and to evaluate optimal capture-detection probe combinations. The information can be used to develop low cost, robust protein-based diagnostic platforms for TB based on these antibodies.

## 3.2 Materials and methods

### 3.2.1 HSP peptides and proteins and VHH proteins

Fourteen overlapping linear peptide epitopes (20 amino acid in length and with a 10 amino acid overlap; numbered 1-14, Fig. 1) covering the entire HSP sequence (Fig. S1) [22, 23], each covalently linked at the C-terminal with either an amide (-NH-R) group or biotin residue for direct and sandwich ELISA studies, were synthesized (Peptide 2.0 inc.). The synthesized peptides were purified by HPLC and their sequences were verified by mass spectrometry by the supplying company (Peptide 2.0 inc.). Two forms of VHH antibodies were used in this study, i.e. biotinylated VHH (VHH-AVI) and VHH with VSV tag (VHH-VSV). The production and purification of these different VHH antibodies were done as described before [18, 24].

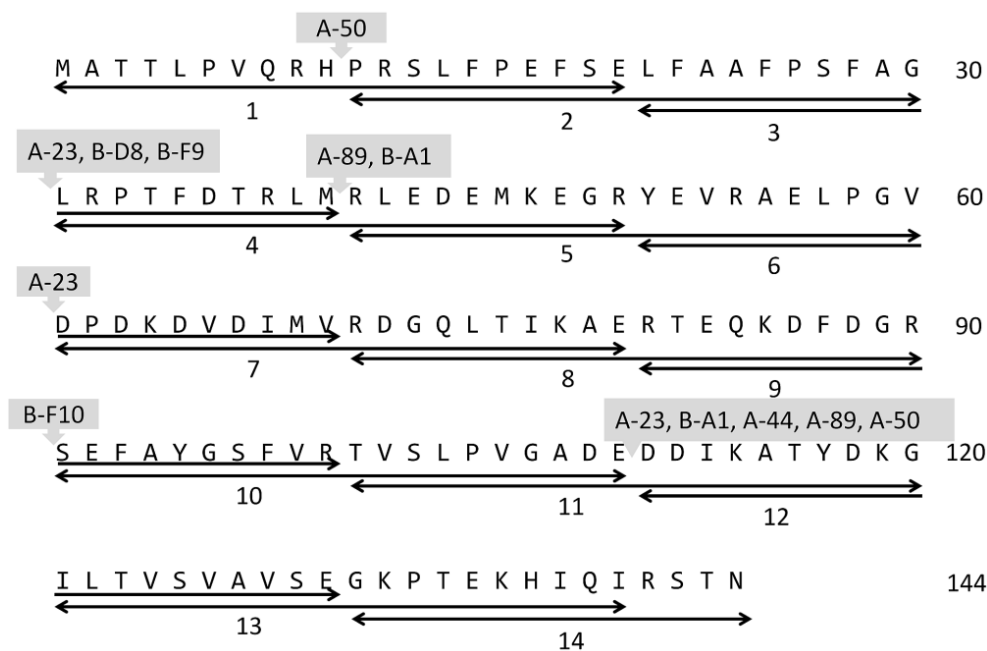


**Figure 1.** Summary of affinity interactions of 14 overlapping peptides derived from the HSP protein with 9 different anti-HSP VHH antibodies. VHH numbering is according to Trilling et al. 2011[18]. VHHs are indicated above the central portions of the interacting peptides

The four forms of HSP used in the present work were:

1. Recombinant HSP with AVI and HIS tag (rHSP-tag), produced and purified recombinant from *E. coli* strain BL21 as described before [18].
2. Recombinant native HSP (rHSP) lysate, produced by PCR-amplifying the HSP from *M.tb.* lysate using the primer HSP16.3-PstI-F (5'-AAAAAACTGCAGAAAATGGCCACCACC CTCCC-3') and HSP16.3-NotI-no.tag-RV(5'-TATATGCGCCGCTTAGTTGGTGGACC GGTCTGA-3') (PstI and NotI restriction sites are underlined). The digested fragment was inserted in a PstI-NotI cut PRI expression vector. This vector is based on the earlier described PRI-VSV expression vector [18]. The construct was transformed into *E. coli* XL-1 blue for multiplication. The cloned HSP sequence is identical to GenBank accession number S79751. Isolated plasmid DNA was transformed into *E. coli* strain BL21-AI for expression. Expression was performed as described before [18] and French press lysis was performed in native extraction buffer (150 mM NaCl, 5mM imidazole, 20µl DNase, 50mM KH<sub>2</sub>PO<sub>4</sub> at pH 8) supplemented with 1mM PMSF and 2 µg/ml aprotinin and 1 mg/ml lysozyme to final concentration.
3. Heated recombinant native HSP (heated-rHSP) lysate, production and expression of heated-rHSP was as described for rHSP. The only difference between the two samples was that, in case of heated-rHSP the cell pellet was heated for 30 min. at 80°C before French press.
4. HSP from *Mycobacterium tuberculosis* (*M.tb.*-HSP) lysate, produced and lysed as described before including a heat treatment as in 3 [18].

### 3.2.2 ELISA-based epitope mapping of HSP

#### 3.2.2.1 Direct ELISA

- I. Linear epitopes as capture species: Flat-bottom medium binding ELISA plates (Greiner Bio One) were coated via physical adsorption with 100 µl of each peptide at a concentration of 10<sup>-4</sup> M in phosphate buffer saline (PBS) by incubating overnight at 4°C. Once these antigen-peptide coated wells were prepared, a standard ELISA method was followed as described by Trilling *et al.* [18] to determine the interacting epitopes of the 9 different VHH antibodies A-23, A-44, A-50, A-89, B-A1, B-B12, B-D8, B-F9 and B-F10.
- II. VHH antibody as capture species: ELISA plate wells (GreinerBioOne) were coated via physical adsorption with VHH antibodies (either A-23 or B-F10) as a capture element by incubating 100 µl of each antibody in PBS at a concentration of 2 µg/ml and incubated overnight at 4°C. These antibody-coated wells were washed with PBS and blocked using a blocking solution of 4% non-fat powdered (w/v) milk in PBS (PBSM) for an h. Later a mixture of 100 µl of each biotinylated peptide in PBS at a

concentration of  $10^{-4}$  M was added and allowed to interact for an h. After incubating with antigen peptides, the wells were washed again with a solution of 200  $\mu$ l of 0.05% TWEEN-20 in PBS (PBST). The wells were then subjected to streptavidin POD conjugate (Sigma Aldrich, USA) for an h at a dilution of 1:4000 in PBSM. Successive washing steps and measurements were done as described above. This procedure was applied to 6 different peptides (i.e. #1, #3, #5, #6, #9 and #11), which were selected on the basis of their response to VHH antibodies A-23, B-F10, A-44 and A-50.

### 3.2.2.2 Sandwich ELISA

Wells of ELISA plates were coated with VHH antibody A-23-AVI as capture element by incubating 100  $\mu$ l of antibody in PBS at a concentration of 2  $\mu$ g/ml and incubated overnight at 4°C, followed by an h of blocking with PBSM at room temperature. Wells were then washed thrice with PBS solution followed by an hour of incubation with either rHSP-tag or *M.tb.*-HSP lysates, as described above. Plates were then blocked again for 1 h with PBSM and washed three times with PBST. Then, the wells were incubated for an h with the secondary sandwich VHH antibody A-23 or B-F10 with VSV tag, followed by three times washing with PBST and incubation for an h with the detection antibody i.e. anti-VSV-HRP (Sigma Aldrich, Missouri, USA) before assay with 1-Step™ Ultra TMB substrate for ELISA (Pierce, IL).

### 3.2.3 Size exclusion chromatography of HSP

For calibration of the column (Superdex 200 10/300 GL with length of 30 cm and diameter of 10 mm, GE life sciences), a mixture of known standards, i.e. Blue Dextran 2000, Ferritin, Catalase, Aldolase, Albumin, Ovalbumin, Chymotrypsinogen A and Ribonuclease A were first injected to obtain a calibration table (Supporting Information, Table S1, Fig. S2). Once the column was calibrated, 250  $\mu$ l of each HSP sample i.e. either rHSP-tag, rHSP, heated-rHSP with a concentration of 750  $\mu$ g/ml or *M.tb.*-HSP lysates with concentration 450  $\mu$ g/ml were loaded on to the column (at a flow of 0.75 ml/min, using PBS as running buffer). Fractions of 1 ml each were collected for further analysis. Diluted samples obtained from individual fractions were concentrated using the Amicon® Ultra centrifugal spin columns (Millipore Ireland Ltd. Ireland) with a cut off 10 kDa following the protocol supplied by the supplier. The concentrated fractions thus obtained were analyzed on dot blot. For dot blot, 100  $\mu$ l of concentrated fractions were blotted in a circular spot with the help of SRC 96D S&S Minifold 1 dot blotter (Schleicher & Schuell, Germany) on nitrocellulose membrane (Trans-Blot, Bio-Rad, Hercules, CA) at room temperature. The membrane was then blocked with PBSM to avoid unspecific binding, washed with PBS and incubated with VHH antibody B-F10-VSV. A blocking step followed by washing and re-incubation of the membrane with anti-VSV-HRP antibody. Detection was done using 3,3',5,5'-Tetramethylbenzidine (TMB) liquid substrate system for membranes (Sigma-Aldrich, The Netherlands), by incubating the membrane for 10 min in the dark with TMB and then washing the substrate off with milliQ water and scanning the bands using a desktop scanner (Biorad GS-710).

### 3.2.4 Electrospray ionization time-of-flight mass spectrometry

Electrospray ionization time-of-flight mass spectrometry (ESI-TOF-MS) is a native mass spectrometry method, which is used to identify oligomerization of non-covalently associated protein oligomers [25, 26]. The method utilizes the soft ionization technique of nanoelectrospray ionization (nESI) to produce gas-phase ions, avoiding structural destruction of thermally labile large supramolecules, such as proteins and non-covalent protein complexes [27, 28]. The rHSP-tag sample was analyzed using nESI-TOF-MS to deduce the oligomerization after urea-based isolation. A small fraction of 20  $\mu$ l of the sample was also retained for samples qualitative analysis on denaturing PAGE gel. The sample was first buffer-exchanged from PBS pH 7.4 to 150 mM ammonium acetate pH 9.0 using 5 kDa molecular weight cut off filter (Vivaspin 500, Sartorius Stedim Biotech GmbH, Goettingen, Germany). The protein was sprayed at a concentration of 20  $\mu$ M on an ESI-TOF mass spectrometer (LCT, Waters, Manchester, UK) using gold-coated borosilicate capillaries made in-house (using a Sutter P-97 puller [Sutter Instruments Co., Novato, CA] and an Edwards Scancoat Six sputter-coater [Edwards Laboratories, Milpitas, CA]). Source backing pressure was increased to 6 mbar. Capillary voltage and cone voltage were set to 1300 and 200 V respectively. Mass calibration was performed using 25 mg/mL Cesium iodide. Data were analyzed using MassLynx V4.1 for experimental mass determination.

### 3.2.5 Epitope mapping using surface plasmon resonance

Surface plasmon resonance (SPR)-based sandwich experiments were performed using streptavidin-coated chips (GE Healthcare) in a Biacore 3000 system at 25°C, using HBS-EP buffer (pH 7.4, consisting of 10 mM 4-(2-hydroxyethyl) piperazine-1-ethane sulfonic acid, 150 mM sodium chloride, 3mM ethylenediaminetetra acetic acid, 0.005% v/v surfactant polysorbate 20) as running buffer at a constant flow of 10  $\mu$ l/min. The experimental setup was same as described before by Trilling *et al.* [18]. The chips had four independent channels out of which the first channel served as reference surface containing of VHH-M200 [18] that does not bind to the HSP (negative control), whereas the second and third channels contained VHH antibodies A-23 and B-F10, respectively. The fourth channel however was left untreated as a blank control. A total immobilization of  $3000 \pm 100$  RU was achieved with every antibody individually, used for anchoring purposes. Once the anchoring VHH antibodies were captured, all four channels were connected and subjected collectively to 50 $\mu$ l of HSP at a concentration of 4  $\mu$ g/ml. Binding yield of 2500RU in channel 2 and 3. The chip was then subjected to 40  $\mu$ l of secondary/sandwiching antibody VHH A-23 and the binding signals were recorded in terms on RU. The surface was regenerated using 10  $\mu$ l of 10 mM hydrogen chloride solution (HCl). The process was then repeated by injecting HSP, followed by secondary/sandwiching VHH antibody B-F10. To verify the reproducibility, the whole experiment was repeated thrice.

### 3.3 Results

#### 3.3.1 ELISA- and SPR-based epitope mapping of HSP

To study the region of the HSP protein responsible for interacting with VHH antibodies ELISA- and SPR-based epitope mapping techniques with HSP peptide overlapping epitopes and HSP intact protein were employed.

##### 3.3.1.1 Epitope mapping using linear peptides in direct ELISA

The interactions of fourteen overlapping linear 20-mer peptides (Fig. 1), based on the 144 amino acid long HSP, with 9 VHH antibodies were first studied using linear peptides as capture species (Fig. 2A, 2C). For each antibody binding peptides were found. Antibody A-23 bound to peptides #3, #6 and #11, antibody A-50 bound to #1 and #11, whereas B-F10 bound only to #9 (Fig. 2B). The summary of interactions of all epitopes with all 9 VHH antibodies is given in Table 1. Overall it was found that as many as 7 out of 14 peptides were recognized by 8 out of 9 different VHH antibodies as summarized in Fig. 1 and Table 1.

*Table 1. Summary of interactions of 14 peptides derived from the HSP protein with 9 different anti-HSP VHH antibodies [18]*

VHH Antibody	Response to different epitopes (#1 to #14) of 16kDa HSP from tuberculosis													
	#1	#2	#3	#4	#5	#6	#7	#8	#9	#10	#11	#12	#13	#14
A-23			X			X					X			
A-44					X						X			
A-50	X										X			
A-89				X							X			
B-A1				X							X			
B-B12														
B-D8			X											
B-F9			X											
B-F10									X					

The binding of antibodies can be grouped in three categories. Group 1 consists of antibodies binding to three different epitopes (A-23), group 2 those binding to two different epitopes (A-44, A-50, A-89 and B-A1), and group 3 those binding to a single epitope (B-D8, D-F9 and B-F10). Interestingly, all antibodies positively selected on purified antigen by a direct phage display selection procedure (represented here with prefix A) recognized peptide #11, whereas most of the ones negatively selected via a depletion strategy (prefix B) recognized other epitopes, which may therefore be more selective. To verify that the

observed interactions were not artefacts of the peptide immobilization method we also carried out a reverse analysis using two VHH antibodies (A-23, B-F10) with the highest binding affinity constants as capture species [18]. For this purpose the peptides #1, #3, #5, #6, #9, and #11 were biotin-tagged and assayed as in Fig. 2C. The results in Fig. 2D confirmed that A-23 binds peptides #3 and #11, while binding to epitope #6 was at background level, and not conclusive. B-F10 was confirmed to only bind to peptide #9.

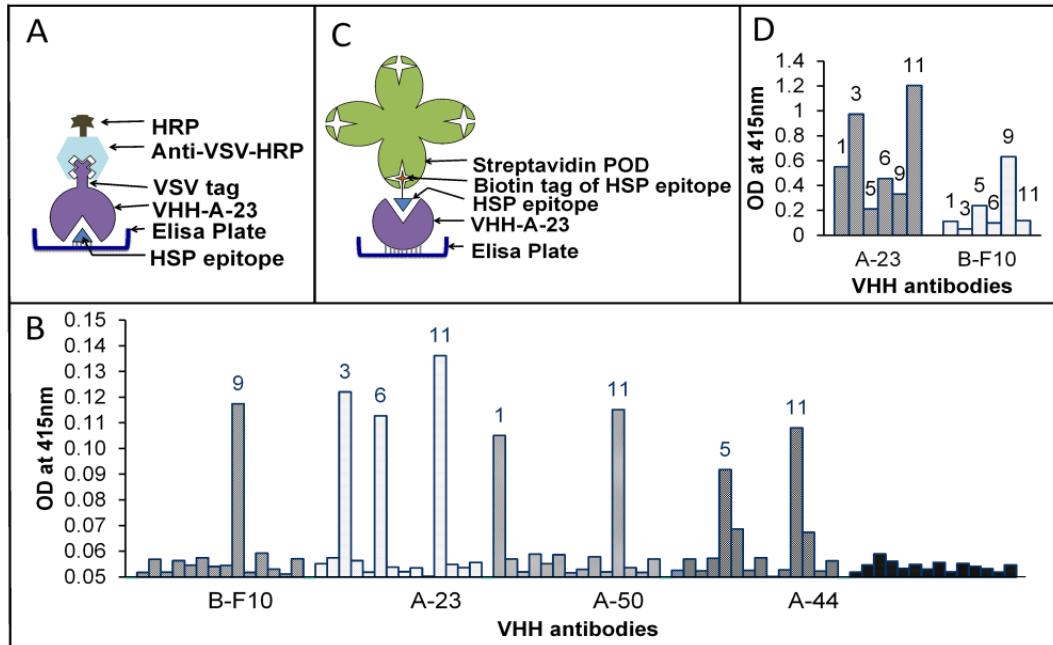


**Figure 2.** Peptides (14 overlapping 20-mers) representing potential epitopes of the HSP protein mapped against different VHH antibodies in direct ELISA. Panel A - Scheme applied in B; Panel B - Results of direct ELISA with coated peptides; Panel C - Scheme applied in D; Panel D - Direct ELISA with VHH antibodies coated to the well

### 3.3.1.2 Epitope mapping using HSP in sandwich ELISAs and SPR measurements

If HSP would behave as a protein monomer then a sandwich ELISA using the same VHH for both capture and detection would not result in a signal, whereas the use of two VHH recognizing distinct epitopes that do not interfere sterically would yield a signal. To test this - sandwich ELISA with rHSP-tag protein captured by A-23-AVI was carried out using the two most potent and distinct VHH antibodies B-F10-VSV and A-23-VSV for detection. In Fig. 3, it is shown that rHSP-tag and *M.tb.*-HSP protein when captured by A-23 could be detected by both secondary antibodies i.e. A-23 as well as B-F10. The A-23 detection suggested that both recombinant HSP and *M.tb.*-HSP do not behave as monomers. For *M.tb.*-HSP, the signal was lower than for 2 µg/ml recombinant HSP protein, presumably due to the lower concentration of the HSP protein in the *M.tb.*-HSP. At lower concentrations, the VHH antibody B-F10 yielded 3-4 times higher signals compared to A-23 for both the recombinant HSP protein as well as the HSP in *M.tb.*-HSP. The basis of this difference could be related to the difference in binding constants of the VHH antibodies (i.e. B-F10 ( $K_d = 0.4 \times 10^{-9}$  M) is more efficient than A-23 ( $K_d = 2.4 \times 10^{-9}$  M)), but also to the reported native higher order (dodecameric, [29]) protein structure in relation to the specific epitopes recognized.

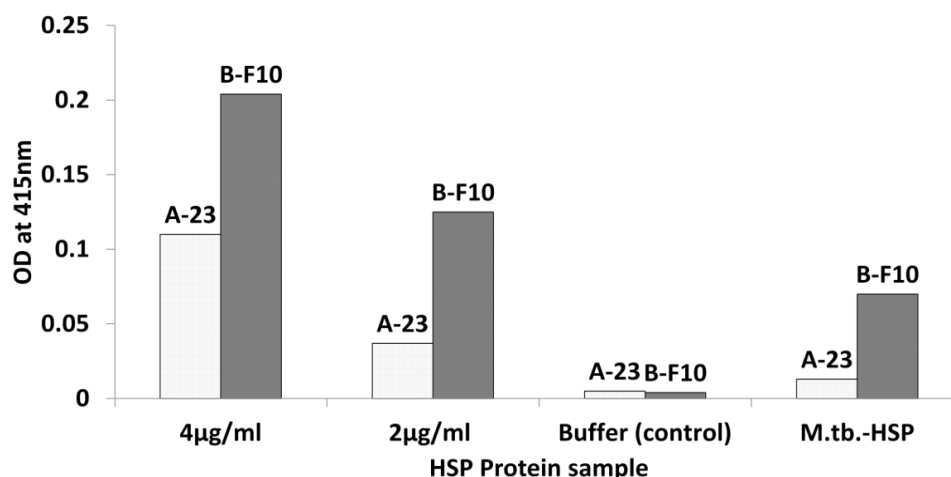


**Figure 3.** Comparison of purified recombinant HSP protein with *M.tb.*-HSP in sandwich ELISA assays with antibody A-23 AVI as capture antibody

To disentangle kinetic, conformational and steric effects, further analysis by “sandwich-SPR” was carried out. A-23 or B-F10 was used to capture recombinant HSP followed by either A-23 or B-F10 as detecting antibody (Fig. 4 and Table 2). With A-23 as capture antibody, B-F10 showed much higher binding to HSP (703RU) compared to A-23 (172RU). This confirmed the peptide study that A-23 and B-F10 bind to distinct epitopes and would support a model of a protein monomer. However, with B-F10 as capture antibody, again B-F10 showed much higher binding (609RU) compared to A-23 (168RU). This contradicted a monomer model for recombinant HSP and called for a more complex multimeric model of HSP.

**Table 2.** SPR assay results showing the observed response units (RU) for rHSP-tag (HSP) and the detection antibodies A-23 and B-F10. These responses are interpreted in terms of secondary binding efficiencies relative to different models of HSP oligomerization

#	Capture/ detection Antibody combinations	HSP (RU)	Detection Antibody (RU)	Observed efficiency			
				Monomer model	Dimer model	Trimer model	Dodecamer model
1	A-23 / HSP / A-23	2664	172	not possible	15%	11%	8%
2	B-F10 / HSP / A-23	2290	168	9%	17%	13%	9%
3	A-23 / HSP / B-F10	2028	703	40%	82%	61%	45%
4	B-F10 / HSP / B-F10	2020	609	not possible	71%	53%	39%

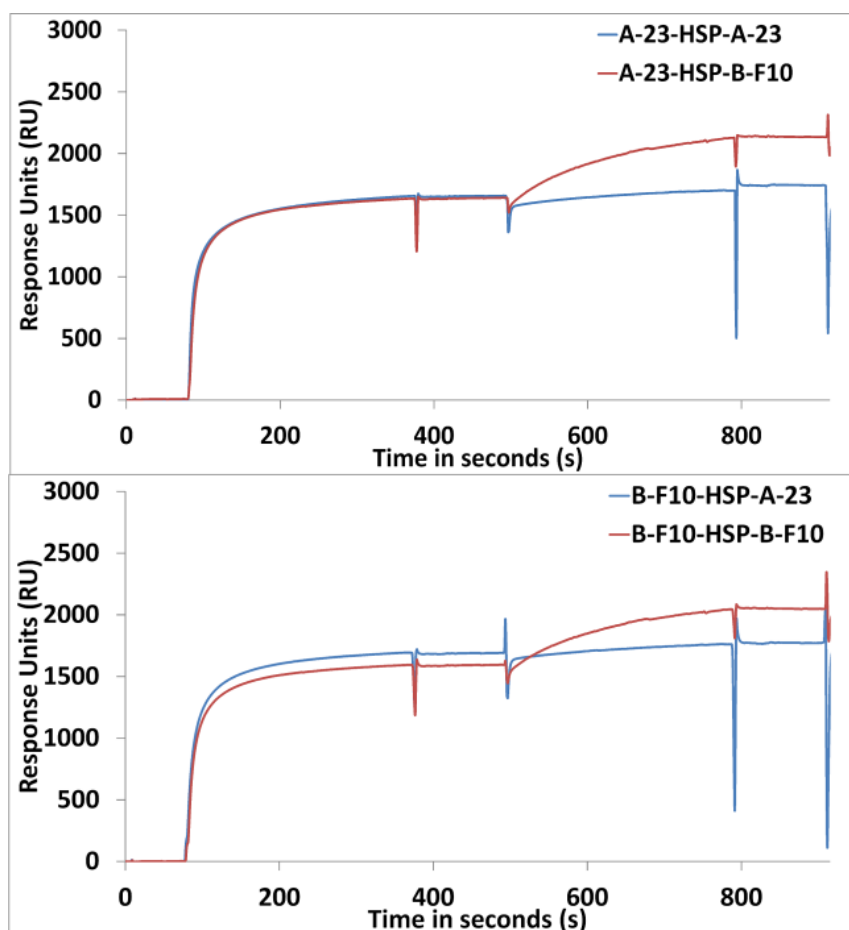


**Figure 4.** Plots of “sandwich SPR” showing the binding kinetics of B-F10 or A-23 binding to HSP as a secondary antibody in a sandwich assay in which HSP was first captured by A-23 or B-F10. Four different sandwich variations are shown: A-23-HSP-A-23 or -B-F10 (top panel) and B-F10-HSP-A-23 or -B-F10 (lower panel)

### 3.3.2 Size exclusion chromatography (SEC) to determine the oligomeric nature of HSP

In the literature, it is reported that the HSP protein exists either as monomer [30, 31], dimer [30, 31], trimer of trimers [31, 32] or dodecamer [29] depending upon the method of extraction from *Mycobacterium* or *E. coli*. To obtain an indication of the quaternary structure of recombinant and native HSP protein after standard isolation procedures, SEC was performed on four samples, i.e. (1) purified recombinant HSP with an AVI and HIS tag on the C-terminus (rHSP-tag) refolded from urea-dissolved inclusion bodies in *E. coli*, (2) French press generated lysate of native recombinant HSP protein without tags expressed in *E. coli* (rHSP), (3) heat inactivated French press generated lysate of native recombinant HSP protein without tags expressed in *E. coli* (Heated-rHSP), and (4) heat-inactivated *M.tb.* lysates generated by mechanical shear with zirconium beads also containing HSP (*M.tb.*-HSP)[18]. In Fig. 5A the elution profiles obtained from each sample are super-imposed. rHSP-tag protein has a monomer size of 20.9 kDa due to the two (AVI and HIS) tags. On SEC, purified protein separated into two peaks with sizes corresponding to  $14 \pm 5$  and  $61 \pm 20$  kDa. Unpurified rHSP with HSP as major component also showed two peaks at  $301 \pm 97$  kDa and  $55 \pm 18$  kDa. After heating heated-rHSP, only the peak at  $55 \pm 18$  kDa remained.

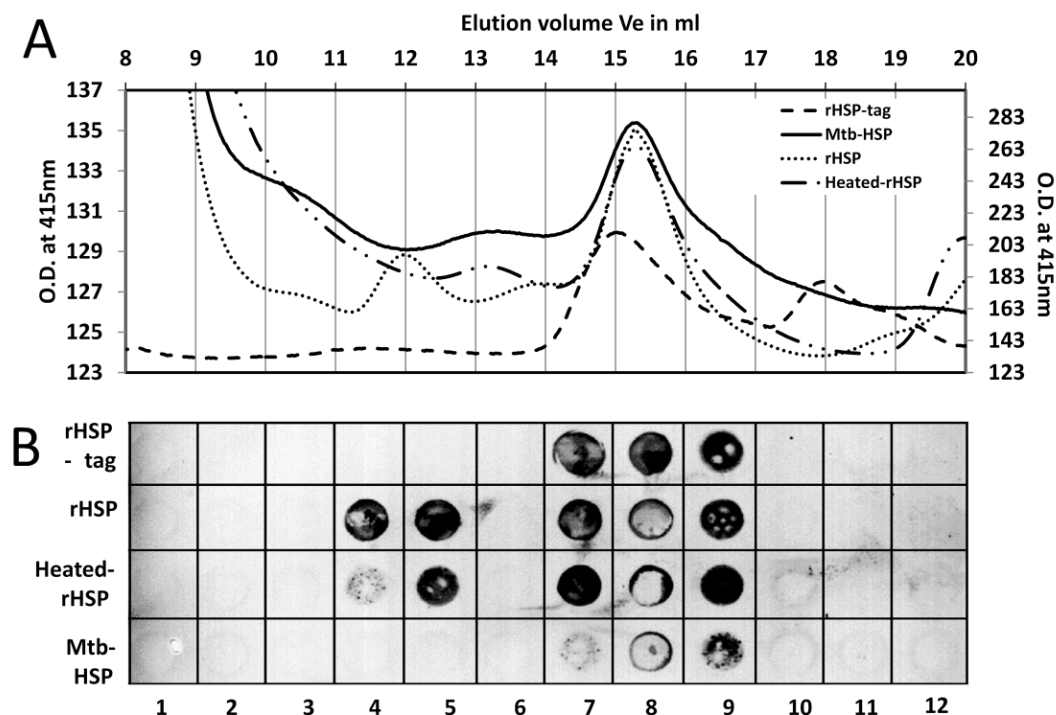


**Figure 5.** SEC for apparent molecular weight determination of HSP. Where figure A shows SEC plot of different HSP samples i.e. purified recombinant HSP with tag (rHSP-tag), unpurified recombinant native HSP (rHSP), heated unpurified recombinant native HSP (heated-rHSP) and *M.tb.* lysates (*M.tb.*-HSP) while figure B shows the dot blot of interaction of 16 kDa protein present in these SEC fractions with antibody B-F10, where lane 4 & 5 shows fractions of different HSP protein eluting at ~301 kDa, lane 7-9 shows fractions of different HSP protein eluting at ~55-61 kDa

Unpurified heated *M.tb.*-HSP also showed only one peak at  $55 \pm 18$  kDa. The presence of HSP protein in samples from these respective fractions was determined using dot blot analysis (Fig. 5B). Major peaks (fractions 7-9) eluting at ~55-61 kDa (33% error margin) all contained HSP protein reactive to A-23 and B-F10, but peak (fraction 10-11) eluting at  $14 \pm 5$  kDa did not. Native rHSP protein peak (fraction 4-5) eluting at ~301 kDa also contained the HSP protein. In case of heated-rHSP the fraction 4-5 eluting at ~301 kDa contained much less HSP compared to non-heated rHSP. This shows that French press generated *E. coli* lysate of rHSP which avoids heating, mostly leaves rHSP in higher eluting (301 kDa) conformation whereas in the case of heated-rHSP it is mostly found to be eluting at ~55-61 kDa. This is also evidence that indeed *M.tb.*-HSP, rHSP, heated-rHSP and rHSP-tag behave like multimers of different sizes and do not occur as monomers.

### 3.3.3 ESI-TOF-MS to determine oligomeric nature of HSP

ESI-TOF-MS is a highly accurate method to determine the quaternary structure of complexes of proteins compared to SEC [33]. A nano electrospray ionization time-of-flight (nESI-TOF) analyzer was used for this mass spectrometric analysis of rHSP-tag under native conditions. The use of a volatile buffer (ammonium acetate) permitted the retention of non-covalent interactions in the gas phase, such that accurate masses of protein complexes could be obtained. The sample of rHSP-tag that was analyzed is shown on an SDS PAGE gel (inset Fig. 6).

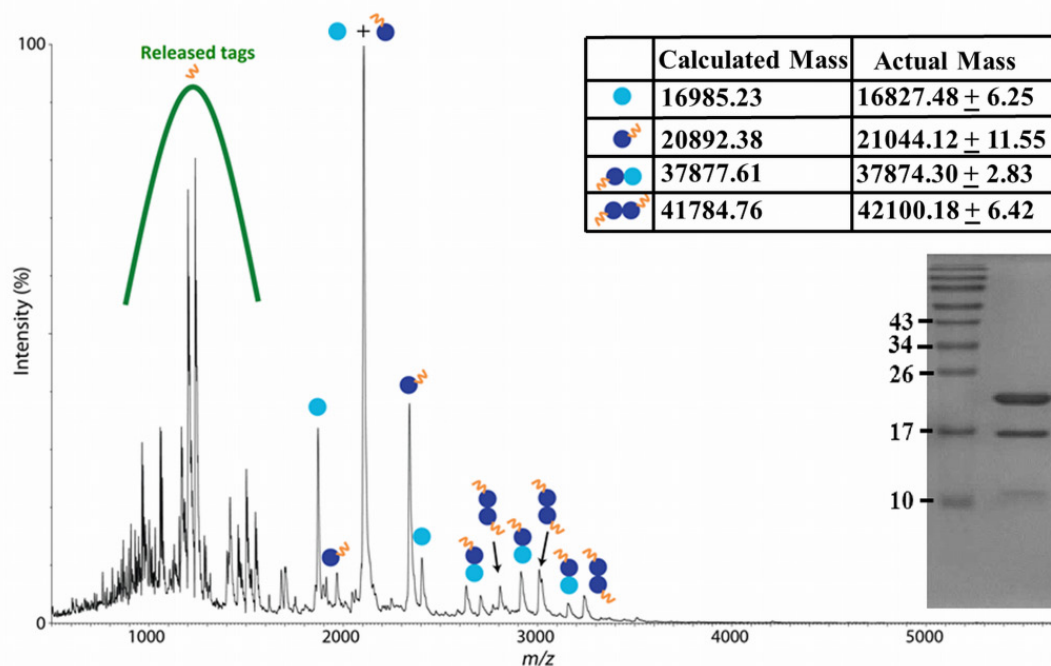


**Figure 6.** Native ESI-TOF-MS spectrum of HSP confirming absence of oligomers greater than the dimer after urea-based isolation. Sample complexity at low  $m/z$  is due to proteolytic loss of tags prior to purification. The various HSP species are indicated in the spectrum: monomer without tag (light blue circle), monomer with tag (dark blue circle), dimer formed from monomers with tags (double dark blue circles), and dimer formed from mixed monomers (double circles, light and dark blue). Other signals in the spectrum stem from contaminants, including the released tags. Deviations of calculated and measured mass values are by exopeptidases pruning the proteins. Denaturing SDS-PAGE coomassie stained gel (inset) shows two prominent bands at 21 and 17 kDa size corresponding to monomers with and without tags

A dominant band of 21 kDa (rHSP-tag) and a less intense band of 17 kDa (rHSP without tag) were observed plus less defined low molecular weight molecules. The nESI-TOF mass spectrum (Fig. 6) shows the presence of these two monomer masses, in addition to peaks corresponding to homo- and hetero-dimers of the two monomers. Interestingly, the homodimer of rHSP without tag was not found, presumably because it was not purified on the His-tag column. The small differences between calculated and observed molecular masses could be due to proteolytic trimming of the protein. The two monomeric species we assume to be derived from the dimers, but to be less stable under the conditions of the ammonium acetate buffer in combination with the nESI-TOF conditions. No oligomers larger than the

dimer were observed, confirming that standard HSP isolation procedures, where HSP is refolded from urea-dissolved inclusion bodies in *E. coli*, reduces the HSP from the native dodecameric form to a dimeric form.

### 3.4 Discussion

In this study, the binding of a set of different VHH antibodies to the 16 kDa HSP was probed with the help of different techniques (ELISA, SPR, and SEC) using both peptides and whole protein. The results demonstrated that after mechanical release from heat-killed bacteria HSP behaves as a dimer. Optimal combinations of antibodies were selected for the development of diagnostic sandwich assays.

TB is a contagious disease so patient samples are usually heat-inactivated at 80°C for 30 mins, before performing any diagnostic test. The heat-killing step was also used in the original procedure to generate *M.tb.* specific antibodies by injecting llamas with heat-killed lysates of *M.tb.* [18]. However, such procedures normally tend to effectively denature most proteins, so that the immunization procedure was likely selective for heat-tolerant proteins. All selected VHH were reactive only with HSP as demonstrated by Trilling *et al.* [18]. This bias for binding of the 16 kDa HSP may, therefore, be the result of the standard heating practice. The heat tolerance adds to HSP being a robust protein marker [18]. Knowledge of the exact conformation of native HSP after applying denaturing conditions by this procedure is necessary for the development of reliable immunological diagnostic procedures that are strongly dependent on protein conformation in specific sandwich assays.

Previous studies have shown immune-response to epitopes #3, #8, #10 and #12 with human T cells [34], epitope #3, #4, #6, #7, #8 and #13 for mouse Mabs, and epitopes #8, and #9 for human B cells [22]. We show using ELISA based on llama monoclonals instead of sera that 7 out of 14 epitopes were recognized by 8 out of 9 different llama VHH antibodies, and that epitopes #3, #4, #6, #11 and #13 were the epitopes recognized most. Immunodominance of epitopes #3, #4, #6 and #13 was shown previously for human sera after natural infection, but epitope #11 emerged as a new target in llama immunizations performed with heated lysates as described above by Trilling *et al.* [18]. Epitope #11 was the most frequently recognized epitope, showing interactions with five different antibodies, although frequencies of phage display selected antibodies may have no direct relationship to dominance of these antibodies in llama serum. Antibodies like B-D8, B-F9, B-F10 that bound to only one peptide, indicated that their recognition sites lie in the centre of the peptide, which in the 3D structure was either a loop or the coil region of the protein (Fig. S1). The overlapping adjacent epitopes may lack the full binding surface as it only represents half of the loop or coil. Several antibodies recognized more than one epitope. Interaction with multiple epitope domains of HSP could be due to a complex recognition site composed of several proximal peptide loops.

In the literature, for HSP, monomer [30], dimer [31], trimer [32], trimer of trimers (nonamers) [32] or dodecamer structures [29] have been described. The monomer and dimer configurations were based on reverse-phase high-performance liquid chromatography (HPLC), and on HSP protein purified by gel filtration chromatography [30, 31]. Trimer and nonamer configurations were based on cryo-electron microscopy [32], whereas the dodecamer configuration was deduced from SEC analysis [29]. These determinations were either based on native or denatured proteins, but for native protein only the SEC analysis has been reliable for size determination. Our SEC analysis initially suggested that HSP (16 kDa) occurred both as a trimer ( $16 \times 3$  i.e. 48 kDa) and a hexamer of trimers (18-mer  $16 \times 18$  i.e. 288 kDa) with observed sizes of 55 kDa and 301 kDa. However, within the SEC margin of error, HSP could also be a dimer and a hexamer of dimers (dodecamer) as reported before [29] and with expected sizes of 32 kDa and 192 kDa respectively. The slightly larger observed size (61 kDa) of the putative dimer of rHSP-tag compared to the putative dimers of the native rHSP, heated-rHSP and M.tb.-HSP proteins with a size of 55 kDa is consistent with the presence of the tags ( $2 \times 5$  kDa). To resolve the issue we analyzed the oligomeric structure by ESI-TOF-MS and concluded that the rHSP-tag sample contains dimers, but not trimers.

In our sandwich ELISA and SPR experiments the immunological reactivity of HSP in SPR did not fit a monomer model, whereas a dimer model resulted in the best fit of our data. This can be seen from Table 2 where we calculated the observed efficiency of binding of the secondary, “sandwich” antibody A-23 and B-F10 relative to the theoretical maximum efficiency in relation to different possible configurations of HSP as a monomer, dimer, trimer or dodecamer using a the following two formulas:

$$\text{Equation detection } RU = \left( \frac{M.Wt. \text{ of antibody} \times (N - 1)}{M.Wt. \text{ of HSP antigen} \times N} \right) \times RU \text{ HSP}$$

$$\text{Observed efficiency} = \left( \frac{\text{Observed detection } RU}{\text{Expected detection } RU} \right) \times 100$$

Where N represents the degree of multimerization. N-1 is used because the HSP antigen is assumed to be captured first by one antibody.

If HSP were a monomer, A-23-HSP-A-23 or B-F10-HSP-B-F10 sandwiching would not be possible. B-F10-HSP-B-F10 (609RU), for which only one epitope was known, showed strong secondary binding, however. If the HSP would be a dodecamer then in theory each of the 12 captured HSP units might bind one secondary antibody each except for the anchoring unit. Given the dodecamer model for A-23-HSP-B-F10 we only observe 45% actual secondary binding, but given the dimer model 82% secondary binding is observed.

An unexpected result of the SPR experiments was that, in contrast to B-F10, A-23 would not bind efficiently to A-23- or B-F10-captured HSP. We think that this was not related to the affinity of A-23 for HSP, because A-23 captured similar amounts of HSP from the solution as B-F10 in the same time period. Rather we think that there are steric reasons why A-23 and B-F10 are behaving so differently. To understand this steric interference it was necessary to map the information on the epitopes recognized by both antibodies i.e. A-23 and B-F10 on to the proposed 3D structure model of HSP (Fig. 7) [29]. To B-F10 only epitope #9 would bind, whereas to A-23 two peptides #3 and #11 were consistently binding. Epitope #3 sites for A-23 are not part of the 3D model, as the dodecameric structure deduced by Kennaway *et al.* does not show its arrangement [29]. We found that the dodecameric structure proposed for HSP by Kennaway *et al.* was built up from 6 dimers, and that the formation of the higher multimeric structure is dependent on interactions of all C-termini with adjacent protein dimers. Dimers are, therefore, the basic conformational unit of HSP, which might survive heat denaturation. Interestingly then, in the dimer 3D model the two positions of epitope #11 of antibody A-23 appear to be in the same plane, whereas the two positions of epitope #9 of antibody B-F10 are diagonally arranged to each other in opposite planes (Fig. 7).

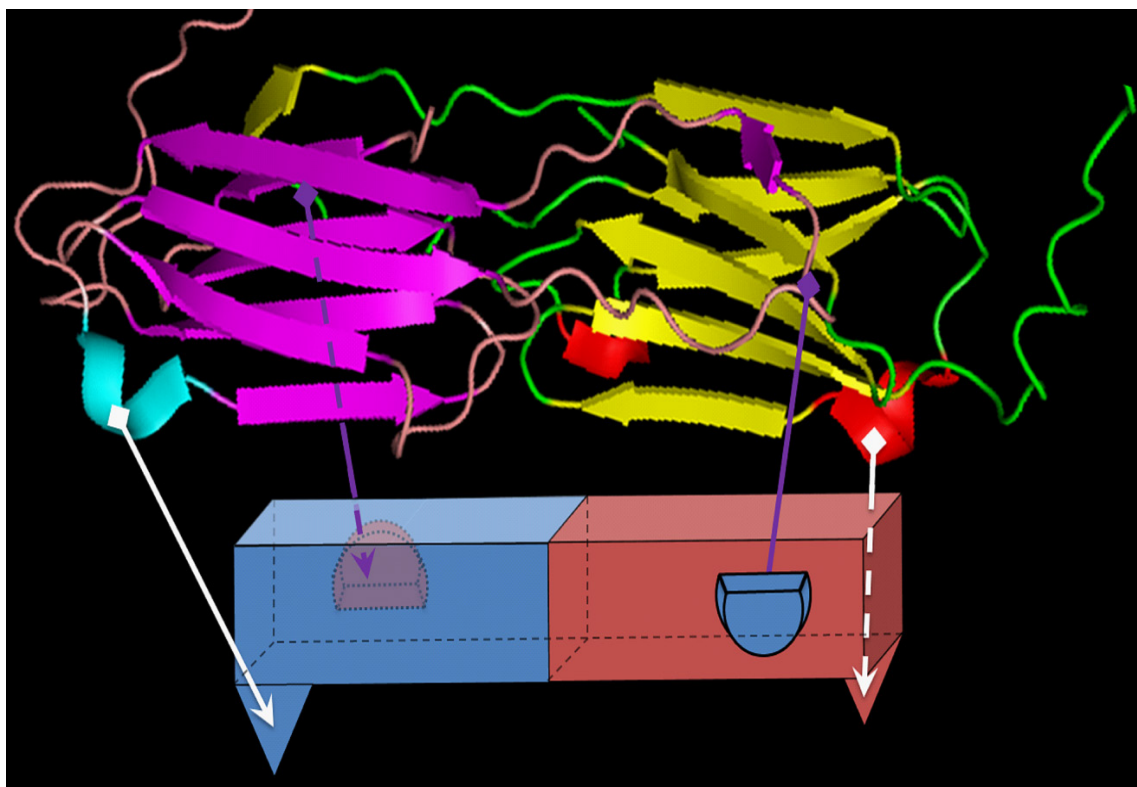


**Figure 7.** Model showing the arrangement of dimer structure of HSP protein along with the representation of possible sites of VHH antibodies B-F10 and A-23

Based on the accumulated evidence from SEC, ESI-TOF-MS, SPR, and the 3D structure of the HSP protein, a model is proposed which shows schematically how B-F10 and A-23 bind to the HSP dimer (Fig. 8). As per this dimer model, all binding sites for A-23 are in the same plane, and thus, upon capture by antibody A-23, the other A-23 binding site is

blocked. Binding of VHH antibody B-F10 is still possible as that binding site is perpendicular to the site of A-23, in a different plane. By contrast, if antibody B-F10 is used for capturing, the binding sites of B-F10 are diagonally arranged in opposite planes, allowing strong binding, while apparently A-23 binding sites remain inaccessible.

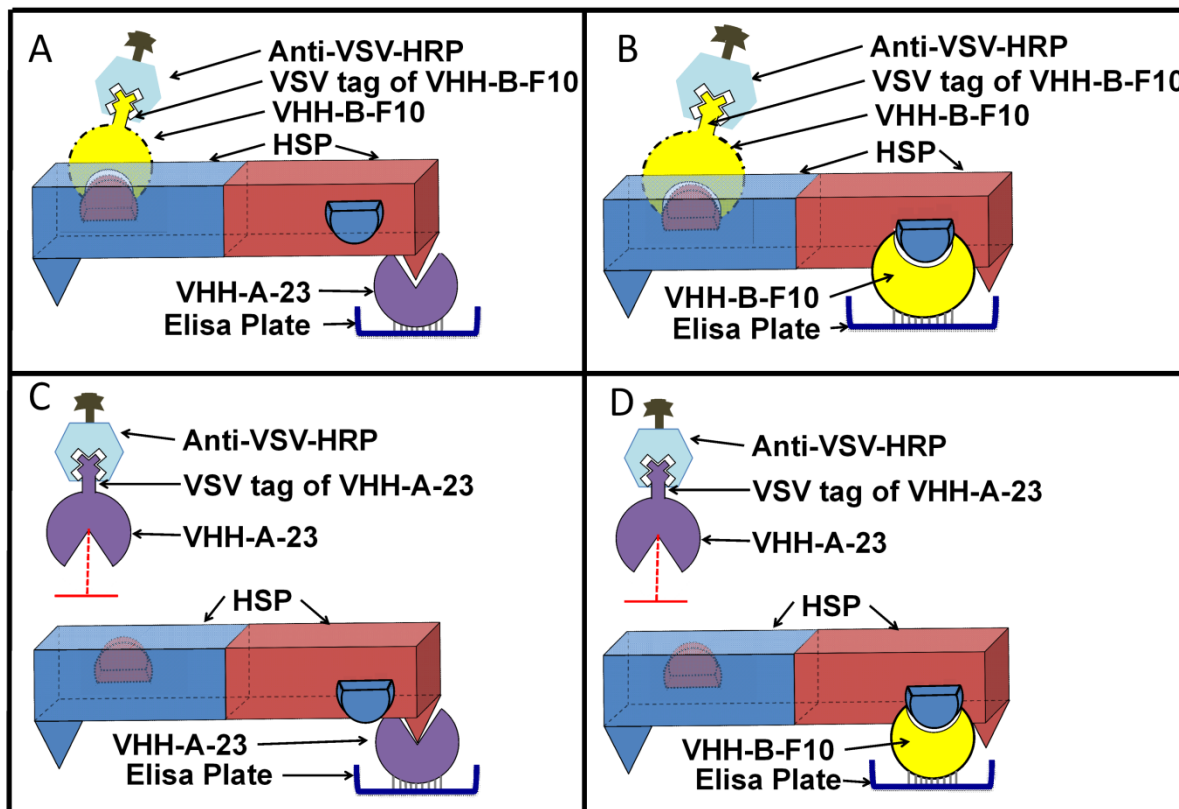


**Figure 8.** Models explaining the blocked detection by A-23 antibodies. The diagrams show the capture of HSP dimer with VHH antibodies B-F10 and A-23 and successful detection with B-F10 (panels A-B) and failed detection with A-23 (panels C-D)

In conclusion, the different VHH antibodies showed specific binding to many different epitopes of the 16 kDa HSP. The VHH's B-F10 and A-23 were the best binders of HSP and are complementary to each other as they recognize non-overlapping epitopes on the HSP dimer. ESI-TOF-MS and SEC in combination with immuno-dot blot analysis showed that although the protein exists as a dodecamer in native state, the HSP is a dimer both as recombinant AVI-HIS-tagged protein (rHSP-tag) and in heat-inactivated *M.tb.* lysates (*M.tb.*-HSP and heated-rHSP). Based on these findings, assays for protein-based diagnosis of tuberculosis could be developed. High concentrations of this non-secreted can be obtained by first concentrating the *M.tb.* cells from liquefied sputum samples using magnetic TB-Beads [35], followed by controlled lysis of the bacteria using mechanical or ultrasonic [36] lysis methods.

## References

1. Nachega JB, Chaisson RE; *Clin Infect Dis*, **2003**, 36, S24
2. The Global Plan to Stop TB 2011–2015; *WHO*, **2010**
3. Ormerod LP; *Br Med Bull*, **2005**, 73-74, 17
4. Kranzer K, Houben RMGJ, Glynn JR, Bekker L-G, Wood R, *et al.*; *Lancet Infect Dis*, **2010**, 10, 93
5. Swaminathan S, Padmapriyadarsini C, Narendran G; *Clin Infect Dis*, **2010**, 50, 1377
6. Toussaint CH, Pritchard EK; *Postgrad Med J*, **1944**, 20, 143
7. Tsara V, Serasli E, Christaki P; *Hippokratia*, **2009**, 13, 20
8. Watterson SA, Drobniewski FA; *J Clin Pathol*, **2000**, 53, 727
9. Landowski CP, Godfrey HP, Bentley-Hibbert SI, Liu XY, Huang ZS, *et al.*; *J Clin Microbiol*, **2001**, 39, 2418
10. Pottumarthy S, Wells VC, Morris AJ; *J Clin Microbiol*, **2000**, 38, 2227
11. Gennaro ML; *Clin Infect Dis*, **2000**, 30, S243
12. Chan ED, Heifets L, Iseman RD; *Tubercul Lung D*, **2000**, 80, 131
13. Grabau JC, DiFerdinando GT, Jr., Novick LF; *Pub Health Rep*, **1995**, 110, 703
14. Pottumarthy S, Morris AJ, Harrison AC, Wells VC; *J Clin Microbiol*, **1999**, 37, 3229
15. van der Linden RHJ, Frenken LGJ, de Geus B, Harmsen MM, Ruuls RC, *et al.*; *Prot Struc Mol Enzymol*, **1999**, 1431, 37
16. Strokappe N, Szynol A, Aasa-Chapman M, Gorlani A, Forsman Quigley A, *et al.*; *PLoS One*, **2012**, 7, e33298
17. Harmsen MM, De Haard HJ; *Appl Microbiol Biotechnol*, **2007**, 77, 13
18. Trilling AK, de Ronde H, Noteboom L, van Houwelingen A, Roelse M, *et al.*; *PLoS One*, **2011**, 6, e26754
19. Bulut Y, Michelsen KS, Hayrapetian L, Naiki Y, Spallek R, *et al.*; *J Biol Chem*, **2005**, 280, 20961
20. Yuan Y, Crane DD, Simpson RM, Zhu YQ, Hickey MJ, *et al.*; *Proc Natl Acad Sci*, **1998**, 95, 9578
21. Lee BY, Hefta SA, Brennan PJ; *Infect Immun*, **1992**, 60, 2066
22. Verbon A, Hartskeerl RA, Moreno C, Kolk AHJ; *Clin Exp Immunol*, **1992**, 89, 395
23. Vordermeier HM, Harris DP, Roman E, Lathigra R, Moreno C, *et al.*; *J Immunol*, **1991**, 147, 1023
24. Trilling AK, Harmsen MM, Ruigrok VJ, Zuilhof H, Beekwilder J; *Biosens Bioelectron*, **2012**, 40, 219
25. Li YT, Hsieh YL, Henion JD, Senko MW, Mclafferty FW, *et al.*; *J Am Chem Soc*, **1993**, 115, 8409
26. Loo JA; *Int J Mass Spec*, **2000**, 200, 175
27. Banerjee S, Mazumdar S; *Int J Anal Chem*, **2012**, 282574
28. Heck AJR; *Nat Methods*, **2008**, 5, 927
29. Kennaway CK, Benesch JL, Gohlke U, Wang L, Robinson CV, *et al.*; *J Biol Chem*, **2005**, 280, 33419
30. Devi KRU, Kumar KSS, Ramalingam B, Alamelu R; *Prot Expr Purif*, **2002**, 24, 188
31. Raja A, Devi KRU, Ramalingam B, Brennan PJ; *Clin Diag Lab Immunol*, **2002**, 9, 308
32. Chang ZY, Primm TP, Jakana J, Lee IH, Serysheva I, *et al.*; *J Biol Chem*, **1996**, 271, 7218
33. Pazehoski KO, Collins TC, Boyle RJ, Jensen-Seaman MI, Dameron CT; *J Inorg Biochem*, **2008**, 102, 522
34. Friscia G, Vordermeier HM, Pasvol G, Harris DP, Moreno C, *et al.*; *Clin Exp Immunol*, **1995**, 102, 53
35. Wilson S, Lane A, Rosedale R, Stanley C; *J Tubercul Lung D*, **2010**, 14, 1164
36. Doeblner RW, Erwin B, Hickerson A, Irvine B, Woyski D, *et al.*; *J Lab Automat*, **2009**, 14, 119

# *Chapter 4*

*Up-concentration and fluorescence based detection of Mycobacterium tuberculosis bacteria and proteins with microsieves*

*Manuscript under preparation.*

## ***Abstract***

Tuberculosis (TB) is a contagious airborne disease, for which diagnosis is challenging due to several limitations with respect to handling, cost, sensitivity and reliability especially in resource poor settings. In the present study we describe the principle of a two-step capture and optical detection procedure of identifying *Mycobacterium tuberculosis* (*M.tb.*). First up-concentrating of mycobacteria with PolyDADMAC functionalized microsieves is shown. In a second step direct fluorescent labelling of whole mycobacteria is possible. Alternatively the sample can be lysed for further assay detection. Here we show the presence of the 16 kDa heat shock protein (HSP) (in this report originating from *E. coli.*) on a second microsieve. The detection was not quantitative as the fluorescent labelling method seemed to induce the agglutination of the antigen, which was confirmed via dynamic light scattering study. However, the combination of up-concentrating *M.tb.* bacteria from sputum on microsieves and subsequent fluorescence assisted microsieve-based detection of HSP may overcome sensitivity issues relating to low bacterial counts and dilute antigen concentrations. Thus, the method may allow earlier detection of *M.tb.* infections in sputum and cultures from patients in resource-poor settings.

## 4.1 Introduction

*M. tuberculosis* (*M.tb.*) is a gram-positive bacterium causing tuberculosis (TB), which is one of the leading causes of global mortality (1.4 million people in 2011) [1]. TB is a contagious airborne disease usually spreading from person to person with every year around 8-9 million new cases reported. The WHO 2012 annual report states that one third of the world population has TB either in active or dormant state [2]. The TB bacterium can remain inactive or in dormant state for years without causing symptoms or spreading to other subjects, but as soon as the immune system of the host subject becomes weakened, the bacterium becomes active and will infect mainly the lungs along with other parts of the body [3, 4]. TB cases are also aggravated by sicknesses or illnesses that decrease body immunity such as HIV, which is prevalent in resource poor countries [5].

The diagnosis of TB is conventionally done using the skin *Mantoux* screening test or by direct acid-fast bacterium testing of sputum smears. The latter may face difficulties in sample collection especially in non-pulmonary TB cases [6, 7]. Plating methods are dependent on the slow growth of the TB bacterium and take around 2-6 weeks [8-11]. Other methods like DNA-based diagnostic procedures are usually very costly as they require an advanced laboratory infrastructure along with skilled personnel [8]. Early detection of TB i.e. either in dormant state or early active stage could enable an earlier treatment with better prognosis or lower epidemiological risks. Though treatment of active TB can be done utilizing one or a combination of several drugs, including rifampicin (Rifadin), ethambutol (Myambutol), pyrazinamide, and streptomycin, the development of drug resistant strains is making treatment of TB much more challenging [12-16]. Diagnostic assays utilizing antibodies have been implemented successfully for various infection diseases [17-19], but in the case of TB not much success was achieved over several decades [20]. To date, no commercial TB immunodiagnostic test is both sufficiently specific and sensitive [21]. Thus, there is an urgent need for rapid, inexpensive, reliable, technically simple and robust methods for the detection of *M.tb.* especially in resource poor settings [5, 22].

Flow-through assays are mature techniques, where the test principle is based on overcoming diffusion limitations by flowing of the analyte through a porous surface, pre-immobilized with capture molecules specific for the analyte. Captured analytes on the porous surface, are then in a second step detected by optical or electrochemical techniques. Flow-through assays are usually very fast and capable of detection of multiple analytes in one test [23]. Though flow-through assays have been around for a long time, very little has been done towards their application in the detection of TB. An attempt was made by Reither *et al.* in 2010 to evaluate a novel flow-through assay i.e. Diagnos TB AG developed by Biomed Industries, Parwanoo, India, for the detection of pulmonary TB. The assay involved the use of four mycobacterial antigens including lipoarabinomannan (LAM) and the 30 kDa antigen [24]. The assay was a three-step assay, where the first step involved the inactivation and lysis of *M.tb.* cells, the second step the formation of antibody-antigen complexes, and the final step red-pink coloration of the membrane in case of positive reaction due to reaction of antibody-antigen complex with protein A conjugate [24]. Application of the test to real cases was

problematic for the following reasons: (1) the test procedure was dependent on sputum viscosity and involved a time consuming mechanical homogenisation step through pipetting, (2) the visual interpretation of the colours in case of a positive test was variable between different researchers and (3) heterogeneous colour development was often observed but difficult to interpret. Thus, the test was evaluated as highly non-specific and not fit for point of care assays [24]. In our opinion, the flaws that were identified in the above method could easily be rectified by utilizing chemical homogenisation of the sputum and using a more advanced fluorescent detection method.

The objective of the present work was to demonstrate the elements that could be part of a new detection method combining capture-based up-concentration of bacteria and fluorescent detection of subsequently released antigens after bacterial lysis captured on a second microsieve. The method potentially overcomes the limitations of the other method by up-concentrating bacterial cells first from chemically homogenized sputum using a microsieve. The concentrated antigens released from these bacteria upon lysis may be detected more reliably using fluorescence.

## 4.2 Materials and Methods

The 2-Epoxy-9-decene (96%), poly (diallyldimethylammonium chloride), high molecular weight (PolyDADMAC) 20 wt.% in water solution, acridine orange (powder phase) and acetone (semiconductor grade) were purchased from Sigma-Aldrich. 1, 2-Epoxy-9-decene was purified by vacuum distillation; the obtained purity was >99% as determined by GC-MS. Ultrapure water from a Barnstead water purification system with a resistivity of 18.3 M $\Omega$ .cm was used. Protein printing buffer solution (PPB) 2 $\times$  was purchased from Arrayit corporation, USA. Biotinylated VHH antibodies were produced as described by Trilling *et al.* [26] Phosphate-buffered saline (PBS) solutions (pH 7.4), (Bovine serum albumin) (10 mg/ml) as blocking solution were used in biological experiments. Micro-engineered membranes (microsieves) made of Si<sub>3</sub>N<sub>4</sub> thin films standing on silicon supports with circular pores of various well-defined sizes (0.45  $\mu$ m and 3.5  $\mu$ m) were provided by Aquamarijn Micro Filtration B.V., The Netherlands.

### 4.2.1 Up-concentration experiments on the microsieve

Microsieves were first coated with PolyDADMAC with the following procedure. Si<sub>3</sub>N<sub>4</sub> microsieves with pore size of 3.5  $\mu$ m were rinsed with acetone for 15 min, followed by piranha treatment for 15 min and washed 3 times with excess of water. Subsequently the samples were dipped into a solution of 2% (w/w) PolyDADMAC in water for 1 min. Any excess of the solution was passed through the microsieves. The microsieves were subsequently dried overnight under vacuum and subsequently rinsed thrice with an excess of water. PolyDADMAC-coated 3.5  $\mu$ m microsieves were mounted into plastic filtration holders. *Mycobacterium smegmatis* (*M. smeg.*) was grown in Middlebrook 7H9 medium supplemented with 10% OADC, inactivated and next stained with acridine orange. A 100  $\mu$ l

sample of stained *M. smeg.* suspension in water ( $10^6$  bacteria/ml) was filtered through the microsieves at a flow rate of 50  $\mu\text{l}/\text{min}$ , and subsequently rinsed with 1 ml of water at a flow rate of 500  $\mu\text{l}/\text{min}$ .

#### 4.2.2 HSP-based detection of *M.tb.* with microsieves

Concentrated bacteria loaded on microsieves can be characterized as mycobacteria using *M.tb.* specific antibodies. For this purpose we used the cellular 16 kDa heat shock protein (HSP) which can be released from mycobacteria by mechanical lysis methods like bead beating, sonication or urea lysis [25-28]. The schematic for this method is described in Fig. 1. We functionalized biotinylated llama VHH antibody for HSP on a second microsieve with a pore size of 0.45  $\mu\text{m}$ . The functionalization of the microsieve was achieved in three steps, first with an epoxide layer, next with a streptavidin (SA) layer over the epoxy layer and finally with biotinylated llama VHH antibody coating. The  $\text{Si}_3\text{N}_4$  microsieves with a pore size of 0.45  $\mu\text{m}$  were provided with an epoxide layer after photochemical ( $\lambda = 254$  nm) attachment of 1, 2-epoxy-9-decene as described by Nguyen *et al.* [29]. The epoxide-coated  $\text{Si}_3\text{N}_4$  microsieves were next incubated with SA in PPB (1.0 mg/ml) for 15 min at room temperature followed by overnight incubation at 4°C. SA-coated microsieves were rinsed with 1 ml of PBS (pH 7.4) [30]. Unreacted epoxide groups on SA-coated microsieves were passivated using BSA solution (10 mg/ml) for 50 min. Subsequently, the microsieves were coated with biotinylated primary antibody VHH-A-23 antibody solution (5 $\mu\text{g}/\text{ml}$ ) or antibody M200 (negative control) solution (5  $\mu\text{g}/\text{ml}$ ) respectively before the capture of HSP.

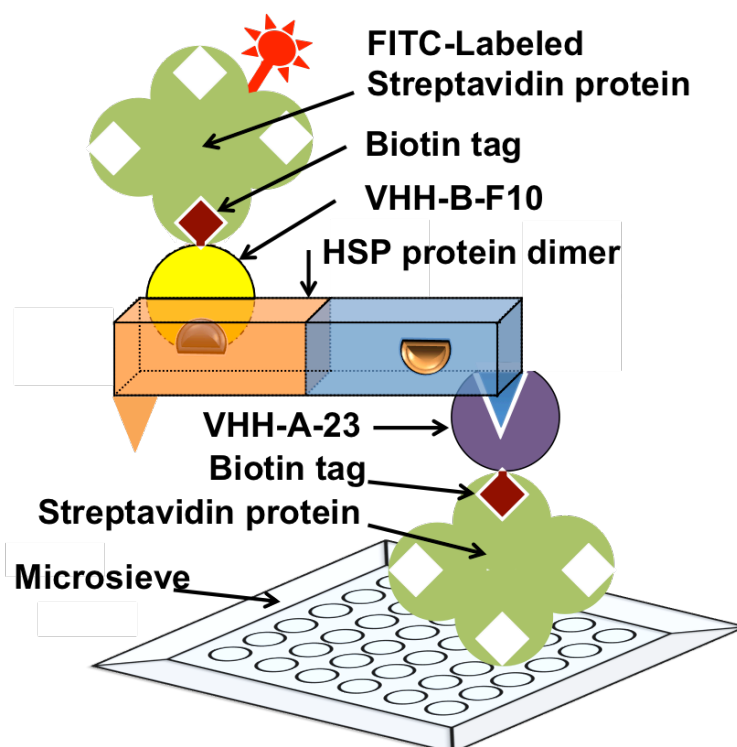


**Figure 1:** Schematic of the microsieve sandwich immunoassay which is built up step by step to first capture the HSP molecule and then the detection antibody VHH-B-F10

All primary capture antibody coated microsieves were blocked using a mixture (1:1) of biotin (5  $\mu\text{g/ml}$ ) and BSA (10  $\text{mg/ml}$ ) for 40 min to block unreacted species, and subsequently rinsed with 1 ml of PBS. A 50  $\mu\text{L}$  volume of HSP solution at different concentrations (5  $\mu\text{g/ml}$ , 2.5  $\mu\text{g/ml}$ , 1  $\mu\text{g/ml}$ , 100  $\text{ng/ml}$ , 10  $\text{ng/ml}$ , 1  $\text{ng/ml}$ ) was subsequently incubated on top of the microsieves for 5 min and filtered through the microsieves. As negative controls, one microsieve was coated with biotinylated primary control antibody M200 (does not bind with HSP) followed by incubation with 50  $\mu\text{l}$  of HSP solution at a concentration of 5  $\mu\text{g/ml}$ . The samples were rinsed with 1 ml of PBS and then blocked with BSA solution for 40 min.

### 4.2.3 Staining procedure to visualize the HSP

In order to visualize the captured HSP, the samples were first incubated with biotinylated VHH-B-F10 antibody solution (5  $\mu\text{g/ml}$ ) for 5 min, followed by first rinsing with 1 ml of PBS and then incubating with FITC-SA (5  $\mu\text{g/ml}$ ) for 10 min. Finally, all samples were rinsed with 1 ml of PBS and dried briefly with nitrogen gas before observation by fluorescence microscopy (excitation at 470 nm and emission at 528 nm).

### 4.2.4 Dynamic light scattering (DLS)

To better understand the results obtained via the capture and detection of HSP in the above sandwich assay, DLS measurements were performed of the agglutination reaction induced by mixing the complex of SA and biotinylated VHH antibody B-F-10 with HSP protein. The hydrodynamic radius ( $R_h$ ) was measured using a nano-zetasizer (Nano-ZS), model: ZEN 3600, Malvern Instruments, Worcestershire, UK. The instrument was equipped with 633 nm laser and the samples were put in a 40  $\mu\text{l}$  (minimum) quartz cuvette with 1 cm path length. The measurements were performed at 25°C in the automatic mode, in which the attenuator and the measurement position were selected automatically with the incident angle for laser to be at 90°. For DLS measurement an equimolar concentration of SA and VHH antibody B-F10 was incubated together for 10 min to obtain a SA-B-F10 complex that was further utilized to perform the experiments. A solution of 25  $\mu\text{l}$  of SA-B-F10 complex was mixed with 25  $\mu\text{l}$  of HSP solution at varied concentrations (5 $\mu\text{g/ml}$ , 2.5 $\mu\text{g/ml}$ , 1 $\mu\text{g/ml}$ , 100  $\text{ng/ml}$ , 10  $\text{ng/ml}$ ) and assayed after a 5 sec time delay of between adding and measuring. Both the VHH and HSP solutions were prepared by dilution from their respective stock solutions in 1  $\times$  PBS pH 7.5 to obtain the desired concentration for the experiment. The intensity fluctuations in the scattered light were measured at 173° for 25 sec. Ten such scans were averaged to obtain the correlation curve. Next, intensity based size distributions were calculated using the standard software of Malvern. The  $R_h$  was calculated in the Malvern software from the calculated diffusion coefficients and using the Stoke-Einstein relation. The diffusion coefficients were calculated from the measured characteristic decay times in the curves of auto-correlation coefficient versus time. Solutions of only SA-bound biotinylated VHH antibodies or HSP alone were measured as controls in order to exclude any agglutination arising from these samples themselves.

## 4.3 Results and Discussion

### 4.3.1 Concentrating *M. smeg.* on microsieves

Sputum is the most obvious sample for the detection of TB. Due to the high viscosity and stickiness of sputum, it is challenging to extract bacteria for further analysis, however. Also, a relatively low bacterium count is an issue for the early detection of TB. Concentrating the bacteria on a sieve could be a solution if known procedures of liquefaction such as salt solutions or household bleach will allow filtering of *M. smeg.* cells [31, 32]. PolyDADMAC-coated microsieves were utilized in our study for up-concentrating mycobacteria of the strain smegmatis suspended in PBS buffer. Fig. 2A and 2B show the fluorescence image of acridine orange pre-stained *M. smeg.* cells on 3.5  $\mu\text{m}$  PolyDADMAC-coated microsieves, whereas on control microsieves (Fig. 2C and 2D) with no PolyDADMAC coating, stained *Mycobacterium* cells pass through the 3.5  $\mu\text{m}$  large pores. *M. smeg.* cells concentrated in this way may easily be lysed using standard procedures such as urea lysis, sonication or bead beating [25-28] to obtain lysates with cellular internal protein.

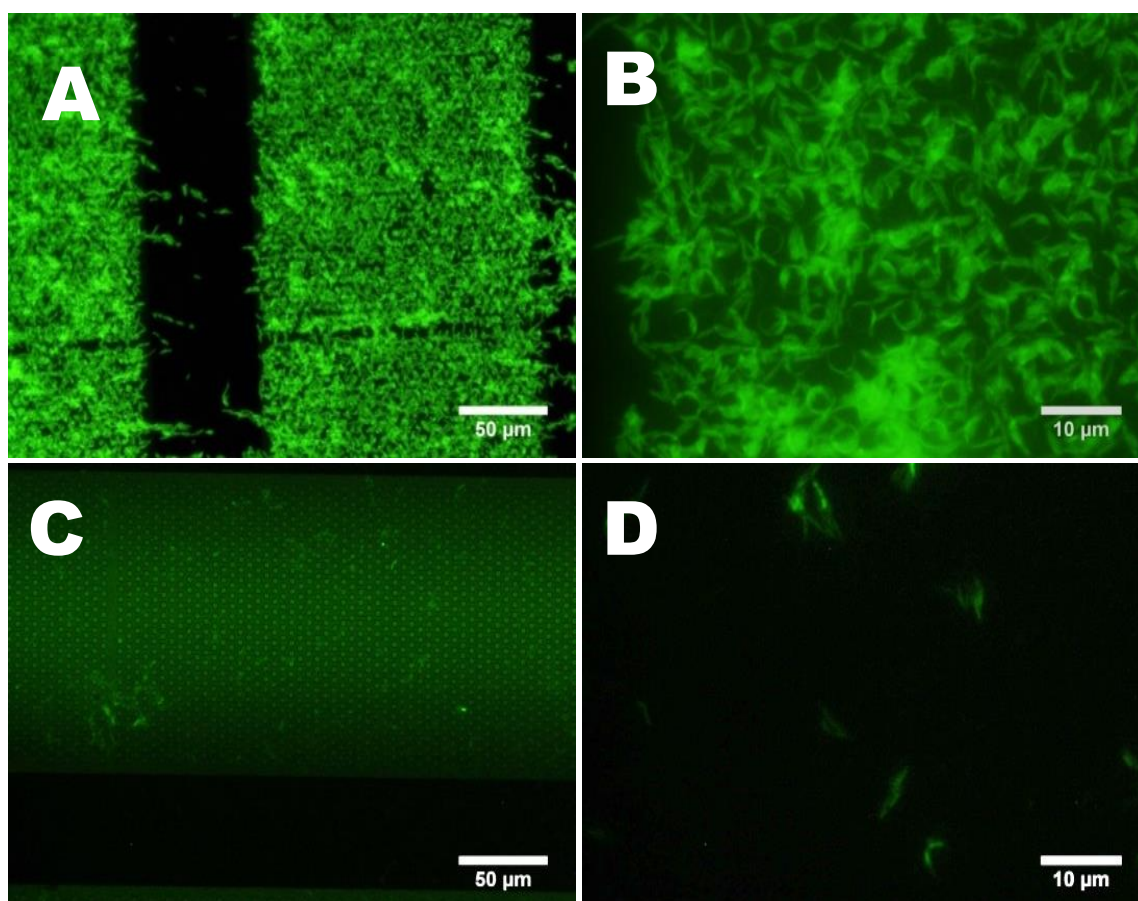


**Figure 2.** Fluorescence microscopy images of *Mycobacteria* stained by acridine orange after capture on PolyDADMAC-coated microsieves with pore size 3.5  $\mu\text{m}$ . Panel A shows the result for PolyDADMAC coated sieves under 5 $\times$  magnification; panel B for 20 $\times$ ; panels C and D the experiment of panel A and B but with uncoated microsieves

### 4.3.2 Fluorescence based detection of HSP on microsieves by immunoassay

Immunoassays have the potential to provide fast, simple and reliable detection methods, though in relation to TB not much success was achieved for several decades. Tested antibodies against whole *M.tb.* cells were either non-specific recognizing all *Mycobacterium sp.* or directed against secreted antigens that were too dilute in sputum test samples to provide a reliable diagnosis [25]. We therefore propose that cell internal proteins may be the better choice for these kinds of immunoassays as they can be pre-concentrated by concentrating the bacteria first.

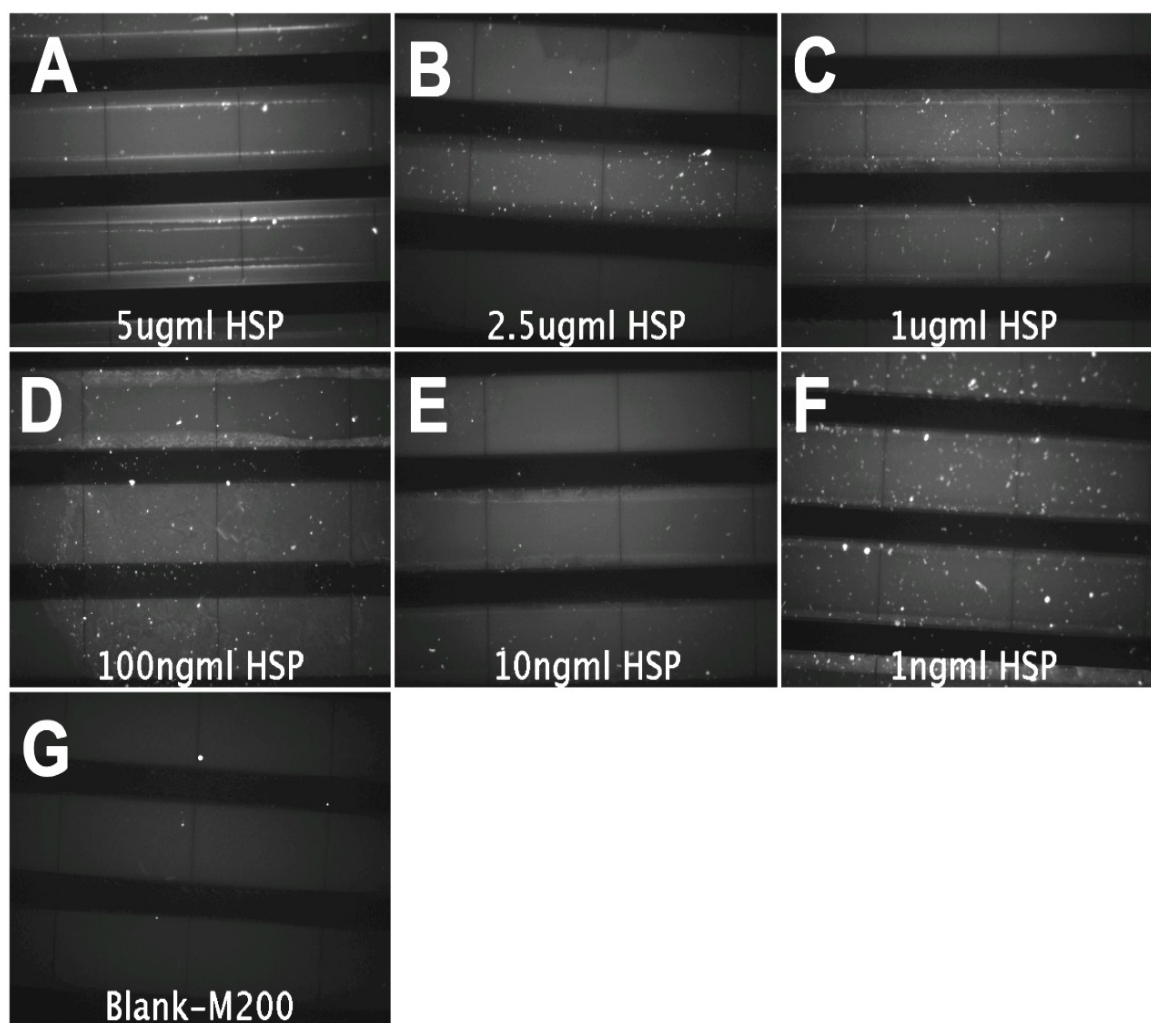


**Figure 3:** Fluorescent images of FITC-SA-B-F10 stained HSP captured by 0.45  $\mu\text{m}$  pore-size microsieves coated with primary antibody VHH-A-23 antibody (test sample) or M200 antibody (negative control) with variable concentrations of HSP in sandwich assay. The sub figures show the test results of HSP concentration of 5  $\mu\text{g/ml}$  (A), 2.5  $\mu\text{g/ml}$  (B), 1  $\mu\text{g/ml}$  (C), 100 ng/ml (D), 10 ng/ml (E), 1 ng/ml (F) while figure G shows the result for the negative control with primary antibody M200 (exposure times and CCD gain are the same for all images)

In our previous work we selected the most optimal antibody pair against the most dominant antigen, HSP, of *M.tb.* [25]. Fig. 3 shows the results obtained using fluorescence based detection of HSP protein in a flow-through based system by performing a sandwich

immunoassay on microsieve surfaces with pore sizes of 0.45  $\mu\text{m}$ . In Fig. 3A-G, the results of a range of applied concentrations of HSP i.e. 5  $\mu\text{g/ml}$ , 2.5  $\mu\text{g/ml}$ , 1  $\mu\text{g/ml}$ , 100  $\text{ng/ml}$ , 10  $\text{ng/ml}$ , 1  $\text{ng/ml}$  are shown. For all concentrations - we surprisingly saw only the presence of aggregates. We suggest that those may be formed by an agglutination reaction as depicted in Fig. 4. Figure 3G is a negative control where primary antibody M200 was used that does not bind with HSP. We did not see significant amounts of aggregates in a range of replicates of that control unlike with the HSP coated sieves. The aggregates obtained in Fig. 3F, and to a lesser degree also visible in Fig. 3A, 3C, 3D and 3E, may possibly be fractal aggregations of the test proteins. They might be formed when SA bound biotinylated VHH antibody B-F-10 comes in contact with the HSP protein dimer although this would require first a release of the HSP dimer from the capture antibody VHH-A-23. To verify that this might be happening DLS measurements were done.

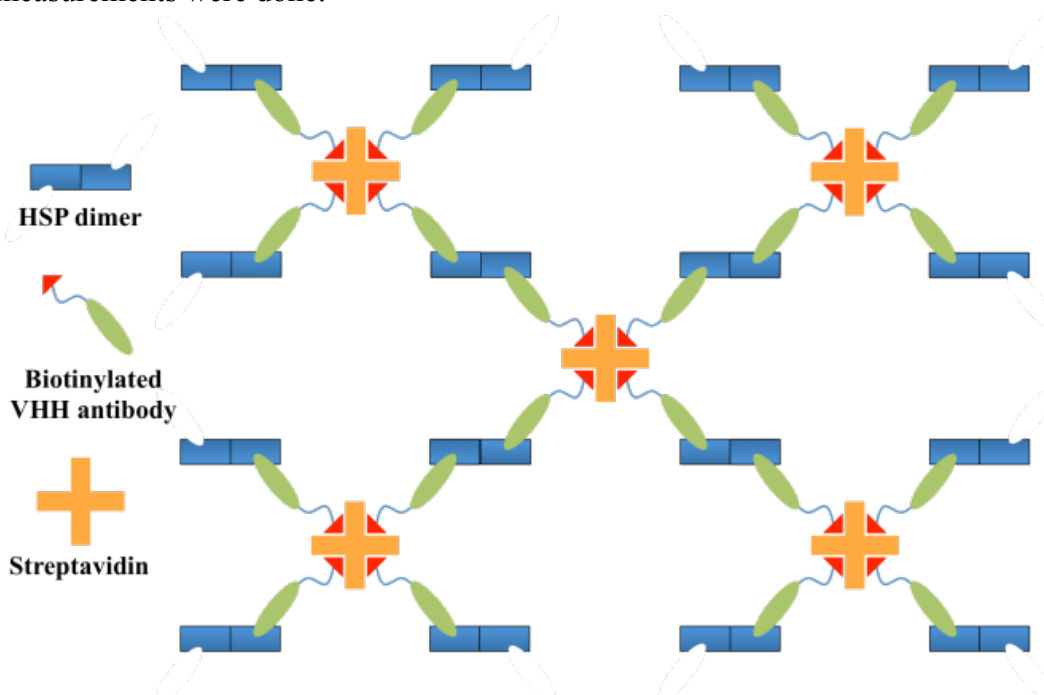


**Figure 4:** Schematics depicting the formation of aggregates due to agglutination between SA-F10 complex and HSP antigen

#### 4.3.3 DLS-based agglutination analysis

In order to understand the agglutination or aggregation observed when SA bound biotinylated VHH antibody B-F-10 contacts HSP protein especially at lower concentrations of HSP, DLS was utilized. In Fig. 5, the results of DLS studies are shown along with the size patterns of agglutinated particles with increasing concentration of the HSP antigen. The control experiments ran with only HSP or SA-F10 complex excluded the possible occurrence of an agglutination reaction with either molecular species (Fig. 5). With increasing concentrations of the antigen, HSP formed polydisperse agglutinated particles. The repeated peaks in the graphs of Fig. 5 suggest the growth and subsequent precipitation of agglutinating particles. After attaining a maximum height the particles settled down by gravity.

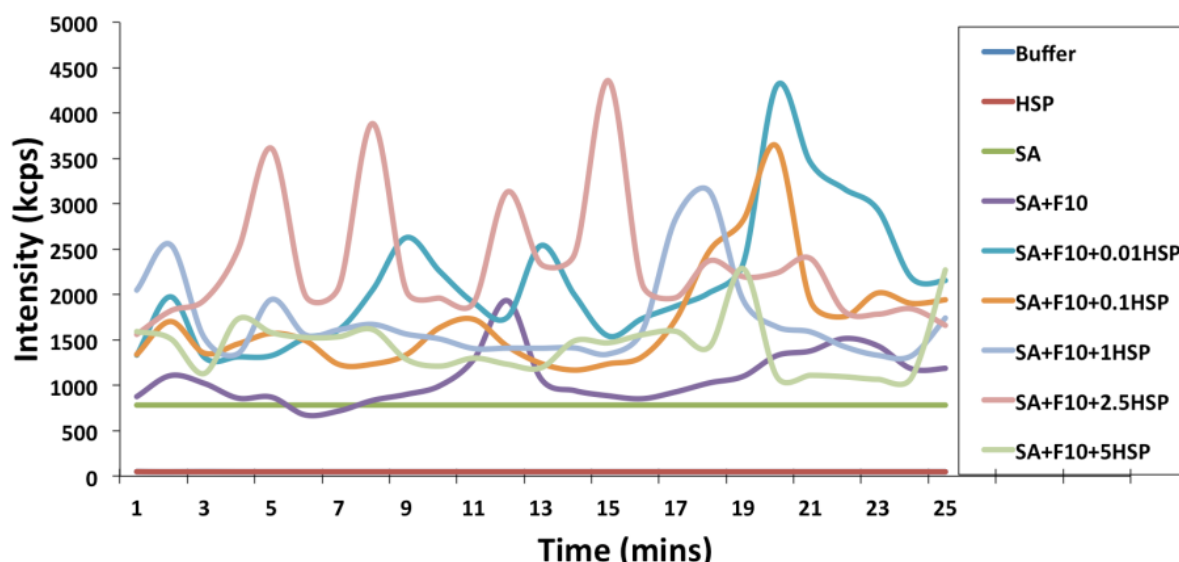


**Figure 5:** DLS plot where intensity is plotted against time showing fractal aggregation for different concentrations of HSP when incubated with antibody VHH-F-10 complexed to SA. HSP and SA alone give straight lines and in combination yield a very low response. Addition of HSP generates intensity fluxes

HSP is known to exist as a homodimer after isolation using a urea lysis procedure resulting in two binding sites for each antibody or a valency of two [25]. Therefore, upon exposure to VHH antibodies that are bound to a SA molecule with a valency of 4, the molecules will induce a chaotic 3D complex formation. This complex formation leads to particles of different sizes and shapes in the measured samples. At a critical lower concentration of antigen HSP, this complex formation would lead to larger aggregates compared to both higher and lower concentrations of HSP (illustrated in Fig. 6). Indeed, with the concentration of SA-F10 complex fixed, but with varying concentrations of antigen HSP (also viewing other experiments), it appeared that more small aggregates were formed at higher concentrations (like 5  $\mu\text{g/ml}$  and 1  $\mu\text{g/ml}$ , except 2.5  $\mu\text{g/ml}$  in this Fig. 3). Possibly, the aggregates formed at higher concentration were also so small that most passed through the microsieve, while at lower titres the aggregates were large enough to be retained.

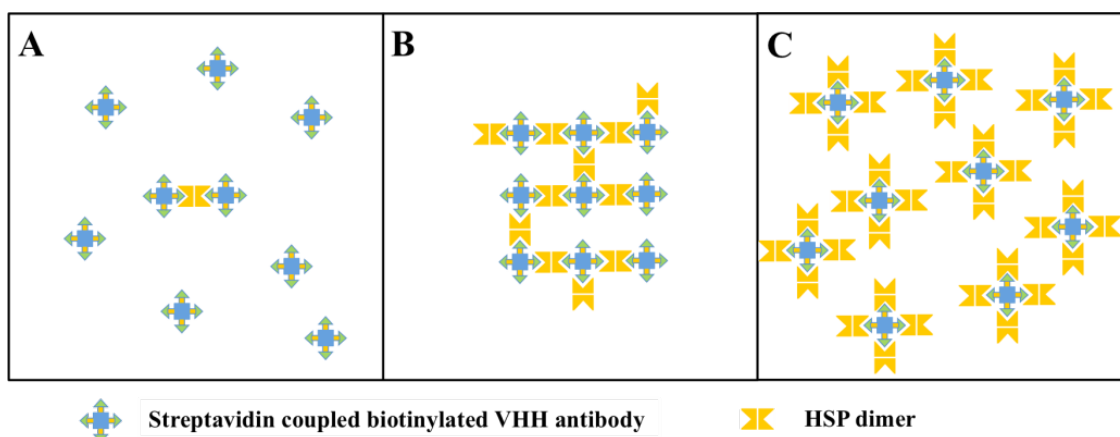


**Figure 6:** Schematics depicting aggregate formation of the detection complex due to agglutination when HSP comes in contact with SA-F10 complex. A: shows the dimer formation when 1 HSP unit is added, B: shows clump formation where 11 HSP units were added while C: shows monomer formation where 36 HSP units were added

## 4.4 Conclusion

Over the last few decades, a lot has been done to develop fast and effective assays for cheap, robust and reliable detection of TB under field conditions, with a main focus on measuring the level of anti-*M.tb.* antibodies in the serum, identifying *M.tb.* cells in sputum (by microscopy or culturing) or detecting biomarkers in urine [6, 33]. Nucleic acid amplification based techniques are fast alternatives, but are complex, expensive and require skilled personnel with high quality standards [34], whereas conventional assays are often not sensitive enough or too time-consuming [33, 35-37].

With additional work, the fluorescence assisted microsieve based platform described here may be developed into a potentially fast, simple and reliable assay. The up-concentration techniques demonstrated here might be useful in obtaining high concentrations of *M.tb.* cells from sputum samples. Up-concentrated cells would greatly enhance the sensitivity of the suggested assay or any other assay that tries to identify *M.tb.* and quantify the bacterial count. The issue which still needs to be addressed is to develop a simple cell lysis protocol to obtain a concentrated protein extract. This might be done utilizing mechanical or ultrasonic [38] lysis methods that preserve the proteins intact and allow subsequent immunoassays. The dominant antigen, 16 kDa HSP, is a good target protein to identify *M.tb.* [25]. However, the agglutination reaction that seems to occur makes it very difficult to obtain quantitative and reproducible data on the quantity of bacteria in the sputum. Possibly protocols can be improved in the future to prevent the occurrence of the agglutination reactions by a better primary capture of the HSP antigen on the sieves first and by using a detection antibody with a valency of one.

## References

1. Global Tuberculosis Report, *WHO*, **2012**
2. Global Tuberculosis Report, *WHO*, **2013**
3. Kranzer K, Houben RMGJ, Glynn JR, Bekker L-G, Wood R, *et al.*; *Lancet Infect Dis*, **2010**, *10*, 93
4. Swaminathan S, Padmapriyadarsini C, Narendran G; *Clin Infect Dis*, **2010**, *50*, 1377
5. Tsara V, Serasli E, Christaki P; *Hippokratia*, **2009**, *13*, 20
6. Minton K; *Nat Rev Immunol*, **2003**, *3*, 355
7. Fernández JG, Fernández-de-Mera I, Reyes LE, Ferreras MC, Pérez V, *et al.*; *J Vet Diag Inv*, **2009**, *21*, 102
8. Landowski CP, Godfrey HP, Bentley-Hibbert SI, Liu XY, Huang ZS, *et al.*; *J Clin Microbiol*, **2001**, *39*, 2418
9. Pottumarthy S, Wells VC, Morris AJ; *J Clin Microbiol*, **2000**, *38*, 2227
10. Gennaro ML; *Clin Infect Dis*, **2000**, *30*, S243
11. Chan ED, Heifets L, Iseman RD; *Tubercle Lung Dis*, **2000**, *80*, 131
12. Mitnick C, Bayona J, Palacios E, Shin S, Furin J, *et al.*; *New Eng J Med*, **2003**, *348*, 119
13. Caminero JA; *Int J Tubercul Lung D*, **2006**, *10*, 829
14. Isaakidis P, Cox HS, Varghese B, Montaldo C, Da Silva E, *et al.*; *PLoS One*, **2011**, *6*, e28066
15. Colijn C, Cohen T, Ganesh A, Murray M; *PLoS One*, **2011**, *6*, e18327
16. Ormerod LP; *Br Med Bull*, **2005**, *73-74*, 17
17. Granberg C, Mansikka A, Lehtonen OP, Kujari H, Gronfors R, *et al.*; *J Clin Microbiol*, **1993**, *31*, 1453
18. Matter L, Germann D; *J Clin Microbiol*, **1995**, *33*, 2338
19. Taye A, Chen H, Duncan K, Zhang Z, Hendrix L, *et al.*; *Ann N Y Acad Sci*, **2005**, *1063*, 280
20. Shen GM, Behera D, Bhalla M, Nadas A, Laal S; *Clin Vacc Immunol*, **2009**, *16*, 49
21. Steingart KR, Henry M, Laal S, Hopewell PC, *et al.*; *PLoS Med*, **2007**, *4*, e202
22. Toussaint CH, Pritchard EK; *Postgrad Med J*, **1944**, *20*, 143
23. Ramachandran S, Singhal M, McKenzie K, Osborn J, Arjyal A, *et al.*; *Diagnostics*, **2013**, *3*, 244
24. Reither K, Saathoff E, Jung J, Minja LT, Machibya H, *et al.*; *Int J Tubercul Lung D*, **2010**, *14*, 238
25. Srivastava SK, Ruigrok VJB, Thompson NJ, Trilling AK, Heck AJR, *et al.*; *PLoS One*, **2013**, *8*, e64040
26. Trilling AK, de Ronde H, Noteboom L, van Houwelingen A, Roelse M, *et al.*; *PLoS One*, **2011**, *6*, e26754
27. Aldous WK, Pounder JI, Cloud JL, Woods GL; *J Clin Microbiol*, **2005**, *43*, 2471
28. Hurley SS, Splitter GA, Welch RA; *J Clin Microbiol*, **1987**, *25*, 2227
29. Nguyen AT, Baggerman J, Paulusse MJM, van Rijn CJM, Zuilhof H; *Langmuir*, **2011**, *27*, 2587
30. Nguyễn TÁ; *PhD thesis*, **2011**, *Wageningen University*, p142
31. Aung WW, Nyein MM, Ti T, Maung W; *J Trop Med Pub Health*, **2001**, *32*, 390
32. Farnia P, Mohammadi F, Zarifi Z, Tabatabaei DJ, Ganavi J, *et al.*; *J Clin Microbiol*, **2002**, *40*, 508
33. Bhaskar S, Banavaliker JN, Hanif M; *FEMS Immunol Med Microbiol*, **2003**, *39*, 235
34. Davis JL, Huang L, Worodria W *et al.*; *PLoS One*, **2011**, *6*, e16321
35. Cosmi L, Maggi L, Santarlasci V, Liotta F, Frosali F, *et al.*; *Int Arch Allergy Immunol*, **2007**, *143*, 1
36. Dinsler R, Fousse M, Sester U, Albrecht K, Singh M, *et al.*; *Rheumatology*, **2008**, *47*, 212
37. Alcaide F, Benitez MA, Escriba JM, Martin R; *J Clin Microbiol*, **2000**, *38*, 398
38. Doebler RW, Erwin B, Hickerson A, Irvine B, Woyski D, *et al.*; *J Lab Automat*, **2009**, *14*, 119

# ***Chapter 5***

***A lateral flow immunoassay for  
Mycobacterium tuberculosis detection***

## ***Abstract***

Most current diagnostic assays for tuberculosis have limitations in terms of reliabilities, sensitivities, costs, ease of use or speed, especially limiting implementation in resource-poor areas. In this study we describe the development of a fast, simple, sensitive lateral flow immunoassay (LFIA) allowing visual identification of the *Mycobacterium tuberculosis* (*M.tb.*) antigen. The LFIA employs variable heavy chain (VHH) llama antibodies to identify the 16 kDa heat shock protein (HSP), an immuno-dominant antigen. Recombinant HSP protein was produced and purified from *E. coli*. The assay detected a lower limit of 0.25 $\mu$ g/ml of purified recombinant HSP antigen. In combination with methods to up-concentrate *M.tb.* bacteria from sputum LFIA of HSP may be a simple and affordable method to detect *M.tb.* infections in sputum and identify *M.tb.* in cultures from patients in resource-poor settings.

## **5.1 Introduction**

Despite many efforts, tuberculosis (TB) remains one of the major unsolved global health problems with ~9.4 million new cases every year and an estimated global mortality of 1.4 million people in 2010 [1]. The situation has deteriorated in several parts of the world mainly due to co-infection with human immunodeficiency virus (HIV), and the subsequently acquired immune deficiency syndrome (AIDS), weakening body immunity against TB [2, 3]. Furthermore, the growing problem of multiple drug resistance aggravates the situation especially in resource-poor countries, where implementation of modern methods to control the TB epidemic is lacking [4].

Initial detection of new cases of TB is mainly based on microscopic inspection of sputum smears for acid-fast bacterium. This method provides high detection rates for patients with active TB, but depends on skilled personnel and is too labour intensive [4]. In terms of sensitivity culture techniques are the gold standard for detection of active TB, with the drawback that they take 2-6 weeks to set a diagnosis [5-8]. Culture plating is also the main method for identifying multi-drug resistant (MDR) TB. An ideal TB test for resource-poor areas should be rapid, simple, reliable, low-cost, specific and sensitive.

Nucleic acid amplification tests (NAATs) are a relatively new strategy in active TB detection [9-11]. This technique can amplify even small amounts of genetic material from TB bacteria. The sample used still has to contain a certain minimum (>100/ml) number of TB bacterium that is not always possible. Often by culturing, the number of bacterium is increased to improve the sensitivity of the test before carrying out PCR [12]. NAAT techniques are also used to identify MDR TB strain mutations causing drug resistance [13]. NAATs require expensive and labour intensive readout systems, like PCR, that are only accessible in well-equipped laboratories [14], although a NAAT coupled lateral flow-based readout have recently become available for malaria diagnosis [15].

Antibody based diagnostic assays have been successful for several other infectious diseases [16-18] but in case of TB diagnosis, no significant success has been achieved for several decades [19]. The commercially available antigen based kits are often used to test the supernatants of cultured bacteria and are not suitable for sputum analysis [12]. Further studies on developing these assays for the diagnosis of TB are in progress due to its potential as a fast, simple and reliable detection method.

The continuous search for simplified, portable, rapid, and sensitive detection assays with immediate “on-the-spot” interpretation for diagnosis of infectious diseases has led to the development of biosensors as well as lateral flow immuno assay (LFIA) platforms [19, 20]. These platforms are especially relevant in the context of their adaptability to resource-poor settings, where a sophisticated laboratory infrastructure and highly trained personnel are not available [21, 22]. LFIA is a rapid (10-20 min), one step, and immuno-chromatographic test. Detection of an antigen is done by sandwiching this antigen between capture antibody

(ligand) on/in the nitrocellulose (NC) membrane and detection antibody (ligand) immobilised onto carbon nanoparticles (CNPs).

This study describes the development of an LFIA for the detection of the 16 kDa heat shock protein (HSP), a species-specific dominant antigen present in TB-causing *Mycobacterium sp.* [23]. It employs VHH (variable heavy chain) llama antibodies which are known to be very stable under harsh conditions. The utility of the method for the diagnosis of infectious *M.tb.* in patients is discussed.

## 5.2 Materials and Methods

### 5.2.1 Chemicals

The 100 mM Borate Buffer (100 mM BB) pH 8.8 was prepared by mixing 100 mM solutions of  $H_3BO_3$  (Merck, Darmstadt, Germany) and  $Na_2B_4O_7 \cdot 10H_2O$  (Sigma-Aldrich Chemie BV, Zwijndrecht, Netherlands). BB buffer, Bovine serum albumin (BSA, Sigma-Aldrich Chemie BV, Zwijndrecht, Netherlands) and Tween 20 (Merck, Amsterdam, The Netherlands) were used to prepare Washing Buffer (WB) with 5 mM BB and 1% (w/v) BSA; Storage Buffer (SB) with 100 mM BB and 1% (w/v) BSA; Running Buffer (RB) with 100 mM BB, 1% (w/v) BSA, and 0.05% (v/v) Tween 20).

### 5.2.2 Biomolecules

VHVs raised against the HSP protein of *M.tb.* as described by Trilling *et al.* [23] were produced in *E. coli* BL-21 wild type strain and purified as described [24]. The highest affinity VHH antibodies A-23 and B-F-10 recognizing non-overlapping epitopes were selected for this study [23]. Both A-23 and B-F-10 were either produced with a VSV-tag or AVI-biotin tag. Rabbit anti-VSV-tag antiserum (Abcam, Cambridge, UK) was used to capture the antibody on the NC strip. NeutrAvidin (NA) biotin binding protein was purchased from Pierce, Rockford, IL, USA. Goat-anti-Mouse-biotin was purchased from Dako (Dako Netherlands BV, Heverlee, Belgium). Recombinant HSP target protein of *M.tb.* with AVI- and HIS-tags was also produced in *E. coli* and purified as described by Trilling *et al.* [23].

### 5.2.3 Preparation of nitrocellulose LFIA strips

LFIA strips were manufactured as described by Posthuma-Trumpie *et al.* [25] using NC membranes cut to a length of 20 cm (HF135, Millipore, Amsterdam, Netherlands or CN140 NC membranes with backing, Sartorius Stedim, Göttingen, Germany). The NC membranes were fixed on a plastic backing along with a cellulose absorbent pad (Schleicher and Schuell, 's-Hertogenbosch, The Netherlands). Capture anti-VSV antibody was diluted in 5 mM BB after buffer exchange using Zeba spin columns (Pierce, Rockford, IL, USA). The antibody concentration was measured using a Nanodrop 2000 spectrophotometer (Thermo Scientific, EttenLeur, Netherlands). Dilutions were made in 5 mM BB to meet the following requirements 500, 250 and 125  $\mu\text{g/ml}$ . Alternatively, NA was sprayed as test line in

concentrations of 1000, 500, 250, 125  $\mu\text{g/ml}$ . A Linomat IV TLC dispenser (Camag, Berlin, Germany) was used to dispense the specific antibody (test line, TL) and the biotinylated antibody (control line, CL) on the NC membrane at a dose of 1  $\mu\text{L}/5\text{ mm}$ . Distance between lines was 3 mm. The NC membranes were dried overnight at 37  $^{\circ}\text{C}$ . Finally, strips were cut at a width of 5 mm using a Bio-Dot Cutter CM4000 (Irvine, California, USA), used immediately, or packaged in aluminium pouches (with a silica desiccation pad), sealed and stored at room temperature until use.

### **5.2.4 Preparation of CNPs**

CNPs with adsorbed NA (CNP-NA) were prepared as described by Posthuma-Trumpie *et al.* [26]. Briefly, 10 mg of carbon (Spezial Schwartz 4, Degussa AG, Frankfurt, Germany) was suspended in 1 ml of MilliQ water and sonicated for 5 min (Branson Model 250 Sonifier, Danbury, Connecticut, USA). The resulting 1% (w/v) carbon suspension was 5-fold diluted in 5 mM BB and sonicated for 5 min. Next, 350  $\mu\text{g}$  NA was added to 1 ml of the diluted carbon suspension and stirred for 3 h at room temperature. This suspension was first centrifuged at  $13.636 \times g$  for 15 min; the supernatant was removed and the pellet was washed with WB to remove unbound protein. To achieve this, 1 ml of WB was added to the pellet, thoroughly mixed and the mixture was centrifuged at  $13.636 \times g$  for 15 min. Subsequently, the supernatant was removed and the pellet was re-suspended in 1 ml WB. This process was repeated twice. After the final wash, the pellet was re-suspended in 1 ml SB. The resulting suspension contained 0.2 % (w/v) carbon conjugate CNP-NA. Alternatively, 350  $\mu\text{g}$  of anti-VSV in 5 mM BB was adsorbed on the carbon using the same procedure as described above and resulting in CNP-VSV.

### **5.2.5 Execution of the test**

The LFIA sandwich assay carried out in this study involved spraying of anchoring protein, binding of capture/detection VHH antibody and detection of HSP target protein. The schematics of these steps are shown in Fig. 1 where first the LFIA strip was coated with anti-VSV or NA protein to capture primary VHH antibody with VSV-tag or biotin tag, respectively. The two VHHs bind the HSP target protein at two different epitopes [24]. Hence, the VHH-HSP-VHH complex can be sandwiched between complementary secondary anti-VSV antibody and NA. Both anti-VSV antibody and NA can serve as the capture (bound to the membrane) and the detection ligand (bound to the CNPs).

The test was executed by vertically inserting an anti-VSV or NA coated LFIA strip in wells of a low protein binding 96-wells microplate containing a thoroughly mixed solution of 25  $\mu\text{l}$  of capture VHH with VSV or biotin-tag, 25  $\mu\text{l}$  of HSP target protein dilution, 25  $\mu\text{l}$  of detection VHH with biotin or VSV-tag (all proteins diluted in RB) and 25  $\mu\text{l}$  of RB containing 1  $\mu\text{l}$  of CNP suspension coated with either anti-VSV or NA protein. After running and drying, the strips were inspected visually or, for documentation purposes, were scanned. Here an Epson Perfection V600 scanner was used, and the pixel gray volumes (PGV) were obtained using image analysis software (Total Lab, Nonlinear Dynamics, Newcastle upon

Tyne, UK). Blank correction was performed with an identical non-modified line right below the test line. Pixel grey volume of the blank was subtracted from the result obtained for the test line.

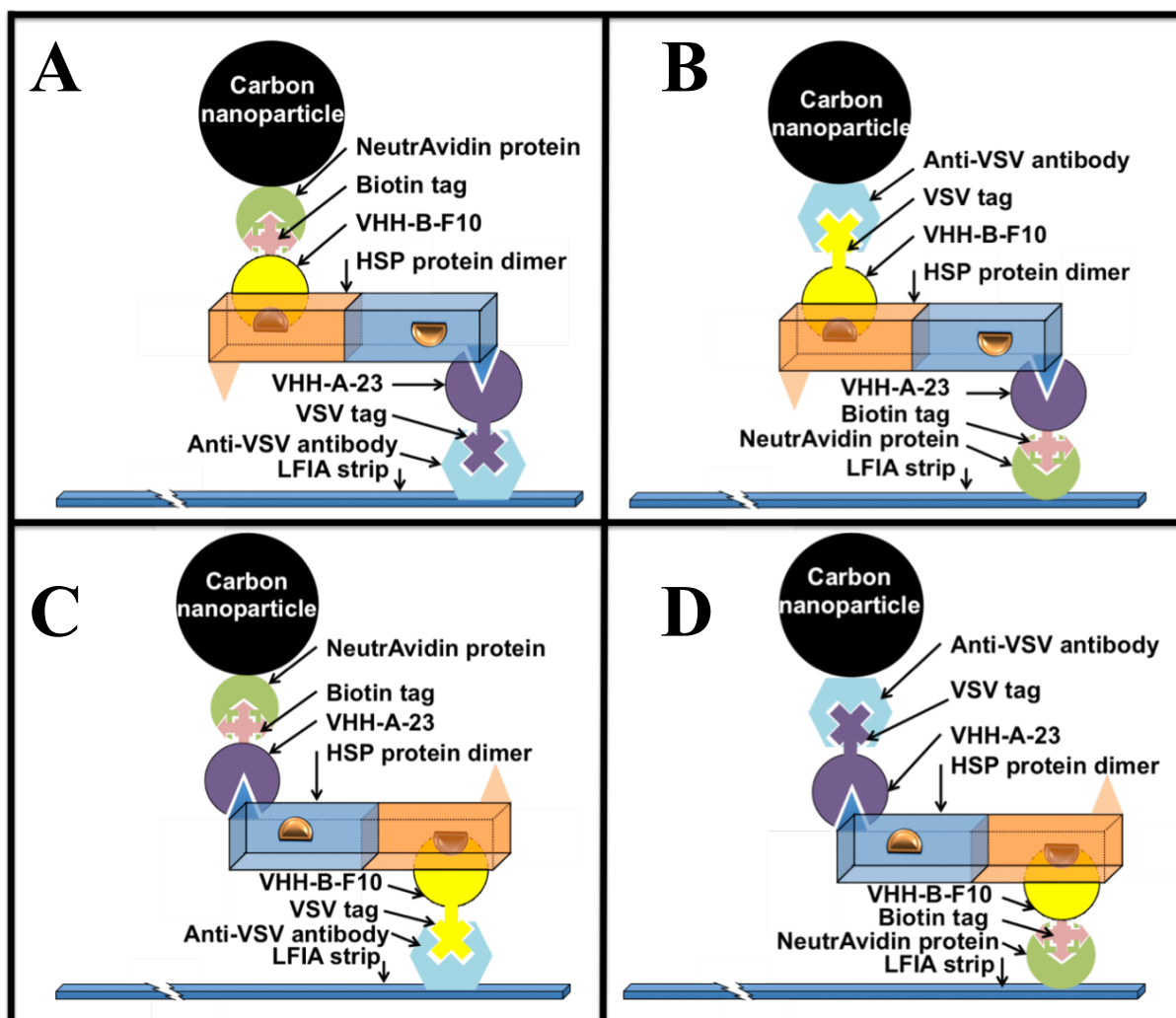


**Figure 1:** Schematic representation of the final LFIA assay sandwich. In each case the anchoring protein on the LFIA strip captures a CNP complex of HSP and two different VHHs by the complementary tag. Panel A: Anti-VSV captures the VHH A-23 with VSV tag and associated complex. Panel B: NA captures the VHH A-23 with biotin tag and associated complex. Panel C: Anti-VSV captures the VHH B-F-10 with VSV tag and associated complex. Panel D: NA captures the VHH B-F-10 with biotin tag and associated complex. The binding model of VHH with HSP is based on Srivastava et al. [24]

### 5.2.6 Determination of a suitable anchoring protein

To determine the best anchoring protein, both anti-VSV and NA were tested on the LFIA strips. For this, either anti-VSV at concentrations of 125, 250 and 500  $\mu\text{g/ml}$  or NA at concentrations of 125, 250, 500 and 1000  $\mu\text{g/ml}$  was sprayed on LFIA strips and dried overnight. An amount of 2  $\mu\text{g/ml}$  capture and detection VHH antibodies in the combinations as described in the scheme of Fig. 1 with either VSV or biotin tag (depending upon the

anchoring protein) was used and mixed with serial dilutions of HSP ranging from 2 µg/ml to 0.25 µg/ml to execute the test. After running and drying the LFIA strips from both experiments, the strips were scanned and analysed as described above.

### **5.2.7 Determination of suitable capture and detection VHH antibodies**

LFIA strips with an anti-VSV concentration of 250 µg/ml were treated with different concentrations and ratios of capture and detection VHH antibodies: both antibodies were tested at either the same (1, 2 or 4 µg/ml) or a different concentration (2 µg/ml capture and 1 µg/ml detection antibody). Antibodies were combined with serial two-fold dilutions of 16 kDa target protein (2 - 0.25 µg/ml). LFIA strips were analysed as described above. Next, whole cell lysate from cultured *Mycobacterium* was tested with 4 µg/ml of both capture and detection VHH. In this experiment - a fixed concentration of 2 µg/ml of whole cell protein lysate from *M.tb.* and *M. smeg.* (a control non-TB causing strain *Mycobacterium smegmatis*) were tested. In order to check whether sequential addition of the two VHH antibodies was preferable over simultaneous mixing, an experiment was done adding the antibody A-23 with VSV tag first followed by HSP, biotinylated antibody B-F-10 and the CNP-NA (Fig. 1A), or in reverse adding biotinylated antibody B-F-10 first followed by the HSP protein, antibody A-23 with VSV tag and the CNP-NA (Fig. 1A). LFIA strips sprayed with 250 µg/ml of anti-VSV were inserted into wells containing these samples and analysed as described above.

## **5.3 Results and Discussion**

### **5.3.1 Determination of a suitable anchoring protein**

For adequate performance of the LFIA test, it was crucial to first identify a suitable anchoring protein concentration to give a sensitive response in the sandwich assay. For this, LFIA strips were sprayed with either anti-VSV or NA at various concentrations. Anti-VSV coated LFIA strips gave a higher response than NA sprayed LFIA strips (Fig. 2). This difference in signal may possibly carry a relationship to the relative purity of the samples or to the fact that NA molecules have four binding sites for the biotinylated VHH antibody, whereas anti-VSV has only two binding sites for the VHH carrying a VSV tags. Overall, anti-VSV was preferred, because the efficiency of binding HSP-CNPs was greatest and the linearity of the response was good. The most linear response to increasing HSP concentrations and lowest background signal was obtained for the 250 µg/ml anti-VSV anchoring antibody concentration, and, therefore, this concentration was chosen for all next experiments.

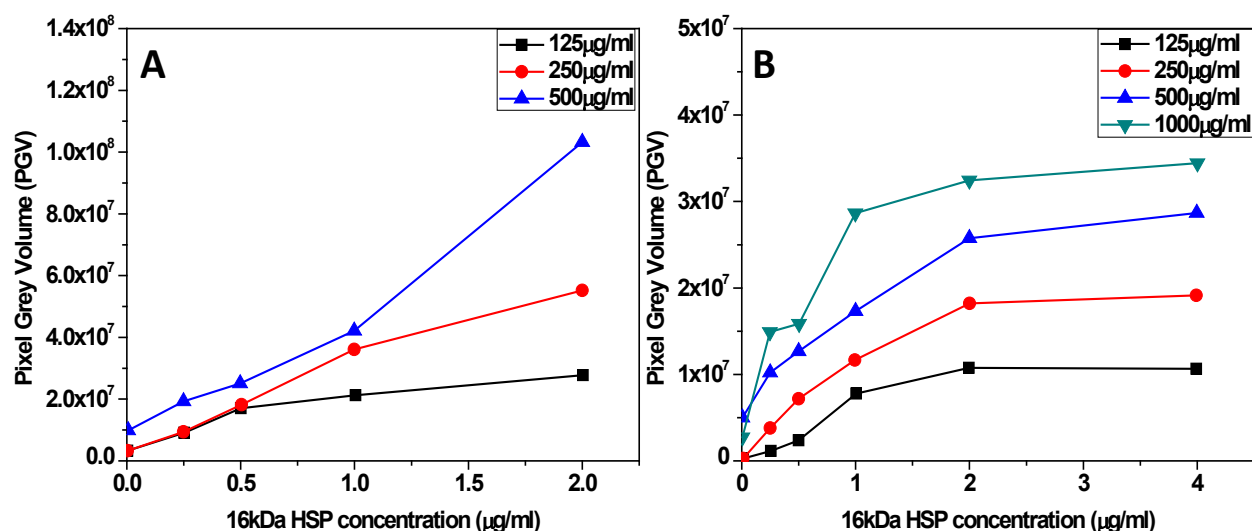


**Figure 2:** LFIA assay responses to different concentrations 16 kDa HSP *M.tb.* antigen with anti-VSV (A) as in Figure 1A or NA (B) as in Figure 1B as capture protein

### 5.3.2 Determination of the suitable capture and detection antibodies

Next, the optimal ratio of the VHH capture and detection antibodies was determined. To evaluate this, an experiment was set up, where either the same concentrations of capture and detection VHH were used, or where the capture VHH concentration was twice higher according to diagram Fig. 1A. Fig. 3 shows that at low HSP concentrations a 2:1 ratio of capture: detection VHH was twice more effective at detecting HSP. The detection VHH at 1 µg/ml was limiting detections above 0.5 µg/ml HSP, however, because a 1:1 ratio at 1 µg/ml of both VHHs would ultimately lead to the same detection sensitivity at 2 µg/ml HSP. Doubling both VHH antibodies to 2 µg/ml only yielded a small increase in total signal, suggesting that the 2:1 ratio of capture: detection VHH is more optimal. This can be understood from Fig. 1A where it is sterically possible for the HSP-CNP complex to be captured by two molecules of VHH-A23 which may be critical for this antibody which is weaker than VHH-BF10. For best sensitivity and a greater linear response concentrations of 4 and 2 µg/ml capture and detection VHH (or even higher concentrations at that ratio) may be the best compromise, but a 1:1 ratio was chosen in the remaining experiments because of the good linear response in Fig. 3.

The optimal concentration and combination of VHH antibodies A-23 or B-F-10 as either capture or detection antibody, was tested by comparing the detection efficiency of the recombinant 16 kDa HSP protein (Fig. 4). At a concentration of 4 µg/ml VHH signals obtained were similar irrespective of the combination of capture or detection VHH. At lower concentrations it was more effective if the B-F-10 VSV-tag was used as capture antibody (Fig. 4B). In that configuration 2 µg/ml gave the best linear signal.

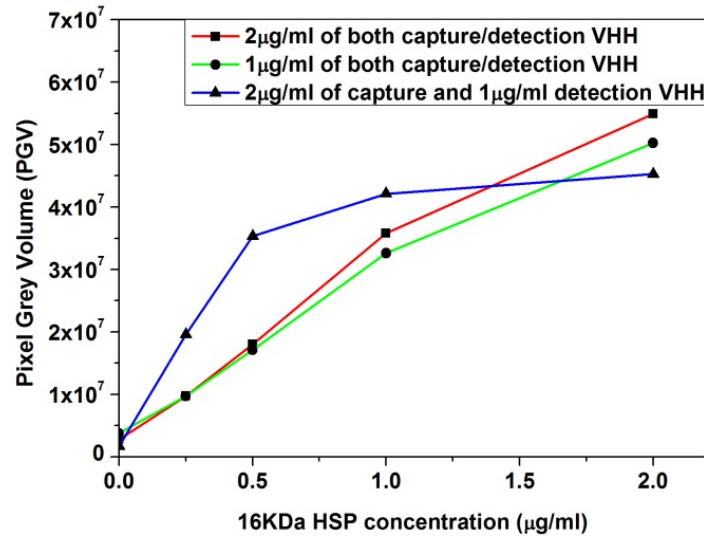


**Figure 3:** LFIA assay results in relation to different combinations of capture and detection VHH antibodies. Anti-VSV was sprayed on the LFIA strip at 250µg/ml. Capture VHH was A-23 with VSV tag, detection VHH was biotinylated B-F-10 as in Figure 1A

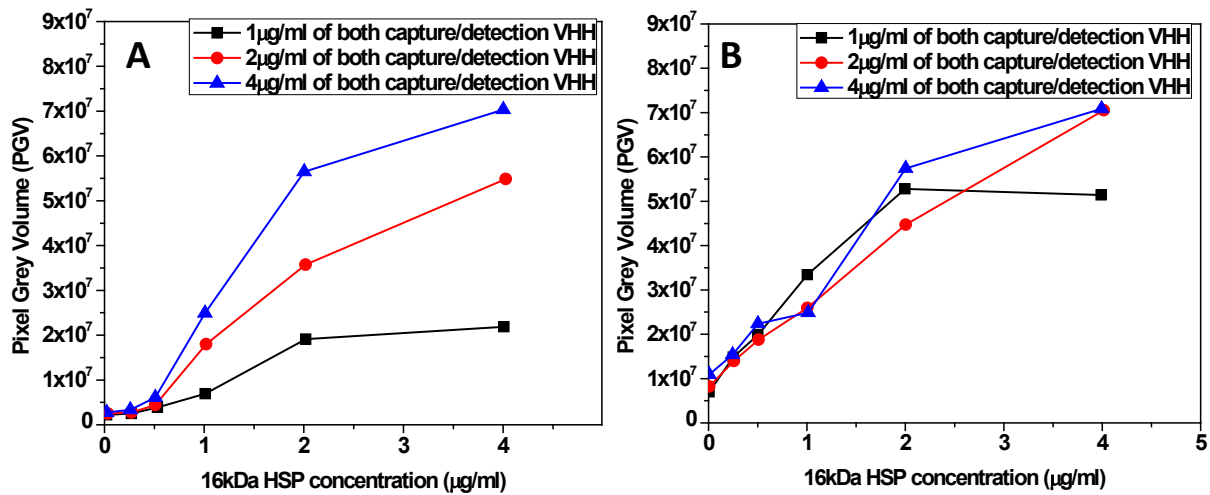


**Figure 4:** Tests of the effect of exchanging capture and detection antibodies at different concentrations on anti-VSV sprayed LFIA strips. Panel A: LFIA assay response with VHH A-23 with VSV-tag as capture and biotinylated B-F-10 as detection antibody as in Figure 1A. Panel B: LFIA assay response with VHH B-F-10 with VSV-tag as capture and biotinylated A-23 as detection antibody as in Figure 1C

For whole cell lysate from cultured *Mycobacterium*, we confirmed that also here the best response was obtained when VHH B-F-10 was used as capture antibody. Fig. 5 shows a comparison of signals obtained for both situations and compared to the low signal from the non-tuberculosis causing strain *M. smeg*. Remarkably the signal strength of the crude lysates was double that of the purified recombinant HSP samples at the same protein concentration. This was unexpected but the reason could be that recombinant HSP with protein tags for purification may have a different and less accessible conformation for VHH binding compared to the native protein.

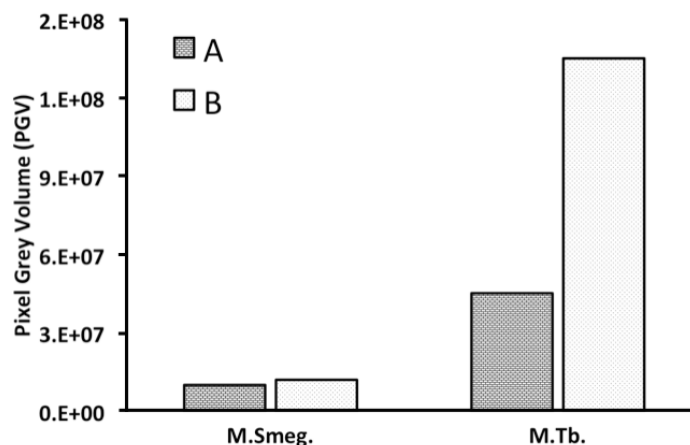


**Figure 5:** Tests of the effect of exchanging capture and detection antibodies on *M. smegmatis* and *M. tuberculosis* samples using anti-VSV sprayed LFIA strips. VHH were used at 4 $\mu$ g/ml. Treatment A: VHH A-23 with VSV tag was used for capture and biotinylated VHH B-F-10 was used as detection antibody. Treatment B: VHH B-F-10 with VSV tag was used as capture and biotinylated A-23 was used as detection antibody

To evaluate the effect of sequential rather than simultaneous addition of the two VHH antibodies i.e. A-23 and B-F-10 to wells containing 16 kDa HSP and CNP-NA, it was observed that when antibody A23-biotin was incubated first with the 16 kDa HSP protein and CNP-NA a higher signal was obtained compared to incubating B-F-10-VSV first (Fig. 6). These results are in agreement with the results obtained by Srivastava *et al.* [24] on a surface plasmon resonance (SPR) platform. There, we also showed that the capture of the HSP dimer on a surface (SPR chip there, CNP here) is best done first with VHH A-23 which has both epitopes facing to the capture surface (Fig. 1C), leaving room for subsequent binding of the 16 kDa HSP by B-F-10. Quite possibly if B-F-10 is added first, a coagulation reaction occurs removing a lot of HSP dimer from effectively binding to CNPs.

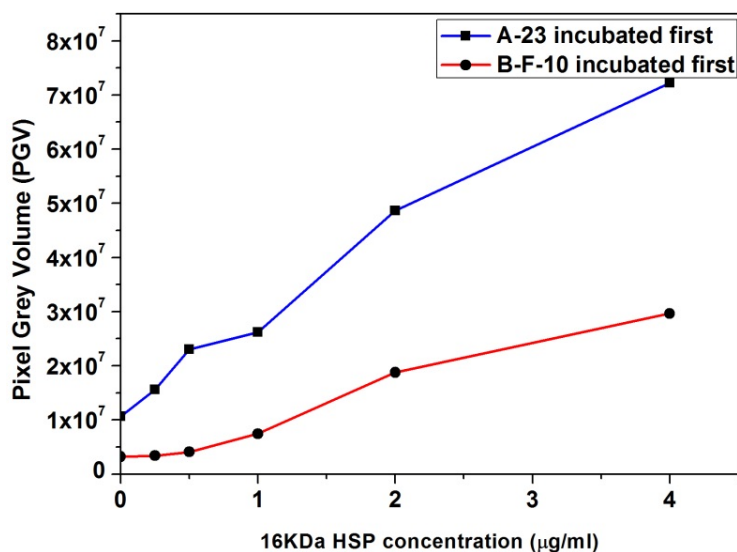


**Figure 6:** LFIA assay response obtained with anti-VSV sprayed LFIA strips when either A23-VSV or B-F-10-VSV was pre-incubated first with 16 kDa HSP protein, followed by the capture VHH (biotinylated A-23 or B-F-10) and CNP-NA of the running mix

### 5.3.3 Sensitivity of HSP detection in sandwich LFIA

The exact amount of 16 kDa HSP protein present in the whole cell lysate was not known. For this reason, recombinantly produced and purified 16 kDa HSP protein in *E. coli* was utilized to demonstrate the sensitivity of the system. Fig. 7 shows the LFIA response at concentration series of 4, 2, 1, 0.5 and 0.25  $\mu\text{g/ml}$  of recombinant 16 kDa HSP. The lowest concentration of 0.25  $\mu\text{g/ml}$  was clearly detected above background in repeated tests. Tests used only 25  $\mu\text{l}$  of sample. A concentration of 0.25  $\mu\text{g/ml}$  16 kDa HSP dimer, therefore, corresponds to an actual protein quantity of 6.25 ng and a concentration of approximately 6 nM just 10-fold above the dissociation constants of these antibodies for HSP. Thus, we conclude this assay to be highly sensitive and potentially effective as a tool to identify *M.tb*.

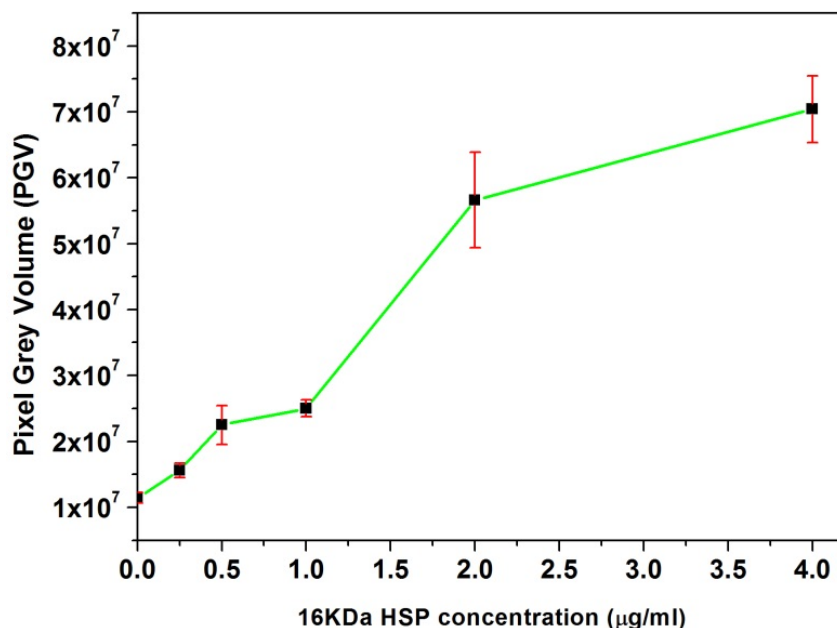


**Figure 7:** LFIA assay response of an anti-VSV sprayed LFIA strip with A23-biotin as detection and B-F-10-VSV as capture antibody for detection of 4 to 0.25  $\mu\text{g/ml}$  16 kDa HSP

### 5.4 Conclusion

A lot of work has been done over the last few decades to develop fast and effective assays for the detection of TB under field conditions that are cheap and robust. These assays mainly focus on detection of TB by measuring the serum response to HSP antigens, identifying *M.tb* cells in sputum or detecting biomarkers in urine [27, 28]. Conventional assays, such as radiometric immunoassays, flow cytometry, rapid cultivation techniques or sputum cultures for acid-fast bacterium are often not sensitive enough or too time-consuming [28-31]. Techniques like nucleic acid amplification are fast and sensitive, but they are complex, expensive and require skilled personnel with high quality standards [5].

The LFIA based platform described here may present a useful alternative by providing an affordable, fast, simple, sensitive and instrument-independent solution for the visualization and identification of 16 kDa HSP protein from lysed *M.tb*. The method identifies a dominant antigen, i.e. the 16 kDa HSP, which is a cell internal protein associated

with the membrane and also known to be a major contributor to the pathogenicity of the TB causing *Mycobacterium* strain. The 16 kDa HSP is produced extensively during the latent phase, and helps the bacterium to survive inside macrophages during latency [24]. The lower limit of detection for LFIA was 0.25µg/ml (6nM) of HSP antigen in 25µl solution. Initially with fresh antibodies and antigen (both recombinant and from *M.tb.*), the results obtained in first series of experiments were reproducible but for the second and third series of experiments the signal deteriorated and were also not reproducible. The main issue which still needs to be addressed is to make the method practical for the detection of *M.tb.* in sputum samples is the pre-concentration of *M.tb.* cells from sputum and a simple cell lysis protocol to obtain a concentrated protein extract. Pre-concentration of *M.tb.* cells from liquefied sputum samples could, for example, be done using magnetic TB-Beads [32] or the up-concentration method described in former chapter, followed by controlled lysis of the bacteria using mechanical or ultrasonic [33] lysis methods.

## References

1. Global Tuberculosis Report; *World Health Organisation (WHO)*, **2012**
2. Kranzer K, Houben RMGJ, Glynn JR, Bekker L-G, Wood R, *et al.*; *Lancet Inf Dis*, **2010**, *10*, 93
3. Swaminathan S, Padmapriyadarsini C, Narendran G; *Clin Inf Dis*, **2010**, *50*, 1377
4. Watterson SA, Drobniewski FA; *J Clin Pathol*, **2000**, *53*, 727
5. Landowski CP, Godfrey HP, Bentley-Hibbert SI, Liu XY, Huang ZS, *et al.*; *J Clin Microbiol*, **2001**, *39*, 2418
6. Pottumarthy S, Wells VC, Morris AJ; *J Clin Microbiol*, **2000**, *38*, 2227
7. Gennaro ML; *Clin Inf Dis*, **2000**, *30*, S243
8. Chan ED, Heifets L, Iseman RD; *Tubercle Lung D*, **2000**, *80*, 131
9. Ling DI, Flores LL, Riley LW, Pai M; *PLoS One*, **2008**, *3*, e1536
10. Davis JL, Huang L, Worodria W, Masur H, Cattamanchi A, *et al.*; *PLoS One*, **2011**, *6*, e16321
11. Laraque F, Griggs A, Slopen M, Munsiff SS; *Clin Inf Dis*, **2009**, *49*, 46
12. Steingart KR, Henry M, Laal S, Hopewell PC, Ramsay A, *et al.*; *PLoS Med*, **2007**, *4*, 1417
13. Felkel M, Exner R, Schleucher R, Lay H, Autenrieth IB, *et al.*; *Eur J Microbiol Immunol*, **2013**, *3*, 252
14. Yang S, Rothman RE; *Lancet Inf Dis*, **2004**, *4*, 337
15. Mens P, Moers A, de Bes L, Flint J, Sak J, *et al.*; *Malaria J*, **2012**, *11*, 1
16. Granberg C, Mansikka A, Lehtonen OP, Kujari H, Gronfors R, *et al.*; *J Clin Microbiol*, **1993**, *31*, 1453
17. Matter L, Germann D; *J Clin Microbiol*, **1995**, *33*, 2338
18. Taye A, Chen H, Duncan K, Zhang Z, Hendrix L, *et al.*; *Ann N Y Acad Sci*, **2005**, *1063*, 280
19. Shen GM, Behera D, Bhalla M, Nadas A, Laal S; *Clin Vaccine Immunol*, **2009**, *16*, 49
20. Zhou LX, He XX, He DG, Wang KM, Qin DL; *Clin Develop Immunol*, **2011**, 193963
21. Hamasur B, Bruchfeld J, Haile M, Pawlowski A, Bjorvatn B, *et al.*; *J Microbiol Methods*, **2001**, *45*, 41
22. Diagnostics for tuberculosis: Global demand and market potential; *WHO*, **2006**
23. Trilling AK, de Ronde H, Noteboom L, van Houwelingen A, Roelse M, *et al.*; *PLoS One*, **2011**, *6*, e26754
24. Srivastava SK, Ruigrok VJB, Thompson NJ, Trilling AK, Heck AJR, *et al.*; *PLoS One*, **2013**, *8*, e64040
25. Posthuma-Trumpie GA, Korf J, van Amerongen A; *Anal Bioanal Chem*, **2009**, *393*, 569
26. Posthuma-Trumpie GA, Wichers JH, Koets M, Berendsen LB, van Amerongen A; *Anal Bioanal Chem*, **2012**, *402*, 593
27. Minton K; *Nat Rev Immunol*, **2003**, *3*, 355
28. Bhaskar S, Banavaliker JN, Hanif M; *FEMS Immunol Med Microbiol*, **2003**, *39*, 235
29. Cosmi L, Maggi L, Santarlasci V, Liotta F, Frosali F, *et al.*; *Int Arch Allergy Immunol*, **2007**, *143*, 1
30. Dinser R, Fousse M, Sester U, Albrecht K, Singh M, *et al.*; *Rheumatology*, **2008**, *47*, 212
31. Alcaide F, Benitez MA, Escriba JM, Martin R; *J Clin Microbiol*, **2000**, *38*, 398
32. Wilson S, Lane A, Rosedale R, Stanley C; *Int J Tubercul Lung D*, **2010**, *14*, 1164
33. Doebler RW, Erwin B, Hickerson A, Irvine B, Woyski D, *et al.*; *J Lab Automat*, **2009**, *14*, 119







# ***Chapter 6***

***A generic microfluidic biosensing module  
for nanowire-based FET measurements***

*Manuscript under prepration.*

## *Abstract*

Biosensors allow label-free measurement of targets or analytes with ample opportunities for multiplexing and miniaturisation relevant for point-of-care assays. Integration of microfluidics brings the added feature of sequential measurements allowing high throughput screening. Here, we report the realization of a compact modular biosensing system capable of carrying out nanowire based FET detections within a microfluidic flow cell. The flow cell is re-sealable on the sensing area of the biosensor chip allowing the attachment of biological capture molecules prior to analysis. The nanowire chips have a size of  $10 \times 15$  mm with 10 outer electrode connections. The module incorporates a printed circuit board soldered with spring probes in contact with the sensing device platform and allows switching between AC impedance and DC conductivity measurements. The flow system is coupled to a set of syringe pumps with valves that allow for automated injection of defined volumes of analyte at a constant flow of buffer. We demonstrate that the nanowire DC conductivity responds predictably to sequential injections of different iso-ionic pH solutions, and that the sequential binding of proteins (streptavidin, antibody, protein ligand) to the surface can be followed in real time with AC impedance spectroscopy of the nanowire.

## **6.1 Introduction**

Clinical analyses based on point-of-care diagnostics require dynamic, rapid and reliable read outs to diagnose diseases without compromising on sensitivity [1]. For this purpose diagnostics based on micro- and nanosystems are being developed which include the use electronic, optical, and mechanical (piezo) actuation principles [2-8] to replace automated analytic systems using classical microtiter plate-based assays [9]. Most current diagnostic assays typically rely on optical spectroscopy, mass spectroscopy, gel electrophoresis or other molecular diagnostic assays which are inherently complex, expensive and often low-throughput due to static or no flow sampling methods [10]. Though these techniques are specific and highly sensitive, they are challenging to miniaturize.

Electrical detection techniques can detect analytes with similar sensitivity to optical techniques [11]. They are different from other bioanalytical systems in the sense that they could provide a direct conversion of a biophysical or biochemical event to an electronic signal, which are detected in real time thereby facilitating rapid and convenient sensing assays [12]. Nanowire (NW) based sensors are electrical sensors which are potentially powerful tools to achieve ultra-sensitive reversible assays due to their large surface to volume ratio and semiconductor properties. They enable the direct electrical detection of changes in the charge density on or near the sensor surface [13]. Since the initial report in 1999 [14, 15] there has been an increased interest towards utilizing NW-based sensors to study the capture of biological entities such as DNA, proteins, viruses, bacteria and cells [16-23]. Biological sensing layers coated on specific NWs can be used as bio-detection platforms to detect captured species in the immediate vicinity of the NW [24]. Both metallic and semiconducting NWs have been used for biological sensing. However, the electronic properties of semiconducting NWs enable a better signal-to-noise ratio and thus a higher sensitivity. A direct electrical readout is also favourable, which is highly attractive for many applications in life sciences and medicine [16, 25, 26]. Due to advances in nanotechnology, NW-devices can also be readily integrated into miniaturized systems thus facilitating the use of above-stated characteristics, which - in turn - would avoid the tedious and time-consuming process of labelling chemistry [11, 25, 26]. Lieber and co-workers were the first to make semiconducting NWs in a field effect transistor (FET) configuration using a bottom-up approach [13-15]. Due to the presence of a thin layer of oxide on top of the NWs, initial experiments were focused on pH, ion sensing, and also the detection of charged biological macromolecules in aqueous solutions including proteins and DNA [13]. This was done with a so-called backgate electrode configuration, without a reference (front or solution gate) electrode.

Ion-sensitive field-effect transistors (ISFETs) are field-effect transistors devices that are designed for sensitive measurement of changes of specific ion concentrations in solution, through monitoring of the current through the transistor in combination with an ion selective coating. ISFETs were aimed for electrophysiology measurements where local ion concentrations as well as their potentials could be measured. For pH/ion sensing, Bergveld determined that planar ISFETs, displaying a typical Nernst limit behaviour, have a maximum

sensitivity limit of 59 mV/pH [27]. However, more recently, Knopfmacher [28] and Go *et al.* [29] have shown that dual-gated NW-based ISFETs can go beyond the Nernst limit, thereby amplifying small signals that are typical for (bio)chemical sensing at the nanoscale [27, 30]. Thus, NWs were evaluated under ISFET configurations with conventional planar ISFETs as benchmarks [31]. For biosensors, the most commonly used insulating surfaces are SiO<sub>2</sub> and Si<sub>3</sub>N<sub>4</sub>, which have been well studied due to their CMOS compatibility although other surfaces such as ZnO, In<sub>2</sub>O<sub>3</sub>, Ta<sub>2</sub>O<sub>3</sub>, GaN, etc. have been explored as well [32-35]. With the development and integration of new device concepts, optimization of the nanosensor devices and their properties is still going on [25].

The sensor performance is critically dependent on the binding efficiency of ligands (biological agents such as antibodies) to the sensor surface. Control of surface (bio)chemistry is, therefore, a critical first step. The sensor performance also depends on the binding of the chemical species and the orientation of the biological agents. The chemistry needs to be tuned to ensure minimal distance between the NWs with the biological sensing entities [36, 37] in the order of a few nm. Binding on surfaces can be influenced by a number of factors that could enhance molecular binding to surfaces through electrostatic, covalent or simply physical interactions [37-39]. Microfabricated electronic devices have surfaces and interfaces that could easily be tuned by adopting different surface modification strategies [40]. The need to develop point-of-care diagnostics leads to high demands to increase the throughput, reduce the size and concentration of samples, and lower the cost without compromising on sensitivity. Implementation of microfluidics provides an excellent solution to these needs. Microfluidics allows the user to control assay time by means of flow rate, mixing, multiplexing and parallel assay designs. Furthermore the assay analysis in such systems is improved as the ligand kinetics is visualized in both on and off rates for ligand binding for example. During the past decade, there has been a strong trend to realize compact microfluidic NW-based biosensing platforms which can monitor specific analytes in a continuous flow format [41-44]. These platforms are still under development and differ in their designs to carry out reliable measurements.

In this report, we describe our own design of a compact, modular, microfluidic biosensing platform and its capability for carrying out NW-based electrical detections inside a re-sealable flow cell. The system is coupled to a set of syringes with valves and syringe pump which allows automated injection of defined volumes of analyte solution and a constant flow of buffer. We demonstrate its application for pH measurements and protein interactions using silicon NW FETs.

## 6.2 Experimental

### 6.2.1 Materials

All chemicals used in the present study were of analytical grade and supplied by Sigma Aldrich. They were used as received. The solutions were prepared using demineralized water (resistivity 18.2 MΩ-cm) obtained using Pure lab Ultra from Elga Lab solutions. The

buffers for pH experiments (pH 4 to pH 7) were prepared using 0.1 M citric acid/0.2 M dibasic sodium phosphate solutions with an ionic strength of 100 mM [45]. A 2% Hellmanex II solution in demineralized water was used for cleaning of new as well as used substrates. Also a 2% HF was utilised for cleaning and surface activation of the new as well as used substrates prior to surface functionalization.

### **6.2.2 NW FET devices**

The p-type, {100} surfaces SiNW (silicon nanowire) FET array devices were fabricated in the class 100 cleanroom (Dimes, Delft University of Technology, The Netherlands) on 4-inch SOI wafers from which SiNWs were patterned via plane dependent etching using photoresist developer which are conventional wafer-scale process without the use of e-beam nanolithography. The width of the SiNWs varied between 100-300 nm while their lengths were 7, 10, 30 and 50  $\mu\text{m}$  depending on application [46, 47]. For both pH and protein sensing, SiNWs with length of 30  $\mu\text{m}$ , height of 300 nm and a width of 300 nm were utilized.

### **6.2.3 Surface modification procedures**

For surface modification, the sensing device was subjected to cleaning via dipping in 2% Hellmanex II solution for 30 sec followed by surface activation with a 2% HF solution for 3 sec. The clean sensing device now obtained was then modified with APTES, which was coated overnight in a desiccator via a chemical vapour deposition method [48].

### **6.2.4 Biosensing measurement setup**

The sensing module along with the sensing chip was coupled to an automated fluid syringe injection pump Chemyx Fusion200 and through BNC connectors to the electronic measurement system, i.e. Autolab PGSTAT302N and/or Keithley 2612A. For pH experiments only the dual channel Keithley 2612A was used, where one channel, i.e. source measure unit (SMU), was utilized to monitor the time-dependent response of different pH buffers, while the second channel/SMU was used to provide the back gate. For the protein binding and antibody-antigen interactions, the Autolab PGSTAT302N was used to provide frequency-dependent AC excitation and monitoring of the time-dependent response, while a Keithley 2612A was utilized for providing the back gate. Data acquisition and automated control of instruments for Autolab PGSTAT302N were carried out using Nova software (V-10.1). Fig. 1 shows the connection scheme of the biosensing platform hosting the biosensing module, the syringe pump with different microfluidics connections and the measurement instruments. A syringe pump that supplied a constant flow of buffer controlled the microfluidics. Injection of ligands was done using an injection valve. An opening in the sensing module right above the sensing area enables optical access to physico-chemical events on the sensing platform.

Prior to the insertion of the flow cell into the flow cell holder (detailed description in section 3.1), the inlet and the outlet of the flow cell channels were manually filled with working buffer to prevent the trapping of air bubbles in the channels during the assembly. The re-sealable flow cell of volume  $\sim 10 \mu\text{l}$  was created by a silicone ring gasket of 4 mm inner diameter and 1 mm height, which created a closed gasket when it was pressed on the sensing device with screws of the flow cell holder. For the sequential injection of a series of predefined volumes of analyte/ligand-spiked buffer over the sensing chip using a piece of capillary tubing of defined length. Characterizations of FET SiNW devices were done under DC mode (I-V sweeps), whereas impedance measurements were done in AC mode for time-dependent measurements. An excitation voltage of 10 to 100 mV and frequencies up to 1 kHz were used for these measurements.

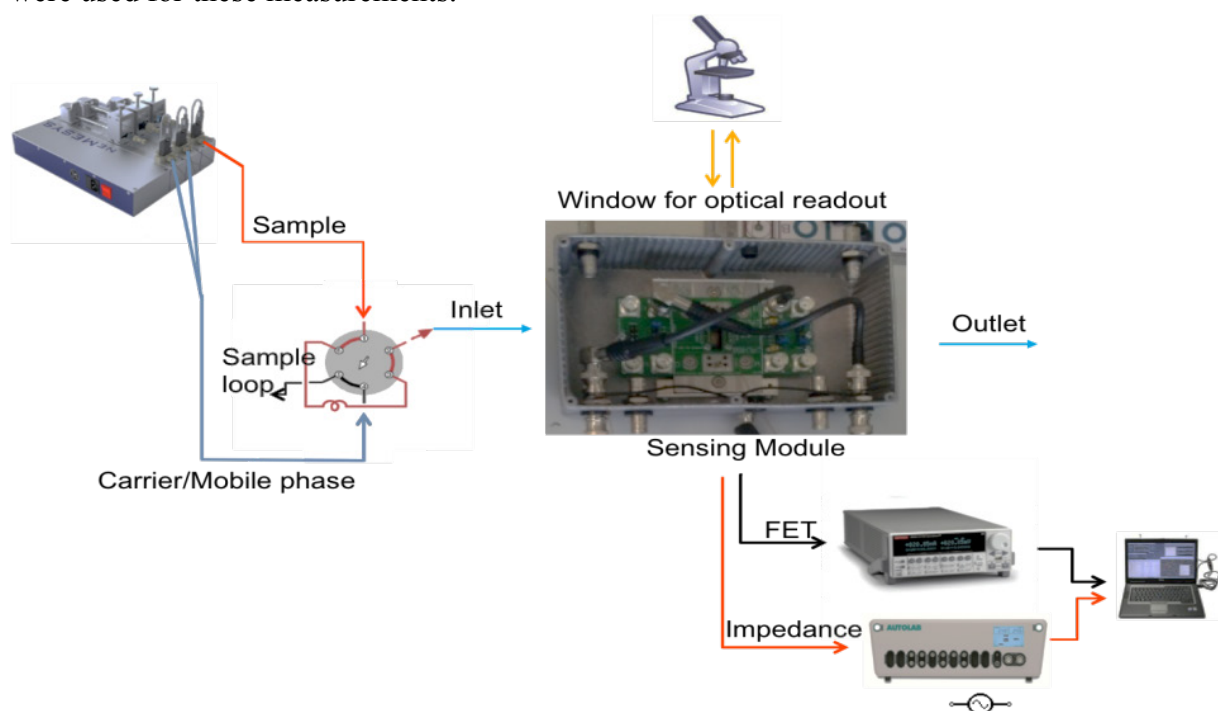


**Figure 1:** Schematics of the biosensing measurement platform with the syringe pump along with the connection scheme of the biosensing module, hosting the sensing chips. The schematics of sensing platform are shown in more detail in the section 3.1

### 6.2.5 pH sensing

To evaluate the performance of the NW FET sensing module, pH measurements were performed on non-functionalized SiNW chips with NWs of 30  $\mu\text{m}$  in length, 300 nm in height and 300 nm in width [46, 47]. A continuous flow of 10  $\mu\text{l}/\text{min}$  of 0.1 M citric acid/0.2 M dibasic sodium phosphate buffer at pH 7 and an ionic strength of 100 mM was applied to the chip. Simultaneous injections of citrate-phosphate buffers of pH 4 or pH 5 for 4 min over continuous flow of pH 7 with an ionic strength of 100 mM were carried out at intervals of 8 min using 4-way valves. Effects of flow rate were studied with a 100 mM citrate-phosphate buffer (pH 4) at flow rates of 0, 5, 10, 15, 20, 25, 30, 40 and 50  $\mu\text{l}/\text{min}$ . Drain currents were recorded online in all cases. The experiments were performed at gate-source voltage ( $V_{\text{gs}}$ ) of -

5 V and drain-source voltage ( $V_{ds}$ ) of 4 V. The SiNW is a p-type accumulation mode device, which means that there is already a measurable drain current at zero gate-source voltage. On applying a negative gate-source voltage the device will be brought in a higher conductive state.

### 6.2.6 Protein sensing

To demonstrate the biomolecular sensing properties of the NW FET, the step-by-step binding of various proteins to the surface was studied. To this end, the FET NW chip was first coated with APTES as described above, followed by a coupling reaction to a PEGylated biotin reagent EZ-Link NHS-PEG12-Biotin (EZ-link in short, obtained from Thermo Fischer Scientific, The Netherlands). In  $0.1 \times$  PBS pH 7.5, EZ-link reacted with the exposed amino groups present on the APTES-modified NW FET surface in 30 min [49]. Activated chips were then mounted in the sensing module and binding of 50  $\mu$ l of 1 nM streptavidin dissolved in  $0.1 \times$  PBS pH 7.5 was measured. Then, 35  $\mu$ l of 5  $\mu$ g/ml, i.e. 300 nM biotinylated VHH llama antibody A-23 was applied [50, 51] in  $0.1 \times$  PBS pH 7.5. Then 65  $\mu$ l 100 ng/ml, i.e. 2.5 nM of *mycobacterium tuberculosis* specific 16 kDa antigen recombinantly produced in *E.coli*, in  $0.1 \times$  PBS pH 7.5 was applied [50]. The experiments were performed at a gate-source voltage ( $V_{gs}$ ) of -20 V and drain-source voltage ( $V_{ds}$ ) of -0.1 V, while the flow speed for all the experiments were kept constant at 10  $\mu$ l/min.

## 6.3 Results and discussion

### 6.3.1 Construction of the sensing module

The prototype biosensing module described here was a compact module that comprised of the following components: a borosilicate glass flow cell with gasket, silicon NW FET with 10 contact pads, a metal flowcell/chip holder and a printed circuit board (PCB) with solder mounted spring probes for connecting to the sensing device. These items were all assembled inside a die-cast aluminium metal alloy LM24 Faraday cage that excluded environmental noise from light and electromagnetic interference along with enabling easy connectivity to the signal readout systems. All components are described in more detail below.

#### 6.3.1.1 Microfluidic flow cell

The top part of the flow cell measured 45 mm  $\times$  15 mm  $\times$  1.5 mm, but the gasket forming the actual flow cell with the NW FET was only 4 mm in diameter (10  $\mu$ l in volume) (Fig. 2). The fluids were supplied to the inlets through plastic tubing with an inner diameter of 250  $\mu$ m, while the outlet tubing had an internal diameter of 750  $\mu$ m to prevent pressure build-up in the flow cell. The top part of the flow cell consisted of two borosilicate glass slides fused together by heating at high temperatures. The top part has an etched fluidic channel to lead the fluid inlet and outlet to the sensing area confined in a gasket of 5 mm in diameter and 1 mm in height. The bottom slide sealed the patterns of the top part and encased

the fluid inlet and outlet to the gasket covered area (Fig. 1). The gasket was either applied to the glass surface using a robotic glue dispenser before it was cured onto a soft elastic material or simply based on a standard natural rubber O-ring. The glass flow cells used here did not leak under a wide range of flow rates from 1  $\mu\text{l}/\text{min}$  to 100  $\mu\text{l}/\text{min}$ .

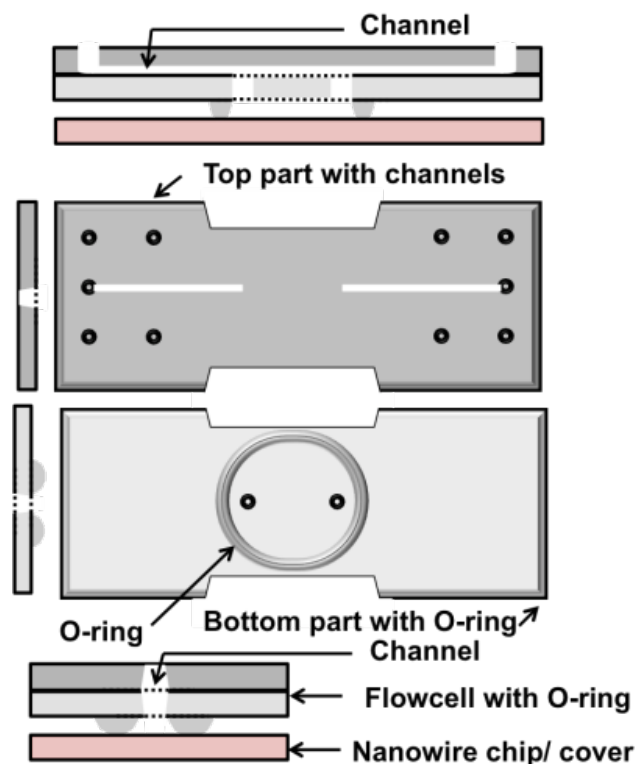


**Figure 2:** Schematic drawing of the construction of the glass flowcell: The top part of the flow cell is made from two fused borosilicate glass sheets (dark and light gray), of which the top one contains a series of holes (black circles) for connecting fluidics along with two etched channels open to the top and two openings for entry/exit to the O-ring compartment and the lower one only contains the two openings for entry/exit to the O-ring compartment (black circle inside the O-ring). The fused glass top part is pressed on the NW chip separated by the flexible O-ring seal thus creating the flow cell

### 6.3.1.2 The flowcell/chip holder

The flow cell and the electronic sensing device are placed inside a compact holder, consisting of two parts. The bottom part of the holder is made up of Teflon that contained slots for placement and alignment of the chip die and the flow cell. The top part is a stainless steel lid that consists of the inlet and outlet for fluidic interconnects to the glass flow cell; as well as a pin-based electrical spring contacts for connecting the contact pads of the sensing chip with the electrical measurement device. To obtain leakage-free flow cells, the top part of the holder is fastened with screws. The holder had dimensions of  $l \times b \times h$ : 8 cm  $\times$  5.5 cm  $\times$  0.56 cm and slot dimensions for placing the flow cell of  $4.5 \pm 0.03$  cm  $\times$   $1.5 \pm 0.03$  cm  $\times$  0.39 cm, and slot dimensions for placing the sensing device of  $1.5 \pm 0.03$  cm  $\times$  1 cm  $\times$  0.17 cm (Fig. 3).

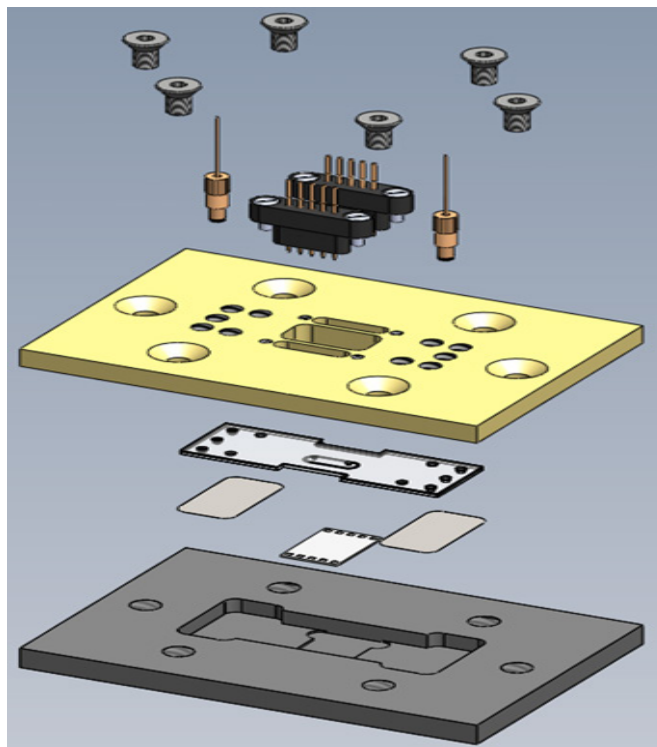


**Figure 3:** Schematics of flowcell/chip holder: sketch showing the Teflon/metal bottom plate where the chip is hosted under a glass flowcell and the top metal part along with the fluidic and electronic connections

### 6.3.1.3 PCB module and the measurement box

The PCB layout is a crucial part of the sensing module, allowing high-quality connectors and switching between AC/DC impedance spectroscopy and NW FET measurements. Switching between DC-based FET measurements and AC-based impedance measurements could be done by the switch indicated in brown in the PCB layout (Fig. 4). The PCB layout had an open window over the sensing chip to enable optical observations. Five soldered mounted spring contacts on either side of this window on the PCB enabled electrical connections to the contact pads of the sensing chip. In addition, the PCB sits in such a way on the flow cell holder, that the micro-fluidic connections are not hindered. The sensing module and measurement setup were grounded via the PCB.

In order to carry out AC-based impedance measurements between pins on either side of the optical window, jumpers are inserted in the respective red boxes between A and D or B and C to establish the connections to the desired pairs of pins where the electrode measurements can be performed. For DC-based FET measurements, connection to the source and drain were realized using BNC connectors to “drain high” and “source low”, with biasing using “gate high” and “gate low”. T-connectors were used to couple the “source low” and “gate low” BNC connections and to keep the entire module at ground potential. Additional sets of BNC sockets were provided for carrying out parallel reference measurements simultaneously.

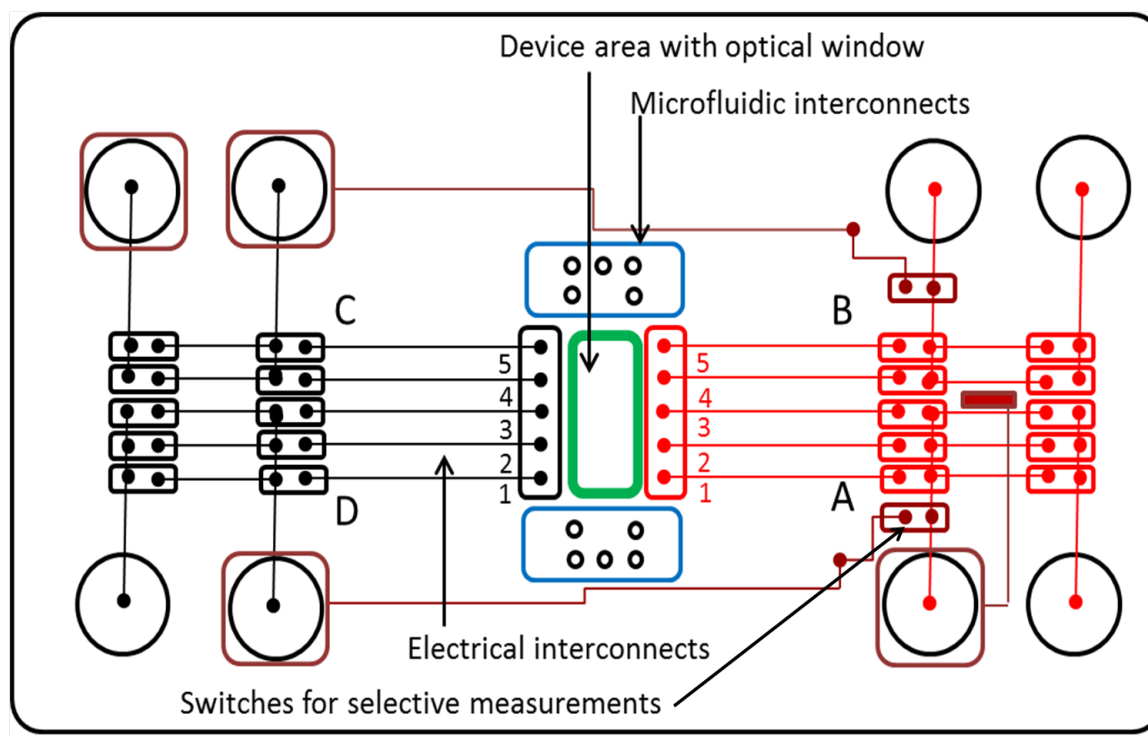


**Figure 4:** Schematics of the PCB layout, used for connecting the NW chip with the readout electronics with two independent, two-point connection systems, i.e. between point A-D and B-C for parallel measurements. A set of two independent BNC connector is available at each point, i.e. A, B, C and D for connection to two adjacent devices, e.g. 1 and 2. (further described in 3.1.3)

### 6.3.2 Platform characterization using NW FET pH sensing

Lieber and co-workers have previously shown how the solution pH affects source-drain currents of functionalized and non-functionalized silicon NWs [13]. The non-functionalized  $\text{SiO}_x$  surfaces are acidic in nature ( $\text{p}K_a=4$ ). The charges induced on the NW surface are dependent on charge polarity of the oxide. At high pH,  $\text{H}^+$  ions are removed i.e.  $\text{Si-OH}$  deprotonates to give negatively charged  $\text{SiO}_x^-$  groups which attract the holes present in the p-doped silicon NW increasing the conductance through the NW. When the pH is decreased, the  $\text{H}^+$  concentration increases, neutralizing the  $\text{SiO}_x^-$  groups (to give  $\text{SiOH}$ , and repelling the (positive) majority charge carriers in the NW and causing the current to decrease. NW FET functionality and behaviour under flow in this platform was, therefore, first tested by pH measurements on non-functionalized silicon NWs covered with a layer of native silicon oxide.

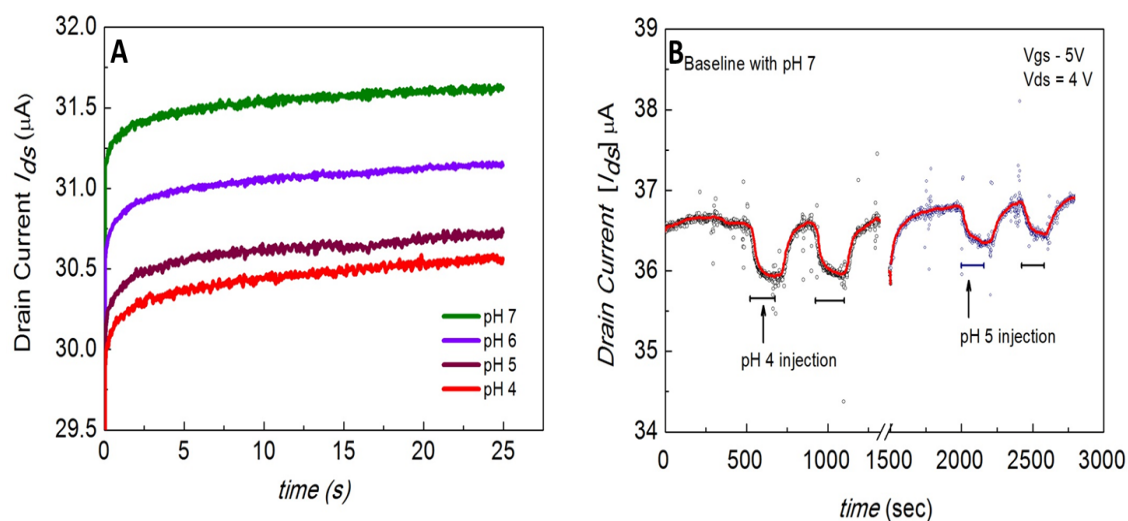


**Figure 5:** The pH response of NW-based sensors. Panel A shows the response of different pH solutions ranging from pH7 to pH 4 on a NW, under a  $V_{gs}$  of -5 V and  $V_{ds}$  of 4 V and a flow rate of 10  $\mu\text{l}/\text{min}$ . The  $V_{ds}$  is set relatively high to obtain an  $I_{ds}$  with good signal to noise ratio. Panel B shows the response of sequential injections for 4 min of either pH 4 or pH 5 over a continuous flow of pH 7 and an interval of 8 min at a flow rate of 10  $\mu\text{l}/\text{min}$ . NWs used in the experiment had the following dimensions: 30  $\mu\text{m}$  in length 300 nm in thickness and 100-300 nm in width

Response profiles to citrate-phosphate solutions (ionic strength of 100 mM) of pH 4-7 under continuous injection are shown in Fig. 5A. As expected, a decrease in drain current of the NW FETs was observed with decreasing pH and rather stable currents of 30-31  $\mu\text{A}$  with only slight drift established within 3 min. The experiments were reproduced with simultaneous injection for 4 min of either pH 4 or 5 buffers over a continuous flow of pH 7 and an interval of 8 min at a flow rate of 10  $\mu\text{l}/\text{min}$  in order to verify the observed pH reversibility effects. Fig. 5B shows the time-dependent pH response of the devices under a flow rate of 10  $\mu\text{l}/\text{min}$  over the non-functionalized SiNW FETs. At pH 7, a stable response was recorded. After 8 min, the device was switched to a 100 mM citrate-phosphate solution of pH 4 for 4 mins. A transient decrease in the order of 1  $\mu\text{A}$  was observed upon re-injecting a buffered solution of pH 4. Similarly for pH 5, reproducible responses of a 0.5  $\mu\text{A}$  current change were recorded. Over time there is a slight increase in the source-drain current  $I_{sd}$ , which may be attributed due to a drift induced by the continuous flow of pH solution in the flowcell. The results obtained here for non-functionalized NWs can be quantitatively compared with the results obtained by Stern *et al.* who tested pH solutions ranging from pH 8 to pH 6 on un-functionalized nanobars for two dimensions, i.e large (1000 nm in width and 80 nm in thickness) and short (100 nm in width and 25 nm in thickness) nanobars. For large electrodes they observed a decrease in drain current of 700 nA and 190 nA for pH change from 8 to 7 and 7 to 6, respectively, whereas for short electrodes the decrease in drain current was 445 nA and 70 nA for a similar transition in pH. It can also be inferred that the change in drain current depends on the dimension on the electrode [52]. Although a direct comparison of our results with the results obtained by Stern *et al.* would be difficult due to different pH ranges measured, but the trends obtained for changes in drain current were in the same

direction [52]. Kim *et al.* reported the effects of flow velocity of ionic solutions on electrical currents through SiO<sub>2</sub>-covered SiNWs [53]. To check for such effects in our set-up a pH 4 citrate-phosphate solution was injected at variable flow speeds from 5 to 50  $\mu\text{l}/\text{min}$ . Although initial changes in the drain current were observed upon changing the flow, no overall change was observed (Fig. 6). Initial changes were presumably caused by the sudden change in flow rate causing a pressure wave with apparent transient electrical consequences. The previously observed effects of flow rate of ionic solutions on NW's conductance (both p-type and n-type devices) [53], were claimed to be due to the formation of streaming potentials when excess counter ions are swept down a pressure-driven flow. We believe the difference between this work on our results may be due to the fact that the flow rate range probed by Kim *et al.* was 60-900  $\mu\text{l}/\text{min}$  with an ionic strength up to 1 mM, while we remained below 50  $\mu\text{l}/\text{min}$  flow rate with an ionic strength of 100 mM. It could thus be inferred that the dependence on the flow rate reduced above 1 mM ionic concentrations. In more detail, from theory we know the value of the streaming potential is inversely related to the electrical conductance of the medium. Since the electrical conductance is proportional to the ionic strength we have an at least 100 times reduced value for the streaming potential than found by Kim *et al.* We understand therefore why the device did not show significant changes within the tested ionic and flow rate range.

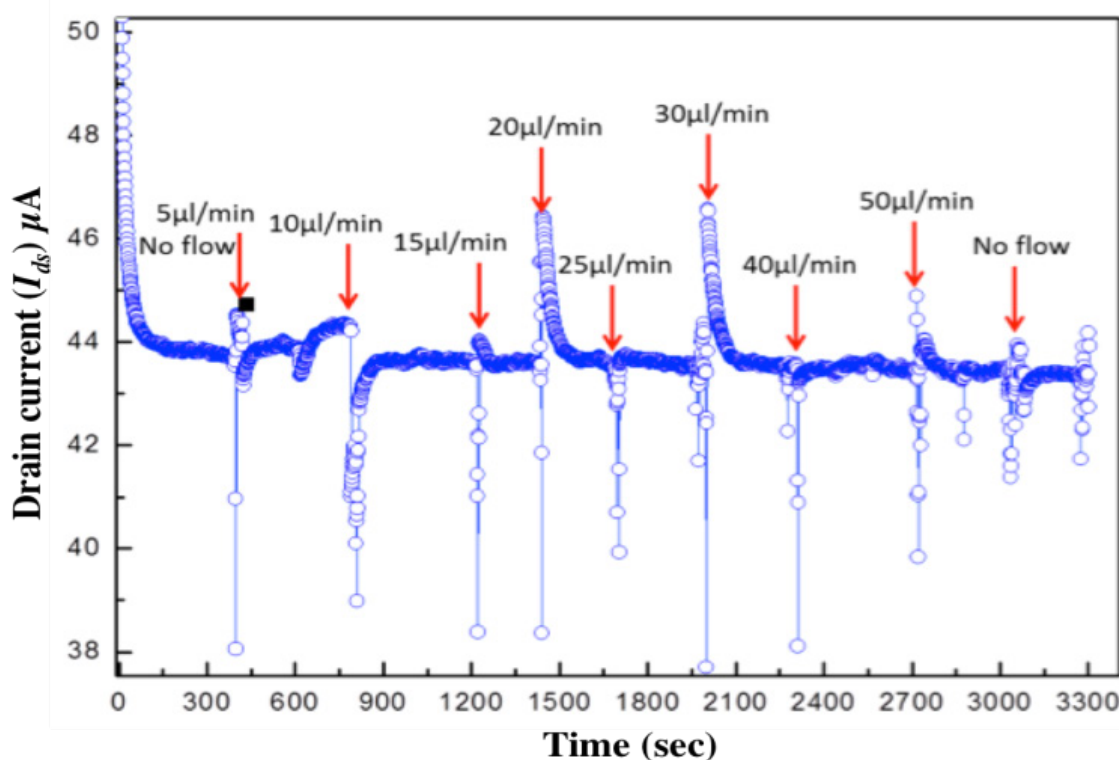


**Figure 6:** Flow rate induced effect on NW with a  $V_{gs}$  of -5 V and  $V_{ds}$  of 4 V: effect of different flow rates ranging from no flow to 50  $\mu\text{l}/\text{min}$  of a pH 4 buffer solution with an ionic strength of 100 mM, under a  $V_{gs}$  of -5 V and  $V_{ds}$  of 4 V and an interval of at least 5 min after every injection

### 6.3.3 Biomolecular sensing using FETs

To demonstrate the suitability of utilizing NW FETs in the present compact biosensing module for the detection of binding of proteins from solutions, an experiment was set up to test the binding of dissolved streptavidin in  $0.1 \times$  PBS solution on biotin-coated NWs, followed by the binding of biotinylated VHH llama antibody A-23, and its specific antigen, *i.e.* the 16 kDa recombinant heat-shock protein produced in *E. coli* [50]. For this purpose, the NW FETs were pre-functionalised with APTES, followed by a PEG<sup>12</sup>-Biotin cross linker that reacts with the amino-groups present on the APTES coating. Fig. 7 shows the resulting binding response in terms of the measured impedance (inverse of the complex analogue of conductance). The change in impedance for 1 nM streptavidin in a  $0.1 \times$  PBS buffer solution was 50 k $\Omega$ , which was a change of about 1%. Elfstrom *et al.* did a similar experiment where they demonstrated the binding of 1 nM streptavidin to biotin-coated NW FETs and observed a decrease in the normalized current using p-type NWs with dimensions of 45 nm in thickness and 100 nm in width [49].

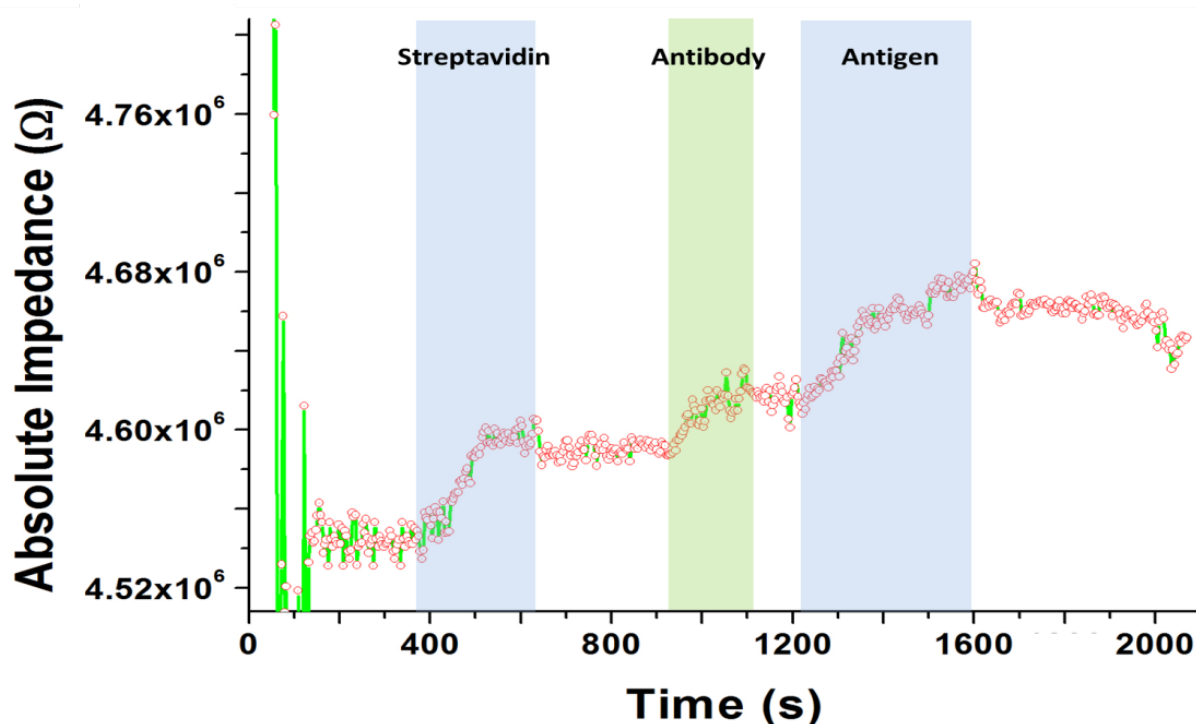


**Figure 7:** Impedance vs time response plot upon binding of different proteins on NWs. The first streptavidin blue bar shows the time during which 1 nM streptavidin was present on a biotin functionalized NW. The green (antibody) bar shows the time during which 300 nM VHH antibody A-23 was present on an streptavidin-functionalized NW, while the blue (antigen) bar shows the duration for a 2.5 nM HSP antigen solution on the antibody functionalized NW. The flow speed for the experiment was kept constant at 10  $\mu$ l/min

Since the current is inversely related to impedance, it could be inferred that the binding of (negatively charged) streptavidin resulted in an increase of the absolute impedance in their case. A similar pattern was observed in our case as well as we also see an increase in impedance of the NW upon binding of 1 nM of negatively charged streptavidin at pH 7.5 (pI

~5.6). Although this is counterintuitive it can be rationalized as follows. The biotin-coated NW will be negatively charged at pH 7.5 and surrounded by small positive counter-ions ( $\text{Na}^+$ ). The negatively charged streptavidin molecule will also be surrounded by positive counter-ions. The streptavidin molecule however is quite large (50-60 kDa) and thus its cloud of counter-ions is more scattered (less dense) around the molecule. Also the isoelectric point of streptavidin is much higher than that of biotin, which means that the streptavidin molecule is less negatively charged than the biotin molecules attached to the NW. When the streptavidin with its counter-ions comes close to the NW, then the positive counter-ions of the streptavidin will also be attracted strongly by the negative groups of the biotin, herewith reducing the strength of the electrical double layer close the NW. The latter means that less negative charge of the biotin groups is felt inside the NW, and that some majority charge carriers (holes) in the NW will be repelled, resulting in higher impedance. Please note that the negatively charged streptavidin molecules are always in distance further away from the NW, and that its electric field gradient is effectively shielded by the Debye Length. With the binding of the biotinylated antibody A-23 having a molecular weight of 17 kDa and HSP antigen dimer of 40 kDa, we again see an increase in the impedance of 30 and 40 K $\Omega$  respectively. Both the antibody (pI ~ 5.9) and antigen (pI ~ 6.1) are negatively charged at pH 7.5 thus this increase in impedance observed is reasonable based on the previous rationale. At around 1600 sec, there is first a small jump down and then a constant level of bound antigen. This pattern is similar to what we observe in SPR and could be attributed to the bulk response when buffer with HSP is exchanged for buffer without as well as slow unbinding of specifically bound antigen as also shown in Srivastava *et al.* using SPR (Chapter 3, Fig. 4).

## 6.4 Conclusion

In conclusion, we have demonstrated a flow-based sensing module for NW-based FET-based biomolecular electrical sensing. We have demonstrated pH-dependent sensitivity, detection of streptavidin and have provided some first evidence of a response to protein binding at flow rates of 10  $\mu\text{l}/\text{min}$ . Unfortunately, due to a shortage of NW chips - additional experiments to corroborate this could not be carried out in the frame of this project. A limitation in the present prototype is the inability to do simultaneous measurement on more than one electrode, due to electrical interferences. In future, integrating an array of sensors enabling multichannel measurements with the aim of performing simultaneously multiple biomolecular sensing could be an extension to the present module.

## References

1. Cheung KC, Di Berardino M, Schade-Kampmann G, Hebeisen M, Pierzchalski A, *et al.*; *Cytometry A*, **2010**, *77*, 648
2. Noy A; *Adv Mater*, **2011**, *23*, 807
3. Anker JN, Hall WP, Lyandres O, Shah NC, Zhao J, Van Duyne RP; *Nat Mater*, **2008**, *7*, 442
4. Chen K-I, Li B-R, Chen Y-T; *Nano Today*, **2011**, *6*, 131
5. Timko BP, Cohen-Karni T, Quan Q, Bozhi T, Lieber CM; *Nanotechnol IEEE Transact*, **2010**, *9*, 269
6. Lee J-H, Oh B-K, Choi B, Jeong S, Choi J-W; *Biochip J*, **2010**, *4*, 1
7. Estevez MC, Alvarez M, Lechuga LM; *Laser Photon Rev*, **2012**, *6*, 463
8. Páscoa RNMJ, Tóth IV, Rangel AOSS; *Anal Chim Acta*, **2012**, *739*, 1
9. Jokerst JV, Jacobson JW, Bhagwandin BD, Floriano PN, Christodoulides N, *et al.*; *Anal Chem*, **2010**, *82*, 1571
10. Nguyen TA, Yin T-I, Reyes D, Urban GA; *Anal Chem*, **2013**, *85*, 11068
11. Vo-Dinh T, Cullum B; *Fresen J Anal Chem*, **2000**, *366*, 540
12. Chen K-I, Li B-R, Chen Y-T; *Nano Today*, **2011**, *6*, 131
13. Patolsky F, Lieber CM; *Mater Today*, **2005**, *8*, 20
14. Hu J, Odom TW, Lieber CM; *Acc Chem Res*, **1999**, *32*, 435
15. Jiangtao H, Min O, Peidong Y, Charles ML; *Nature*, **1999**, *399*, 48
16. Cui Y, Wei Q, Park H, Lieber CM; *Science*, **2001**, *293*, 1289
17. Gao A, Lu N, Dai P, Li T, Pei H, *et al.*; *Nano Lett*, **2011**, *11*, 3974
18. Lu N, Gao A, Dai P, Li T, Wang Y, *et al.*; *Methods*, **2013**, *63*, 212
19. Wang WU, Chen C, Lin KH, Fang Y, Lieber CM; *Proc Natl Acad Sci*, **2005**, *102*, 3208
20. Duan X, Gao R, Xie P, Cohen-Karni T, Qing Q, *et al.*; *Nat Nano*, **2012**, *7*, 174
21. Parpura V; *Nat Nano*, **2012**, *7*, 143
22. Lee Y-EK, Kopelman R; *Nat Nano*, **2012**, *7*, 148
23. Cohen-Karni T, Qing Q, Li Q, Fang Y, Lieber CM; *Nano Lett*, **2010**, *10*, 1098
24. Lagarde F, Jaffrezic-Renault; *Anal Bioanal Chem*, **2011**, *400*, 947
25. Wujcik EK, Wei H, Zhang X *et al.*; *RSC Adv*, **2014**, *4*, 43725
26. Patolsky F, Zheng G, Lieber CM; *Nanomedicine*, **2006**, *1*, 51
27. Bergveld P; *IEEE Transact*, **1972**, *19*, 342
28. Knopfmacher O, Tarasov A, Fu W, Wipf M, Niesen B, *et al.*; *Nano Lett*, **2010**, *10*, 2268
29. Go J, Nair PR, Reddy B, Jr., Dorvel B, Bashir R, *et al.*; *ACS Nano*, **2012**, *6*, 5972
30. Tarasov A, Fu W, Knopfmacher O, Brunner J, Calame M, *et al.*; *Appl Phys Lett*, **2011**, *98*, 012114
31. Kim S, Rim T, Kim K, Lee U, Baek E, *et al.*; *Analyst*, **2011**, *136*, 5012
32. Sahoo P, Suresh S, Dhara S, Saini G, Rangarajan S, *et al.*; *Biosens Bioelectron*, **2013**, *44*, 164
33. Huang Y, Duan X, Cui Y, Lieber CM; *Nano Lett*, **2002**, *2*, 101
34. Yang P, Yan H, Mao S, Russo R, Johnson J, *et al.*; *Adv Func Mater*, **2002**, *12*, 323
35. Lin J, Huang Y, Bando Y, Tang C, Li C, *et al.*; *ACS Nano*, **2010**, *4*, 2452
36. Castner DG, Ratner BD; *Surf Sci*, **2002**, *500*, 28
37. Sorribas H, Braun D, Leder L, Sonderegger P, Tiefenauer L; *J Neurosci Method*, **2001**, *104*, 133
38. Andrew L Neal TLB, Michael F Hochella, Kevin M Rosso; *Geochem Transact*, **2005**, *6*, 77
39. Major R, Bruckert F, Lackner JM, Waldhauser W, Pietrzyk M, Major B; *B Pol Acad Sci-Tech*, **2008**, *56*, 223
40. Matsuo T, Esashi M; *Sensor Actuat*, **1981**, *1*, 77
41. Shen F, Tan M, Wang Z, Yao M, Xu Z, *et al.*; *Environ Sci Technol*, **2011**, *45*, 7473
42. Ma Y, Zhao M, Cai B, Wang W, Ye Z, Huang J; *Chem Commun*, **2014**, *50*, 11135
43. Prakash S, Pinti M, Bhushan B; *Philos T R Soc A*, **2012**, *370*, 2269

44. Lu Y, Peng S, Luo D, Lal A; *Nat Commun*, **2011**, 2, 578
45. Ruzin SE; *Plant Microtechnique and Microscopy*, **1999**, Oxford University Press
46. Moh TSY, Srivastava SK, Milosavljevic S, Roelse M, Pandraud G, *et al.*; *MEMS*, **2012**, 1344
47. Moh TSY, Maruyama Y, Shen C, Pandraud G, Smet LCPMd, *et al.*; *Proceeding of International Conference on Solid State Sensors and Actuators*, **2011**, 1590
48. Zhang F, Sautter K, Larsen AM, Findley DA, Davis RC, *et al.*; *Langmuir*, **2010**, 26, 14648
49. Elfstrom N, Karlstrom AE, Linnros J; *Nano Lett*, **2008**, 8, 945
50. Srivastava SK, Ruigrok VJB, Thompson NJ, Trilling AK, Heck AJR, *et al.*; *PLoS One*, **2013**, 8, e64040
51. Trilling AK, de Ronde H, Noteboom L, van Houwelingen A, Roelse M, *et al.*; *PLoS One*, **2011**, 6, e26754
52. Stern E, Klemic JF, Routenberg DA, Wyrembak PN, Turner-Evans DB, *et al.*; *Nature*, **2007**, 445, 519
53. Kim DR, Lee CH, Zheng XL; *Nano Lett*, **2009**, 9, 1984

# ***Chapter 7***

***A generic microfluidic biosensor of G protein-coupled receptor activation – impedance measurements of reversible morphological changes of reverse transfected HEK293 cells on microelectrodes***

*This chapter is submitted for publication*

## *Abstract*

Impedance spectroscopy of cell lines on interdigitated electrodes (IDEs) is an established method of monitoring receptor-specific cell shape changes in response to certain analytes. Normally, assays are done in multiwells making it a bulky, static and single use procedure. Here, we present a biosensor allowing sequential application of biological test samples with an automated microfluidic system. It is capable of monitoring relative changes in impedance using castellated IDEs of 250–500  $\mu\text{m}$  diameters, covered with stable or reverse transfected HEK293 cells. Reversible activation of the Neurokinin 1 (NK1) receptor in stable cell lines was observed in response to a series of 5 minute exposures from 1 pM – 10 nM of the specific ligand Substance P (SP) using impedance measurements at 10 mV and 15 kHz. An optimal flow speed of 10  $\mu\text{l}/\text{min}$  was chosen for the 10  $\mu\text{l}$  flow cell. The EC<sub>50</sub> of ~10 pM was about 10 times lower than the EC<sub>50</sub> based on measuring changes in the calcium ion concentration. The method was also shown to work with reverse transfected cells. Plasmid DNA encoding the NK1 gene was spotted onto the electrodes and pre-incubated with a transfection agent. The overlaid HEK 293 cells were subsequently transfected by the underlying DNA. After challenge with SP, the cells induced an activation response similar to the stable cell line. The microfluidic micro-electrode reverse transfection system opens up possibilities to perform parallel measurements on IDE arrays with distinct receptors per IDE in a single flow channel. The potential of the system for measuring host-derived biomarkers of patients is discussed.

## 7.1 Introduction

The use of label-free sensing in cell-based screening is gaining increasing interest as a tool to enable the discovery of analytes specific for G protein-coupled receptors (GPCRs) in applications involving pharmaceutical drug screening [1, 2]. A strong potential exists to use these receptors as well for monitoring of food quality and safety, and disease diagnosis. However, the microtiter plate-based platforms tend to be too costly for these tasks [3, 4]. Responses of live cells expressing GPCRs to specific analytes are usually immediate, transient (1-5 min) and can be highly sensitive (nM–pM range). In comparison to conventional diagnostic methods for example PCR for DNA/RNA detection and ELISA for immunodetection, the activation of GPCRs identify a sample's bioactivity, but not its identity. This can be an advantage when the potential ligand is unknown or diverse [5]. Broader application of GPCR-based assays for diagnostics will hinge on our ability to scale down the assays to save on handling and material costs and to integrate them with automated microfluidic formats allowing multiple sequential use and internal calibration [6].

GPCRs play important roles in sensory, physiological and disease-related signalling processes. As such they can be utilized for screening assays in both medical and food related industries. Collectively the ~800 receptors known in humans specifically recognize extracellular stimulants ranging from glycoproteins, cytokines, hormones, neurotransmitters, growth factors, to tastants and odorant molecules [7]. Once activated, the dissociating G proteins trigger one or more pathways that finally generate an intracellular response [8]. Generally, for measurement of GPCR activation assays, concentration dynamics of secondary messengers like  $\text{Ca}^{2+}$  and cAMP are studied in real time utilizing various fluorescent indicator dyes [9, 10]. Alternatively, field-effect transistors, impedance spectroscopy, light-addressable potentiometry, patch clamp and piezoelectric methods have been used [11]. Impedance spectroscopy is a well-established technique for studying effects of biomolecules on a wide range of prokaryotic and eukaryotic cells [12]. The technique measures the combined resistive and capacitive changes due to morphological or mass redistribution changes of cells on electrodes [13].

Yu *et al.* (2006) showed for the first time that impedance measurements of cells transfected with different GPCRs allowed measurements of morphological changes; however, those were measured in terms of h rather than min [14]. Since then, the advent of dedicated instruments has opened a large research field, and dedicated assays were demonstrated to be similarly sensitive as label-based methods, but operate on a scale of minutes rather than seconds [1, 2]. In 2009 Meshki *et al.* demonstrated substance P (SP)-dependent activation of the  $G_{\alpha 12/13}$  pathway using HEK293 cells expressing the NK1 receptor. The pathway causes apoptosis-independent cellular blebbing, and is mediated by the Rho/Rho-associated coiled-coil kinase pathway [15]. The activation of this receptor has been associated with the transmission of stress signals and pain, the contraction of smooth muscles and inflammation [16]. The morphological changes of the cells after the activation of the  $G_{\alpha 12/13}$  pathway could be monitored using impedance spectroscopy, and there have been similar demonstrations for other receptors and activation pathways [14, 17-19]. In general, it is thought that also

activation of  $G_{as}$ ,  $G_{ai/o}$  and  $G_{\alpha q/11}$  pathways can lead to changes in actin and myosin complexes of the membrane cortex that are essential for cell shape and locomotion [20].

At present there are four commercial electric cell-substrate impedance-sensing (ECIS) platforms available in the market (ECIS, xCELLigence (RT-CES), Bionas Discovery 2500, Cellkey). These systems have been utilized for a large variety of studies, including cell adhesion, proliferation, cytotoxicity, receptor-mediated signalling, barrier function and immune cell signalling [21, 22]. These systems utilize interdigitated electrodes (IDEs) of similar dimensions (i.e. electrode features of 30  $\mu\text{m}$  and line gap of 50  $\mu\text{m}$ ) [23] in 8, 16, 96 or 384 (RT-CES and Cellkey) well microplate formats. However, other IDE dimensions are needed to expose cells transiently and/or repeatedly to a ligand, including integration with microfluidic auto-samplers. These changes would make them amenable to automated internal calibration and create possibilities of screening or monitoring of biological targets with lower material and labor costs [6, 24, 25]. To also match the power for parallel measurements solutions are needed to generate and read cell arrays in flow cells. Some approaches have focused on top down dispensing methods of transfected cells into semi-open array structures [26]. A potentially more elegant and low cost solution can be found in reverse transfection of spotted plasmid DNA [27]. This method allows the formation of cell arrays by overlaying the DNA arrays with a single cell type. However, until now, the method has not been applied to IDE based methods or flowcells [27].

In this study, we aimed to demonstrate for GPCRs the possibility of doing sequential impedance measurements on stable cell lines and reverse transfected cells by monitoring impedance changes during serial injections of analyte in a microfluidic flow configuration.

## 7.2 Materials and Methods

### 7.2.1 Materials

All chemicals were analytical grade and supplied by Sigma Aldrich, unless specified otherwise. The NK1 receptor gene construct NK1-T2ANC YC3.6 for stable and reverse transfection cell lines as well as the cell culture conditions were as described by Roelse *et al.* [28]. All solutions were prepared in demineralized water (conductivity 18.2  $\text{M}\Omega\cdot\text{cm}$ ) obtained using Pure lab Ultra from Elga Lab solutions.

### 7.2.2 IDE preparation

The gold interdigitated electrodes IDEs were fabricated (Nanosens BV, Zutphen NL) using a standard micro-photolithography process on thermally oxidized silicon oxide/silicon substrates of 10  $\times$  15 mm dimensions. Interdigitated chromium-gold patterns of 20  $\mu\text{m}$  line width with castellated features of 40  $\mu\text{m}$  length and a line spacing of 12  $\mu\text{m}$  were printed on the silicon substrates as a series of 5 sensing electrodes with a unit-to-unit distance of 500  $\mu\text{m}$ , and electrode dimensions of 500  $\times$  500 (central three) or 250  $\times$  250  $\mu\text{m}$  (terminal two) (Fig. 1A). Prior to use, the sensing chips were subjected to cleaning, surface activation and

modification procedures. New and used IDE sensor chips were cleaned with 2% Hellmanex II in MilliQ water followed by exposing the chips to a 2% HF solution for 10 sec and rinsing with de-mineralized water. For adherence of cells, surface functionalization of both gold and silicon oxide was required. First, the gold electrodes were surface functionalized via drop casting with 25 mM of cysteamine in ethanol for 30 min [29] followed by a modification of the SiO<sub>2</sub> surface with APTES through chemical vapor deposition on the chip [30]. Subsequently, the gold arms connecting the sensing area with the contact pads were covered with a negative photoresist SR3170 PR. Finally, bovine fibronectin (100 µg/ml, Mw ~220 kDa) was drop-casted, incubated for 30 min at 37°C, and unbound fibronectin was rinsed off the chips with MilliQ water [29, 31].

### **7.2.3 Flowcell set up**

A re-sealable and re-usable flow cell was designed to allow connection to a microfluidics system. The flow cell had dimensions of 4.5 cm × 1.5 cm × 0.15 cm. On the top of the borosilicate glass flowcell the in- and outlets were spaced 3.5 cm apart and on the downside 4 mm apart, connected by an internal microfluidic channel. A poly-silicone gasket of 5 mm in diameter and 1 mm in height yielded a compact encasing around the 5 IDEs and resulted in a flow cell volume of 10 µl. The fluids were supplied to the inlets through a Teflon connection tubing of inner diameter 250 µm while the outlet tubing had an internal diameter of 750 µm to prevent any pressure build-up and leakage from the flow cell. Cultured chips were placed in a tailor made stainless steel chip holder of dimensions of l × b × h: 8 cm × 5.5 cm × 0.56 cm with slot dimensions for placing the flow cell of 4.5±0.03 cm × 1.5±0.03 cm × 0.39 cm, and with slot dimensions for placing the sensing device of 1.5±0.03 cm × 1 cm × 0.17 cm (Micronit Microfluidics BV, Enschede, NL). A printed circuit board (PCB) with solder-mounted spring probes for connection to the sensing device was assembled over the chip holder. This flow cell device was mounted inside a die-cast aluminium metal alloy LM24 Faraday cage to exclude environmental noise from light and external electromagnetic interference and enable easily accessible connections to the signal readout systems.

### **7.2.4 IDE preparation with stable cell lines and reverse transfected cells**

The fibronectin coated IDE chips were seeded and incubated for 15 min with 0.5 ml of freshly harvested NK1 expressing stable HEK293 cell lines [28] by drop casting at either a density of 1×10<sup>4</sup> or 1×10<sup>6</sup> cells/ml, followed by the addition of 9.5 ml of freshly prepared DMEM medium in a dish of 5.5 cm in diameter. A uniform monolayer of cells with ~50% coverage for lower and ~80-100% for higher seeding density had formed after 48 h of incubation at 37°C in a 5% CO<sub>2</sub> environment. All subsequent experiments were performed at room temperature in HEPES assay buffer composed of 20 mM HEPES pH 7.4, 137 mM NaCl, 5.4 mM KCl, 1.8 mM CaCl<sub>2</sub>, 0.8 mM MgSO<sub>4</sub> and 20 mM glucose. Serial injections of various freshly prepared dilutions of NK1 ligand SP (Bachem AG, Switzerland, product nr. H-1890, stock solution of 0.5 mM (0.67 mg/ml in 50% acetic acid) in HEPES assay buffer was carried out at a constant flow rate of 10 µl/min.

For reverse transfection experiments fibronectin-modified chips were used as described above. The 0.5 mm diameter sensing area of the IDE was spotted with 1  $\mu\text{l}$  of DNA-gelatin mixture (1  $\mu\text{g}$  of transfection grade NK1-T2ANC YC3.6 as described by Roelse *et al.* [28] with 1  $\mu\text{l}$  of 1.5 M sucrose and 12  $\mu\text{l}$  1% gelatin in total of 30  $\mu\text{l}$  MilliQ) using a micropipette, followed by drying for 1 h in a 50–60% humidity chamber. Spotted chips were stored in a dry box. For experiments, the chips were drop casted with 30  $\mu\text{l}$  of effectene mixture (30  $\mu\text{l}$  of buffer EC, 3.2  $\mu\text{l}$  of enhancer and 5  $\mu\text{l}$  of effectene reagent, all taken from the Qiagen effectene transfection kit) on top of the DNA spotted area and incubated for 10–20 min at room temperature. The chips were then rinsed with DMEM medium and seeded with freshly harvested wild type HEK293 cells at a density of either  $1 \times 10^4$  cells/ml (the multiple loop injections of 1 nM SP experiment) or  $1 \times 10^6$  cells/ml (the multiple-loop injections of 1 pM to 100 pM SP experiment) and cultured in DMEM medium for 48 h in an incubator with 5%  $\text{CO}_2$  at 37°C.

### 7.2.5. Impedance measurements

Impedance measurements were performed at a fixed voltage of 10 mV and a fixed frequency of 15 kHz as described previously [32] and cell responses were measured as a function of time using an Auto Lab PGSTAT302N with FRA2 module (Metrohm Autolab B.V., The Netherlands) at a frequency interval of 3 sec. The sensitivity of the instrument was in the range of  $\sim 0.1 \Omega + 2\% - 1 \Omega + 0.3\%$ . Before and after each series of measurements a frequency-impedance sweep of the cell covered electrode and the bare electrode was carried out in the range of 1 Hz to 1 MHz in order to quantify the impedance contributed by the cells covering the IDEs.

## 7.3 Results

### 7.3.1 Impedance characterization of cell covered IDEs

To allow experiments in the flow cell the first requisite was proper adhesion of the cells to the gold electrodes under the shear of the applied flow rate. For this, IDE chips were given a surface modification using cysteamine, APTES and fibronectin to enhance cell adhesion under flow as described in Materials and Methods. Stable NK1 receptor expressing HEK 293 cells ( $1 \times 10^6$  cells/ml) were applied on the IDEs and after 2 days of culturing a nearly complete monolayer of cells was formed (Fig. 1B). After the flow cell was integrated into the stainless steel chip holder, a flow of 10  $\mu\text{l}/\text{min}$  was applied. The absolute impedance response as a function of frequency sweep (Bode plot) was recorded for both cell-covered and cell-free IDEs in a set up as shown in Fig. 1A. Absolute impedance was found to increase in the range of 100 Hz to 1 MHz due to the coverage of cells on the electrodes. For time-dependent measurements we chose to work at a frequency of 15 kHz where electrode surface-related effects are dominant and the cells induced an additional impedance of around 2 k $\Omega$  for 500  $\mu\text{m}$  IDEs (Fig. 1C), and 2.5 k $\Omega$  for 250  $\mu\text{m}$  IDEs.

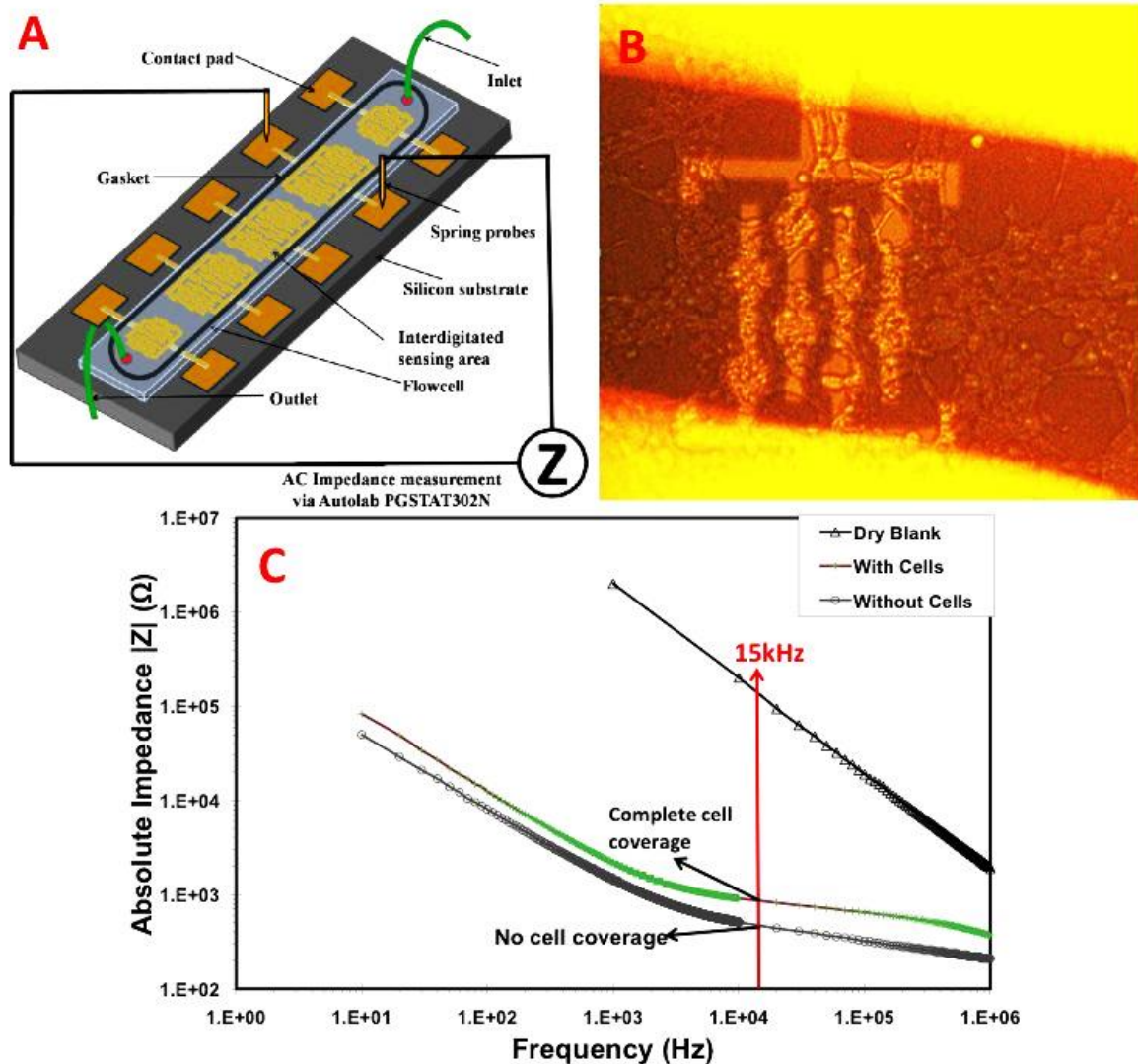


**Figure 1:** Optical and electrical characterization of IDE electrode chips. *A:* Schematic representation of the sensing device. *B:* Microscopic image of a 250  $\mu\text{m}$  IDE coated with NK1-HEK293 cells [28] showing  $\sim 80\%$  coverage on the electrode between the yellow layers of photoresist after the measurement. *C:* A Bode impedance spectrum of an IDE of 500  $\mu\text{m}$  with and without cell coverage in HEPES buffer or without liquid medium exposed to ambient air (dry blank)

Prior to further analysis each electrode, covered with stable NK1 receptor expressing HEK293 cells, was first characterized with a Bode plot (Fig. 2A) and a Nyquist plot (Fig. 2B). The Bode plot was generated under a 10  $\mu\text{l}/\text{min}$  flow of HEPES medium. At around 1 kHz, the phase shift of the Bode plot reached a maximum of around  $70^\circ$ , which was indicative of a quasi-capacitive behaviour originating from the nearly confluent cell layer on the electrode, which slowly decreased upon increasing frequency [33, 34]. In the sample analysed in Fig. 2B, the Nyquist plot shows quasi-parallel resistive-capacitive RC component behaviour for the central cell-covered electrodes (500  $\mu\text{m}$ ) (Fig. 2B and 2C) [34].

### 7.3.2 Impedance responses of stable NK1 receptor-expressing HEK293 cells to SP

Based on the response obtained from impedance spectra of the Bode and Nyquist plots (Fig. 2), a single pair of 500  $\mu\text{m}$  IDEs covered with stable NK1 receptor expressing cells was chosen to measure the specific cell response to activation by a series of injections of SP. Following literature and from Fig. 1, a frequency of 15 kHz and amplitude of 10 mV was chosen to record the induced changes in cell-electrode coverage [32, 35]. A 50  $\mu\text{l}$  sample of SP was loop-injected at concentrations ranging from 1 pM to 10 nM. Samples were diluted in the same HEPES buffer also used for continuous flow. Due to the constant flow rate of 10  $\mu\text{l}/\text{min}$  - each 50  $\mu\text{l}$  injection lasted 5 min and was always followed by a recovery period of at least 2–3 min.

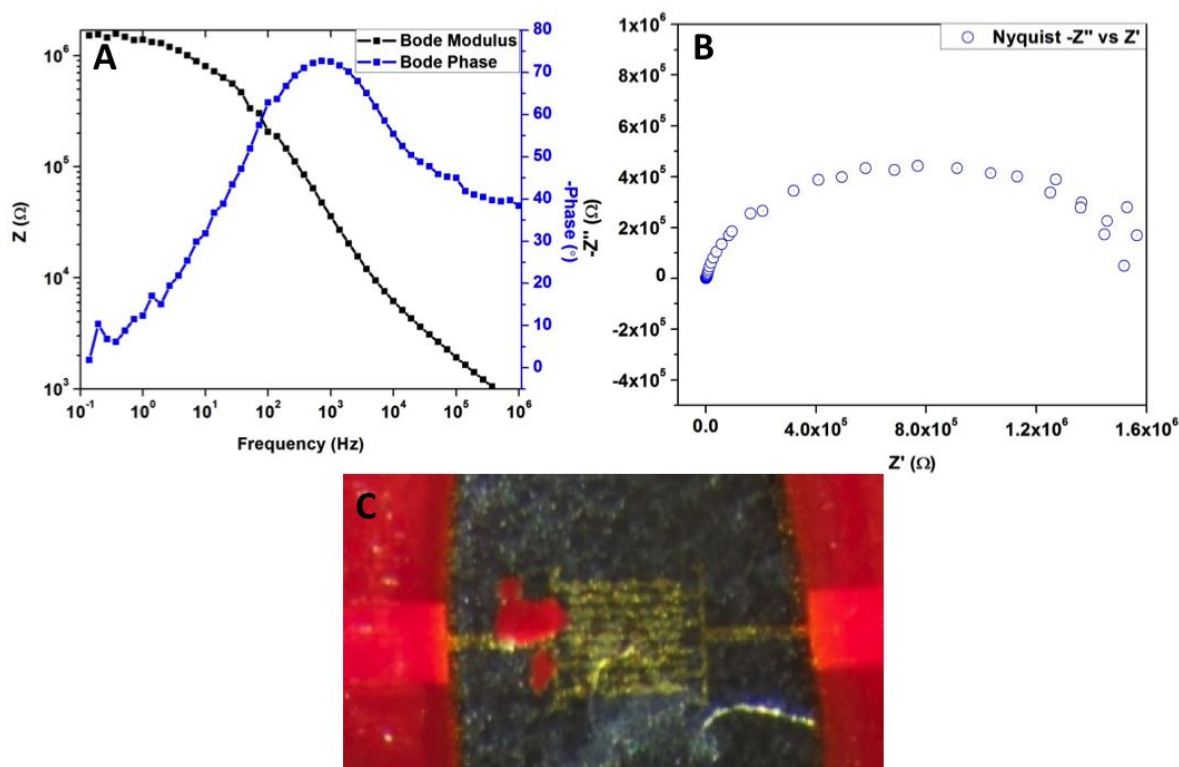


**Figure 2:** Optical and electrical characterization of a 500  $\mu\text{m}$  IDE with stable NK1 HEK293 cells. *A:* Bode plot of an IDE covered with NK1-HEK293 cells. The black line indicates the impedance, and the blue line shows the phase. *B:* Nyquist plot of the same IDE and *C:* optical microscope image with normal light of a cell covered microelectrode of 500  $\mu\text{m}$  after the experiment. In red is the photoresist (SR3170 PR) shielding the connecting electrodes from the assay solution. The plots were obtained from the central 500  $\mu\text{m}$  electrode.

In detail, Fig. 3A shows the combined signals obtained from stable NK1 receptor expressing covered electrodes during and after exposure to 1 pM to 10 nM SP as a function of time. Subplots of Fig. 3B-3F show the same for individual SP concentrations compared to the blank measurement. The overall sample resistance of the sensing area coated with cells was around  $\sim 5$  k $\Omega$  with a contribution from cells of  $\sim 2$  k $\Omega$ . As a control for non-specific buffer effects or drifts from switching the valve, blank injections were done by injecting only buffer on stable NK1 receptor expressing cells (Fig. 3).

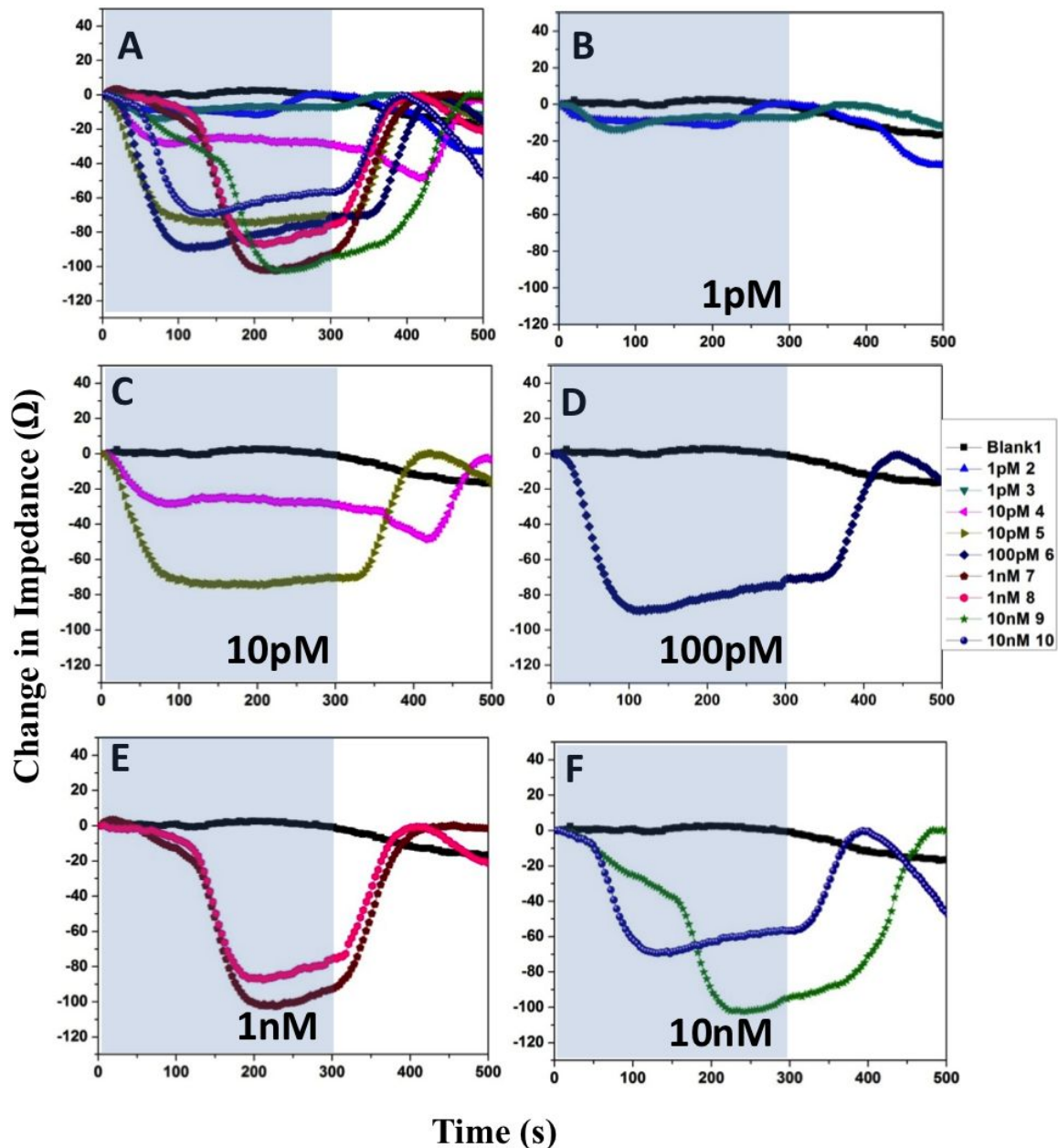


**Figure 3:** Impedance change of a 500  $\mu\text{m}$  IDE covered with a stable NK1 receptor expressing cell line in response to 300 sec injections of different concentrations of ligand SP. *Panel A:* the combined data of impedance response to different concentrations of ligand doses ranging from 1 pM to 10 nM on interdigitated electrodes covered with stable NK1 receptor expressing cells. *Panels 3B-3F:* the changes in impedance for individual ligand dose concentrations. The intervals in light blue background color represent the period that SP was contacting the cells, while areas in white represent recovery periods with buffer flow without ligand. The notation 1–10 in the ligand of the plot represents the sequence of injection. Assay-independent drift was corrected in all cases by subtracting a linear slope coefficient of a line drawn between  $t = 0$  and the highest recovery point between  $t = 400$ – $500$  s post injection ( $t = 300$  s for the blank).

As a negative control to verify that the signals obtained were due to GPCR activation only and not due to changing concentrations of SP, different concentrations of SP were tested on wild type HEK293 cells (Fig. 4). The baseline noise level was below  $\sim 2 \Omega$  for this sample. The system could detect cell morphological changes after challenges with concentrations of SP down to 1 pM even when the electrodes were fully covered with cells. An average impedance change of around  $14 \Omega$  was observed for 1 pM concentrations, whereas the higher concentrations (10 pM, 100 pM, 1 nM and 10 nM) showed average changes of 60, 89, 94 and  $87 \Omega$ , respectively. Impedance changes associated with the mechanical injection process were found to be negligible. Every injection of SP followed a typical response pattern, with a maximum response being reached typically 100–200 sec after injection, followed by decreasing impedance and a recovery period after removal of SP of again 100–200 sec. The activation and recovery slopes of the curves were very similar, independent of the ligand concentration, but the response valleys were deeper at higher ligand concentrations. There was some uncontrolled variation in both the onset (e.g. Fig. 3F) of the strong response and also in the response duration (e.g. Fig. 3E vs. the rest). Also the tenth injection of 10 nM SP, showed a lower response compared to the ninth injection of the same concentration of SP. This could be due to saturation of the receptor as described by Roelse *et al.* 2013 [28].

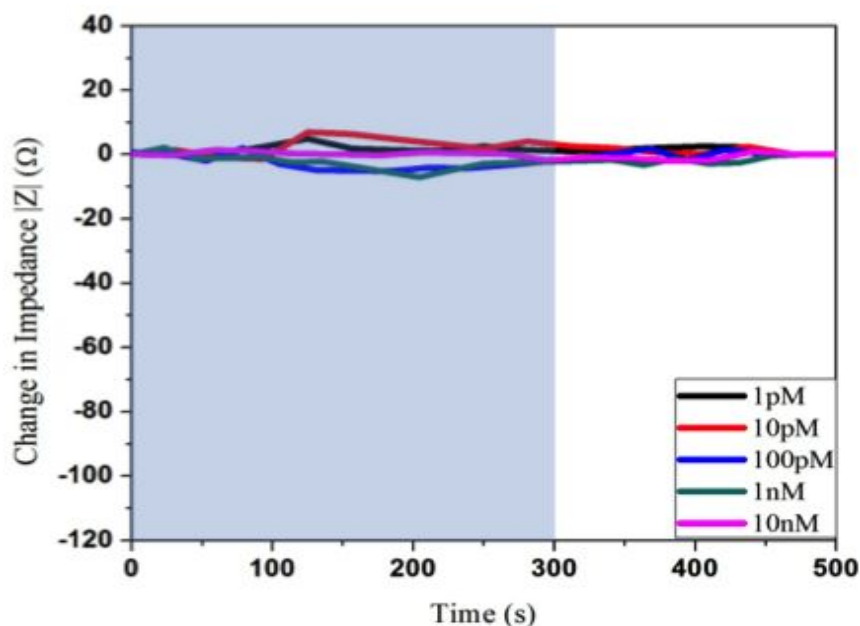


**Figure 4.** Transient response of wild type HEK293 cell lines coated IDEs ( $500 \mu\text{m}$ ) to the SP ligand (1 pM–10 nM). Assay-independent drift was corrected as in Figure 3.

### 7.3.3 Impedance responses to SP on NK1-expressing reverse transfected wild type HEK293 cells

Arrays of electrodes in a single flow cell can be individually transfected with different receptors by means of reverse transfection. HEK293 cells, reverse transfected with NK1 plasmid DNA on  $500 \mu\text{m}$  electrodes, were first characterized with Bode (Fig. 5A) and Nyquist (Fig. 5B) plots when full cell coverage was reached after 48 h. These plots were generated under a  $10 \mu\text{l}/\text{min}$  flow of HEPES medium and the phase response was plotted for reference purposes. Two-phase shifts at 1–15 kHz, and 0.1–1 Hz were evident in the Bode

plot (Fig. 5A) suggesting two independent electrical Resistance-Capacitance circuits (RC circuit). This is also evident in the Nyquist plot (Fig. 5B) where two corresponding semicircular regions are observed. The large semi-circle corresponds to a low frequency RC-circuit formed by the internal IDE electrical capacity and an electrical resistance, originating from the transport/diffusion of ions via the bulk liquid towards the electrodes. The small semi-circle corresponds to a second RC-circuit formed by the electrical capacity of the cell-envelopes and the electrical conductance within the cells and of the exo-ions towards the electrodes. Both RC circuits are present in parallel (cf. extended Randle equivalent circuit) and at 15 kHz mainly the presence of the second RC-circuit are probed, herewith recording sensitive changes in the electrical capacity of the cell-envelopes.

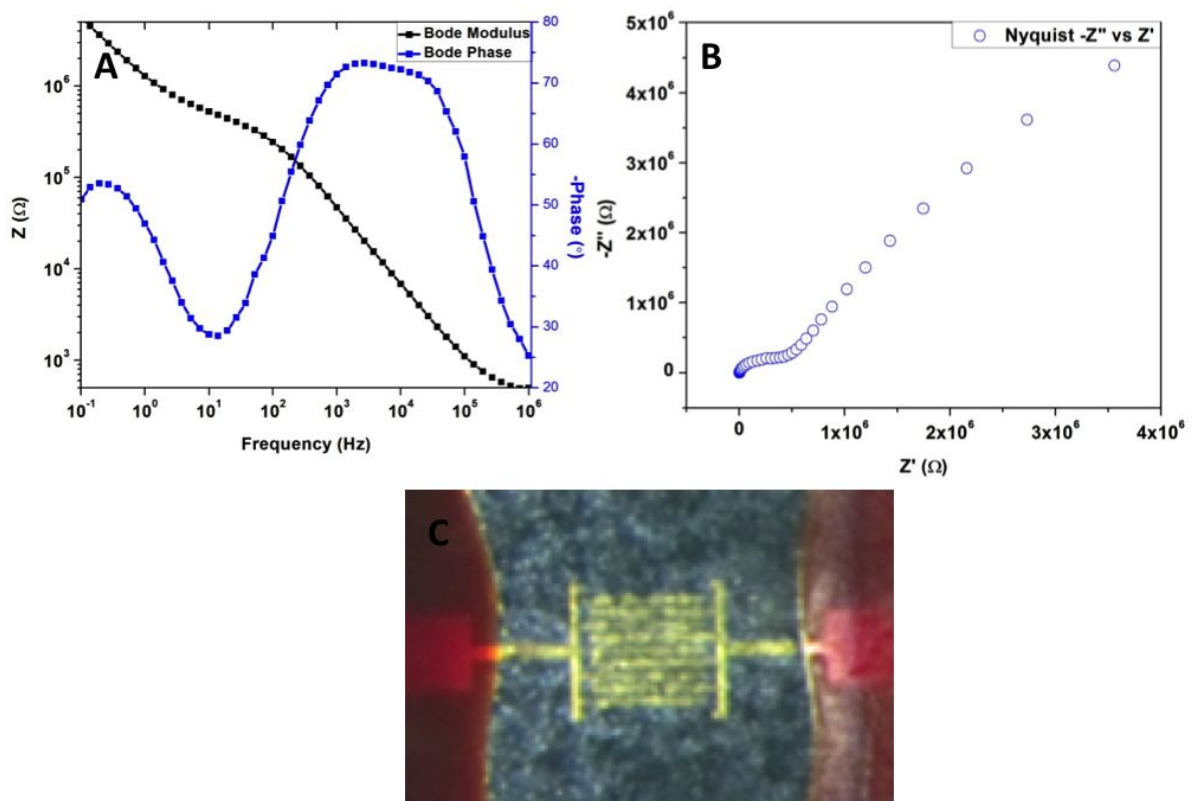


**Figure 5:** Optical and electrical characterization of IDE (500  $\mu\text{m}$ ) electrode chip used for the experiments with reverse transfected HEK293 cells expressing NK1 receptor. A: Bode plot from an electrode covered with reverse transfected HEK293 cells expressing NK1 receptors. B: Nyquist plot from a cell-covered electrode and C: optical image of cell-covered electrodes of 500  $\mu\text{m}$ . In red is the photoresist (SR3170 PR) covering the thick connecting electrodes.

To test the compatibility of the process of reverse transfection with impedance measurements, two distinct experiments were performed. First, doses of 1 nM SP were repeatedly passed over reverse transfected cells with chips seeded at a lower cell density ( $1 \times 10^4$  cells/ml), and after that, doses ranging from 1–100 pM SP were tested on a different chip seeded at high cell density ( $1 \times 10^6$  cells/ml). Fig. 6A shows the combined signal obtained from reverse transfected cell-covered electrodes exposed to repeated 1 nM SP injections. An average maximum response amplitude of  $\sim 18 \Omega$  was obtained which was 2–3  $\Omega$  less than the

signal obtained for 1 nM with stable transfected NK1 cell lines seeded at the same cell density of  $1 \times 10^4$  cells/ml (data not shown), but  $\sim 76 \Omega$  less compared to electrodes seeded with 100 times more cells. Transient response curves were different from the shapes obtained with stable cell lines as the deepest point of the curve was usually reached after removal of SP. The apparent decrease in the signal response (slope and depth) in the later two injections (-5 and -6) may be attributed to temporary desensitization of the NK1 receptor cells due to receptor recycling of SP-activated receptors [28].

In the second experiment a different single pair of IDE electrodes covered with NK1 reverse transfected HEK293 was selected to measure the signal responses to doses ranging from 1 to 100 pM SP. The overall sample resistance for all the cell covered electrodes on different chips were in the range of 4–4.5 k $\Omega$  with baseline noise level of 2  $\Omega$ . The change in absolute impedance for 1 pM SP was similar to the stable NK1 expressing HEK293 cells ( $\sim 16 \Omega$ ). For higher concentrations of 10 and 100 pM, the average impedance changes were 37 and 62  $\Omega$  respectively (Fig. 6B). No significant impedance changes were observed in the blank experiment with no SP in HEPES media.

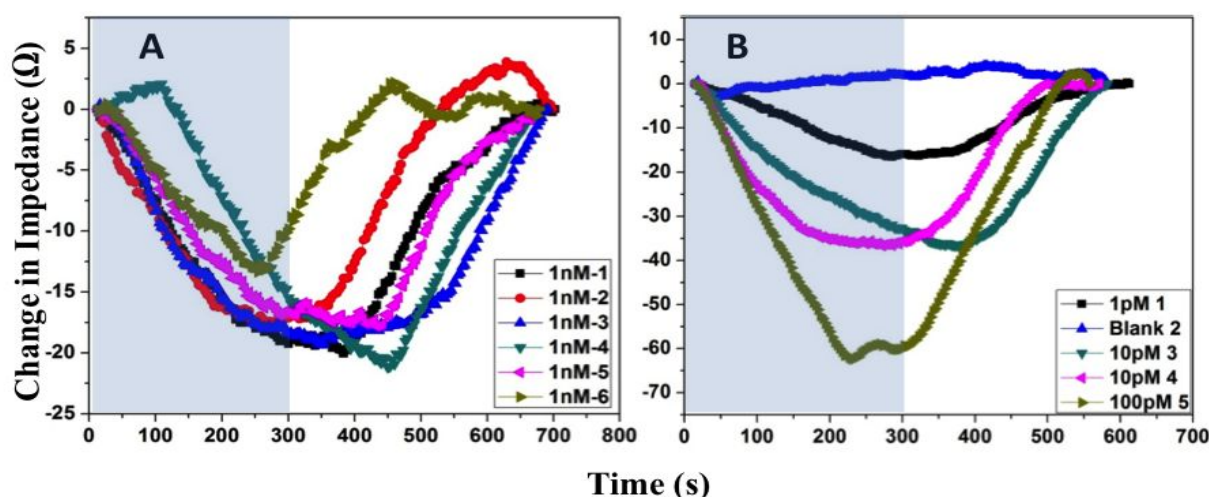


**Figure 6.** Transient response of NK1 reverse transfected HEK293 cell lines on 500  $\mu\text{m}$  IDE's to the SP ligand. A: shows the combined data of the impedance response as a result of a series of injections of 1 nM SP on reverse transfected HEK293 cells with NK1 plasmid DNA at cell seeding density of  $1 \times 10^4$  cells/ml, the sequence of injection is represented by the notation 1–6 in the legend of the plot, where 1 represents the first injection while 6 represents the last injection. B: shows the combined data for impedance response with different concentrations of ligand doses ranging from 1 pM to 100 pM on interdigitated electrodes covered with reverse transfected NK1 HEK293 cells at cell seeding density of  $1 \times 10^6$  cells/ml. The notation 1–5 in the legend of the plot represents the sequence of injection. Assay-independent drift was corrected as in Figure 3.

## 7.4 Discussion

Multiwell assays are the basis of the current impedance- and molecular probe-based analytical platforms of measuring specific cell or receptor responses [15, 43, 44]. These static assays are relatively costly, labor and reagent intensive, wasteful (single use only), and with a relatively low information content (only on-rates of compound addition, no off rates of compound removal, no internal calibration with injection of a standard) [45, 46]. In view of the demand for smaller, parallel, multiple use, dynamic fluidic assays, we therefore developed a prototype system potentially combining all these desirable traits. The system consists of a flowcell enclosing multiple interdigitated micro-electrodes that can be specifically reverse transfected with DNA plasmids encoding different cell membrane receptors to create receptor cell arrays. DNA-printed electrodes can be stored for months until use and the cell arrays can be addressed repeatedly due to the reversible nature of the morphological changes. In addition, the transient activation provides the kinetic profile of both activation and de-activation at the level of changes in cell morphology.

Cell-based biosensors exploit cellular receptors of specific analytes to trigger an intracellular signalling pathway and measure cellular responses (e.g. changes in calcium ion concentrations) as the sensing principle. A wide variety of transducers such as electrical, optical, mechanical, thermal principles have been utilized for cell based sensing [47]. Cell impedance spectroscopy in a microfluidic setting was set up to develop an assay which could potentially detect infections such as tuberculosis in body fluids. As a model, a HEK293 mammalian cell line expressing the NK1 GPCR receptor was immobilized as the biosensing layer, on the hybrid surface of an interdigitated electrode chip. Ligand SP specifically was shown to trigger the NK1 receptor already at very low concentrations. IDE arrays in a single flow cell would enable the possibility of multiplexed assays and detection of multiple analytes in one sample. We have shown that by means of reverse transfection receptor cell arrays may be generated on chip from a wild type cell line, thereby excluding the need for tedious procedures involving maintaining and depositing separate receptor cell lines on one IDE array chip. Thus, a generic application of impedance based measurements of changes in cell shape induced by the specific activation of arrays of receptors potentially provides a novel tool for diagnosing a broad set of disease conditions including TB in human body fluids.

Human infections with pathogens such as *Mycobacterium tuberculosis* trigger specific endogenous biomarkers in the human host. On the one hand, those are antibodies targeting components of the pathogen, but on the other hand there is also a large range of other factors specifically inducing or induced by the human cellular defense. These factors often act via interaction with certain cellular receptors some of which belong to the GPCR family. The biomarkers that are known to be correlated with a TB infection are interferon gamma (IFN- $\gamma$ ), fork-head box P3 (FOXP3), interleukins (IL-1RA, IL-8, IL-18, IL-12), IP-10 and mast cell protease (MCP-1, MCP-2, MCP-3) [36-41]. IL-8 in the group of interleukins is specifically recognized by the GPCRs, CXCR1 and CSCR2. A closely related  $G_{\alpha i}$  dependent chemokine receptor CXCR3 was shown in cells to yield impedance changes when specifically

challenged by CXC chemokine [42]. The potential exists, therefore, to develop cell impedance-based biosensors for tuberculosis infection that can assist in disease diagnosis.

Current limitations of the system prototype are: (i) Due to electrode interference during simultaneous measurements the technical set up did not allow reading more than one sensing electrode. Systems sequentially addressing electrodes at intervals have been developed for the existing microtiter plate formats, however, so that we do not foresee a technical hurdle for flow cell arrays; (ii) the design of the flow cell did not allow higher flows than one flowcell volume per minute. Future designs with wider and/or higher flow cells will allow larger flow volumes as described by Roelse *et al.* with greater convenience in terms of the speed of delivery of series of samples [28]; (iii) The non-monotonous drift could not be addressed in the present system with a read out of only a single receptor. Drift compensation methods need to be realised by adapting the design of the chip layout for example by arranging a rows-column format with electrical connections lying plane perpendicular and at the underside of the sensing area thereby minimizing the chances of drift due to thermal and electrical interferences from neighbouring electrodes [48]. If drift is IDE independent compensation may also be achieved by subtracting the signals of control electrodes. If drift is IDE dependent the process of cell division may be responsible. The mitotic cycle induces strong morphological changes that likely disturb signal stability on small electrodes with only few cells contributing to the total signal. Arresting the cell cycle with chemicals may therefore be another effective way of suppressing drift.

HEK293 cells were seeded on the chip typically 48 h prior to use. Depending on the chosen cell densities, this yielded well-attached, uniform, 50-100% confluent cell layers. Loading higher densities and spinning cells down to reduce the adhesion time from 48 h to < 2 h was not effective, as cells could not withstand medium flow speeds higher than 2  $\mu\text{l}/\text{min}$ , due to poor adherence (data not shown). It is noted that the morphological changes of cells can involve both shrinking and stretching, depending on the nature of the activated receptor [49, 50]. This probably has some implications for the most adequate cell coverage in case of mixed cell responses. In the present study the NK1 receptor activation with SP resulted in shrinkage of cells (blebbing), and therefore, near confluent cell coverage yielded the best differential signal. In a mixed situation it may be better to aim for 70–80% cell coverage, in order to allow for efficient measurements of cell stretching as well.

The signal responses obtained with various ligand doses were generally reproducible for both stable as well as reverse transfected cell lines. Noise levels were typically 2~5% relative to response signals of  $\sim 20 \Omega$  and higher. The response profiles of stable and reverse transfected cell lines were, however, a little different. Stable cell lines displayed an initial 1–2 min steep decrease followed by a 3–4 min slightly rising saturation plateau, succeeded by a 1–2 min steep rise when the ligand was removed. Both the fall and rise of the signals could be delayed up to 100 sec. We suspect that this might be due to failure of the pump to deliver a constant low flow in our system. By comparison for reverse transfected cell lines the decrease was less steep, taking 4–5 min to reach a shorter, yet still decreasing, saturation plateau, which would extend 1–2 min beyond the point that the ligand was removed. Recovery was

also slower taking up to 4–5 min. A possible explanation might be that HEK293 cells were present in a multilayer, with only the lower layer being transfected and responding. In comparison to uniform stable transfected cell lines, the ligand may reach the bottom reverse transfected cells less efficiently.

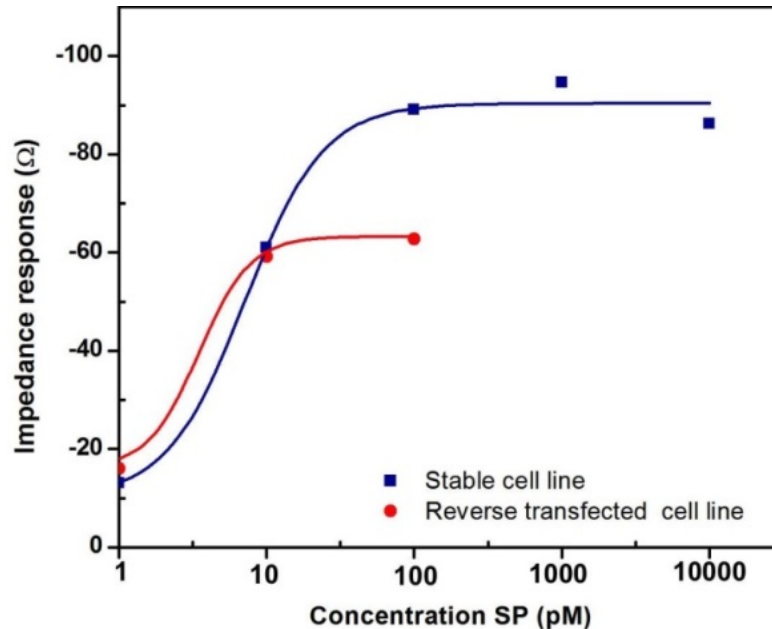


**Figure 7:** Dose-response curve of the relative change in impedance at 15 kHz, 10 mV, for different SP concentrations for both stable and reverse transfected NK1 cell lines seeded at a density of  $1 \times 10^6$  cells/ml. All changes were negative, resulting in a lower impedance as a result of the interaction with SP. The data points are mean values obtained from 2 or 3 injections of the same concentration

The dose response curve for the stable cell line showed an estimated EC<sub>50</sub> value of ~10 pM (Fig. 7), which was 140 times lower compared to the EC<sub>50</sub> reported by Meshki *et al.* experiments in a microtiter plate on large electrodes [15] and about 10 times lower than a complementary microfluidic system where cytoplasmic [Ca<sup>2+</sup>] changes were measured [28]. One reason for this higher sensitivity could be the very low cell density used by Meshki *et al.* in the wells, i.e. 4000 cells/6.4 mm well diameter. Based on a cell size of 100 μm<sup>2</sup> these results in coverage of only 1.25% compared to 80-100% coverage in our sample preparations. This was also evident with the experiment involving repeated injections of 1 nM, where the signal obtained was diminished for lower cell inoculation of 10<sup>4</sup> cells/ml compared to higher cell inoculation 10<sup>6</sup> cells/ml. In addition, we incubated cells 3 times longer (48 h) allowing stronger electrode adhesion of cells. Secondly, the reported lower sensitivity values from Meshki *et al.* could be due to SP not being fully active as it quickly inactivates after dilution in buffer according to our experience. Thirdly, considering the mean cell size (10 μm), the line spacing used in our case was very narrow (12 μm) compared to commercial devices (50 μm) used by Meshki *et al.* As described by Radke and Alocilja, for sensitive impedance measurement of cellular organisms, electrode spacing should be proportional to the dimensions of cells [49], so as to minimize the influence of events occurring due to some random particle floating over the sensor electrode. In their study where they utilized *E. coli*

bacteria with average length of 2.5  $\mu\text{m}$ , the optimum spacing between the electrodes was 4  $\mu\text{m}$  which minimized up to 98% of external interference caused by random particles floating at a distance of 10  $\mu\text{m}$  over the sensing area [51].

For proof of concept, the NK1 receptor was utilized as a model GPCR. Upon activation by SP, the NK1 receptor triggers both the  $G_{\alpha_q}$  and the  $G_{\alpha_{12/13}}$  pathways. Presumably, the activation of the  $G_{\alpha_{12/13}}$  pathway induces a contraction of the membrane cortex termed as blebbing [52]. There are three main GPCR pathways, which are mediated by four ( $G_{\alpha_s}$ ,  $G_{\alpha_{i/o}}$ ,  $G_{\alpha_{q/11}}$  and  $G_{\alpha_{12/13}}$ ) subclasses of G-proteins [53]. Although, the pathway best known to induce such morphological changes is the  $G_{\alpha_{12/13}}$  pathway, it appears that the activation of other pathways might also lead to changes in actin and myosin complexes of the membrane cortex that are essential for cell shape and locomotion [52]. There have been similar demonstrations, however, for the histamine (H1), serotonin (5-HT1A) [14], dopamine (D2, D5), cannabinoid 1 (CB1), melanocortin-4 (MC4R) [17], cannabinoid 2 (CB2), metabotropic glutamate 1 (mGluR1) [18] and chemokine CXCR3 [19] receptors with activation pathways mainly involving  $G_{\alpha_s}$ ,  $G_{\alpha_{i/o}}$  and  $G_{\alpha_{q/11}}$ . Furthermore, also the ligands of nuclear receptors such as glucocorticoid, mineral corticoid, progesterone, androgen receptor induce morphological changes in cells [54]. The presented novel microfluidic system of impedance measurements on microelectrodes in a flow cell is therefore potentially useful for a much wider array of receptors. In fact, if they do not naturally change shape, their signalling pathway can be altered in order to do so. Recently,  $G_{\alpha_q}$  proteins could be engineered into chimeric versions with  $G_{\alpha_{12/13}}$ , which would bind  $G_{\alpha_q}$  GPCRs, but trigger the  $G_{\alpha_{12/13}}$  pathway [55], thus opening up further possibilities to use impedance measurements as a generic platform for GPCR research.

## References

1. Scott CW, Peters MF; *Drug Discov Today*, **2010**, *15*, 704
2. Fang Y, Frutos AG, Verklereen R; *Comb Chem High Throughput Screen*, **2008**, *11*, 357
3. Beets I, Lindemans M, Janssen T, Verleyen P; *Methods Mol Bio*, **2011**, *789*, 377
4. Lappano R, Maggiolini M; *Nat Rev Drug Discov*, **2011**, *10*, 47
5. Cheng X, Chen G, Rodriguez WR; *Anal Bioanal Chem*, **2009**, *393*, 487
6. Martins SA, Trabuco JR, Monteiro GA, Chu V, Conde JP, *et al.*; *Trends Biotechnol*, **2012**, *30*, 566
7. Zhang R, Xie X; *Acta Pharmacol Sin*, **2012**, *33*, 372
8. Hermans E; *Pharmacol Therap*, **2003**, *99*, 25
9. Berridge MJ, Bootman MD, Roderick HL; *Nat Rev Mol Cell Biol*, **2003**, *4*, 517
10. Paredes RM, Etzler JC, Watts LT, Zheng W, Lechleiter JD; *Methods*, **2008**, *46*, 143
11. Liu Q, Wu C, Cai H, Hu N, Zhou J, Wang P; *Chem Rev*, **2014**, *114*, 6423
12. Randviir EP, Banks CE; *Anal Methods*, **2013**, *5*, 1098
13. Ding L, Du D, Zhang XJ, Ju HX; *Curr Med Chem*, **2008**, *15*, 3160
14. Yu N, Atienza JM, Bernard J, Blanc S, Zhu J, *et al.*; *Anal Chem*, **2006**, *78*, 35
15. Meshki J, Douglas SD, Lai JP, Schwartz L, Kilpatrick LE, *et al.*; *J Biol Chem*, **2009**, *284*, 9280
16. Seto S, Tanioka A, Ikeda M, Izawa S; *Bioorg Med Chem Lett*, **2005**, *15*, 1479
17. Peters MF, Scott CW; *J Biomol Screen*, **2009**, *14*, 246
18. Scandroglio P, Brusa R, Lozza G, Mancini I, Petro R, *et al.*; *J Biomol Screen*, **2010**, *15*, 1238
19. Watts AO, Scholten DJ, Heitman LH, Vischer HF, Leurs R; *Biochem Biophys Res Commun*, **2012**, *419*, 412
20. Perez V, Bouschet T, Fernandez C, Bockaert J, Journot L; *Eur J Neurosci*, **2005**, *21*, 26
21. Solly K, Wang XB, Xu X, Strulovici B, Zheng W; *Assay Drug Dev Techn*, **2004**, *2*, 363
22. Thedinga E, Kob A, Holst H, Keuer A, Drechsler S, *et al.*; *Toxicol Appl Pharmacol*, **2007**, *220*, 33
23. Xu X, Abassi Y, Wang X; USA Patent (US-WO2005077104 A3), **2008**
24. Allen JA, Roth BL; *Annu Rev Pharmacol Toxicol*, **2011**, *51*, 117
25. Wu M-H, Huang S-B, Lee G-B; *Lab Chip*, **2010**, *10*, 939
26. Tsai S-L, Chiang Y, Wang M-H, Chen M-K, Jang L-S; *Electrophoresis*, **2014**, *35*, 2392
27. Mishina YM, Wilson CJ, Bruett L, Smith JJ, Stoop-Myer C, *et al.*; *J Biomol Screen*, **2004**, *9*, 196
28. Roelse M, de Ruijter NCA, Vrouwe EX, Jongsma MA; *Biosens Bioelectron*, **2013**, *47*, 436
29. Slaughter GE, Bieberich E, Wnek GE, Wynne KJ, Guiseppi-Elie A; *Langmuir*, **2004**, *20*, 7189
30. Zhang F, Sautter K, Larsen AM, Findley DA, Davis RC, *et al.*; *Langmuir*, **2010**, *26*, 14648
31. Meyburg S, Stockmann R, Moers J, Offenhäusser A, Ingebrandt S; *Sensor Actuat B-Chem*, **2007**, *128*, 208
32. Shih SC, Barbulovic-Nad I, Yang X, Fobel R, Wheeler AR; *Biosens Bioelectron*, **2013**, *42*, 314
33. Wegener J, Keese CR, Giaever I; *Exp Cell Res*, **2000**, *259*, 158
34. Cho S (2011); *Biochip J*, **2011**, *5*, 327
35. Hatanaka K, Lanahan AA, Murakami M, Simons M; *PLoS One*, **2012**, *7*, e37600
36. Ameixa C, Friedland JS; *Infect Immun*, **2002**, *70*, 4743
37. Lin YG, Gong JH, Zhang M, Xue WF, Barnes PF; *Infect Immun*, **1998**, *66*, 2319
38. Ruhwald M, Bjerregaard-Andersen M, Rabna P, Eugen-Olsen J, Ravn P; *BMC Res Note*, **2009**, *2*, 19
39. Sutherland JS, Hill PC, Adetifa IM, de Jong BC, Donkor S, *et al.*; *PLoS One*, **2011**, *6*, e25230

40. Wu B, Huang C, Kato-Maeda M, Hopewell PC, Daley CL, *et al.*; *J Immunol*, **2007**, *178*, 3688
41. Zhang Y, Broser M, Cohen H, Bodkin M, Law K, *et al.*; *J Clin Inv*, **1995**, *95*, 586
42. Deng MC, Eisen HJ, Mehra MR *et al.*; *Am J Transplant*, **2006**, *6*, 150
43. Wang J, Wu C, Hu N, Zhou J, Du L, *et al.*; *Biosensors*, **2012**, *2*, 127
44. Fang Y; *Int J Electrochem*, **2011**, *16*, 460850
45. Rocheville M, Jerman JC; *Curr Opin Pharmacol*, **2009**, *9*, 643
46. McGuinness R; *Curr Opin Pharmacol*, **2007**, *7*, 535
47. Perfezou M, Turner A, Merkoci A; *Chem Soc Rev*, **2012**, *41*, 2606
49. Chachisvilis M, Zhang YL, Frangos JA; *Proc Natl Acad Sci*, **2006**, *103*, 15463
50. Voets T, Nilius B; *EMBO J*, 2009, *28*, 4
51. Radke SM, Alocilja EC; *Sensors J*, **2004**, *4*, 434
52. Ye RD; *J Leukocyte Biol*, **2001**, *70*, 839
53. Hermans E; *Pharmacol Therap*, **2003**, *99*, 25
54. Abassi YA, Xi B, Zhang W, Ye P, Kirstein SL, *et al.*; *Chem Biol*, **2009**, *16*, 712
55. Vazquez-Prado J, Miyazaki H, Castellone MD, Teramoto H, Gutkind JS; *J Biol Chem*, **2004**, *279*, 54283

# *Chapter 8*

## *General Discussion*

In this PhD project, various diagnostic methods were developed for potentially sensitive and early detection of TB, which in some cases may also be applied in resource-poor areas. This final chapter focuses on the achievements of the project and highlights the further work required along with future perspectives.

## 8.1 Need for better biosensing tools in TB

Tuberculosis (TB) is affecting people across all continents, and is a global problem for our modern society demanding urgent attention. Early and sensitive detection techniques applicable in remote areas remain the mainstay for the fight against TB. Unfortunately, detection tools for TB still fall short from the required qualities.

As mentioned throughout in this thesis, a crucial step towards TB management is early detection. In Chapter 2 we introduced the different diagnostic platforms that have been developed and used so far for TB detection and we stressed that a highly sensitive and user-friendly diagnostic tool to analyze biological samples (like – sputum or blood) for the presence of *Mycobacterium tuberculosis* (*M.tb.*) is still not available. Moreover the situation is complicated by the fact that TB is most prevalent in tropical and poor countries with inadequate infrastructure and lack of funds to support the current diagnostic tools.

In summary the motivation for this thesis work has been as follows:

- (1) The seriousness of the problem - TB as a disease has a worldwide presence and the socio-economic burden that it projects on a global scale is enormous [23].
- (2) The key point in TB management is early detection – if possible even at the latent infection stage. It needs to be emphasized that the major hurdle lies here as most of the latent TB cases are either asymptomatic or with few symptoms which makes it difficult to diagnose at an early stage [24]. However, medical literature has reiterated over and over that a diagnostic tool that can be used in detecting such (a) symptomatic cases would greatly improve the opportunities for TB management. In other words – there is strong support for developing a diagnostic tool that can be implemented to screen entire populations irrespective of symptoms [55].
- (3) As *M.tb.* infections stimulate the production of specific antibodies – a set of serological assays have been reported over the last few decades [56,57]. Unfortunately, most of these assays are not user-friendly, require strong logistic support, are expensive, offer inadequate sensitivities and cannot distinguish between old and new infections. Moreover, in July 2011 the World Health Organisation issued a warning against the use of such tests stating, “*Test results are inconsistent, imprecise and put patients’ lives in danger*” [23]. In a nutshell, the current available biosensing tools fail to live up both to the expectations and performance standards.

(4) During the last few years, nano- and microtechnology have experienced explosive growth. Unique properties of these materials and techniques (such as – superconductivity, paramagnetism, fluorescence, higher chemical reactivity, microfluidics) over bulk materials and volumes offer unprecedented opportunities to develop novel tools for medical diagnostics [58].

## 8.2 Biosensor-based detection of TB biomarkers and research questions

Despite the fact that recently there have been remarkable advancements in biosensing based approaches towards detection of TB, the currently available techniques are still limited to laboratories. The expected features/criteria that an effective and suitable biosensor for TB detection should possess are: 1) high cost-effectiveness, 2) high sensitivity, 3) good reliability, 4) portability, 5) simple use and 6) having disposable parts.

In chapter 2, classification of biosensors was done on the basis of their signal transduction principle.

For electrical biosensors, an electronic nose-based method has been developed for detection of TB. Electronic nose based biosensors recognize volatile substances that are produced by the *M.tb.* in liquid medium [1-3].

For optical biosensors, techniques utilizing fibre-optics, surface plasmon resonance (SPR), resonant mirror and breathalyzer based biosensing methods have been demonstrated for TB detection. Fibre-optic based biosensors were shown to recognize compounds that are secreted by *M.tb.* into sputum [4], while SPR [5-12], resonant mirror [13] and breathalyzer based biosensors focused on the recognition of *M.tb.* produced byproducts or the whole *M.tb.* bacterium [14-16].

For mechanical biosensors techniques like quartz crystal microbalance (QCM), multichannel series piezoelectric quartz crystal (MSPQC) and acoustic wave biosensors have been explored in relation to TB. Where QCM based methods rely on the detection of whole *M.tb.* bacterium [17], MSPQC and acoustic based sensors recognize volatile and non-volatile products that are produced due to the growth of *M.tb.* bacterium [17-19]. For magnetoelastic and magnetic TB biosensors, techniques such as magnetoelastic strip, diagnostic magnetic resonance (DMR) and magnetic barcode-based biosensors have been developed. Magnetoelastic strip-based sensors are designed to detect by-products produced from *M.tb.* from their specific signature, while the other two techniques are lab-on-a-chip techniques, where whole *M.tb.* bacterium are analysed in crude sputum samples in an automated, high throughput, miniaturized NMR platform towards identification of on-chip RT-PCR amplified 16S rRNA [20-22].

The research presented in this thesis has been part of a large interdisciplinary project initiative of the Dutch technology foundation STW involving four main partners with one PhD student at three location i.e. Laboratory of Organic Chemistry/ Plant Research

International (Wageningen University), NanoOrganic Chemistry Group (Technical University Delft) and the Delft Institute of Microsystems and Nanoelectronics (Technical University Delft) and a technician at Viroscience division (Erasmus Medical Center-Rotterdam). The role for Wageningen was to work on the biosensing layer and test and apply nanowires for the detection of pathogens like TB. The technician involved in the project at Rotterdam had the task to provide virus-specific antibodies and recombinant virus proteins for initial assay set-up, along with clinical specimens for test validations. The other two PhD students involved in the project at Delft were expected to construct the nanowires and functionalize them with chemical monolayers suitable for the immobilization of a biosensing layer by the Wageningen PhD. However, due to a delay in the deliverables from the project partners, alternative detection platforms were improvised and initiated. As a result, lateral flow immunoassays, microsieves for upconcentration and detection, and cell-based biosensors were developed and evaluated, with the original global aim to address the existing challenges of sensitivity and simple use in TB diagnosis utilizing micro- and nanomaterials, and testing novel electronic and optical options for detecting either pathogen or host biomarkers in simple one step procedures. The resulting research questions addressed in this thesis were:

1. Development of antibody pairs for a novel TB biomarker HSP which can be concentrated by concentrating the bacteria first to meet the sensitivity benchmark (8.3).
2. Development of a one step capture and detection procedure of HSP with those antibodies to meet the simplicity benchmark (8.4 and 8.5).
3. Development of label-free one step detection of host biomarkers using cellular membrane receptors to meet both the sensitivity and simplicity benchmark (8.6).

### **8.3 Characterization and upconcentration of the *M.tb.* HSP internal antigen**

For the development of antibody pairs for a novel TB biomarker that could be upconcentrated by concentrating the bacteria, it was crucial to identify a suitable intracellular target and bacteria capture method. In the selection of the biomarker protein we looked for a protein, which would be abundant and immunogenic. A good candidate was the 16 kDa heat shock protein (HSP) which has long been known to be a critical pathogenic component of infectious TB. It is highly immunogenic leading to high titres in patients' sera. It has been claimed to exist as monomer, dimer, trimer, trimer of trimers (i.e. nonamers) or dodecamer structures and was analysed using various techniques like reverse-phase high performance liquid chromatography, cryoelectron microscopy and size exclusion chromatography (SEC) analysis [26]. In earlier research, a set of llama antibodies had been selected using phage display against this protein [11]. In order to understand the optimal capture-detection probe combinations and, in continuation, to design highly sensitive biosensing tools, it was important that the protein epitopes of HSP in relation to existing antibodies were sorted out. In Chapter 3 the multimeric structure of HSP was investigated. The denaturation due to heat and harsh isolation and purification methods was coupled to an SEC and mass spec analysis that allowed for the first time a reliable size determination of the various protein forms [26].

We demonstrated the configuration of denatured-renatured protein to be a dimer, and identified and characterized via epitope mapping experiments the antigenic regions of the HSP protein, with a collection of HSP-specific VHH llama antibodies. Different VHH antibodies showed specific binding to many different epitopes of 16 kDa HSP. It was observed that the best binders of HSP, VHH A-23 and B-F-10, recognized non-overlapping epitopes of the HSP protein [26]. Binding of HSP epitopes, protein and lysates to different VHH antibodies was modelled leading to recommendations of the most suitable capture-detection probe combinations for detection of TB.

The elucidation of the antigenic structure of the 16 kDa HSP has been a matter of debate for a long time. The improved understanding of the structure and the availability of VHH antibodies against this clinically and pathologically relevant protein of *M.tb.* may be relevant towards the development of sensitive biosensors specific to diagnose HSP. The use of VHH llama antibodies [27] has been quite successful in a range of diagnostic applications due to their unusually robust properties. This work, therefore, laid the foundation for research towards the development of novel biosensing tools in TB especially if also straightforward methods of upconcentrating mycobacteria from sputum would be available. A method to achieve that was described in Chapter 4. A homopolymer of diallylimethylammonium chloride (polyDADMAC) was coated as capturing agent on microsieves and was used to concentrate acid-fast Gram-positive Mycobacterium from test samples. The concentrated Mycobacteria, may subsequently be lysed and the released biomolecules (DNA, RNA, proteins like HSP) will be available in concentrated form for various detection assays. This may be useful in detecting Mycobacteria not only in human samples but also in other media like milk or water [29]. Furthermore, with the use of other specific capturing agents, the scope for such functionalised microsieves could be broadened to other pathogens.

#### **8.4 Sandwich immunoassays of TB HSP antigen**

Sandwich assays are usually more specific than direct assays if the capture and detection of the analyte molecule is done using two different epitopes, i.e. first epitope 1 by the capture antibody and subsequently epitope 2 by the detection antibody [28]. A positive signal is only obtained when both the capture and detection antibodies have bound the same target molecule, thus making the system more specific than systems depending on one capturing epitope. Two strategies were followed, that focused on capture/detection of *M.tb.* cellular internal 16 kDa HSP antigen protein using sandwich assays (Chapters 4 and 5).

In the first strategy, the detection of HSP was based on a step-by-step build-up of a sandwich assay involving two complementary biotinylated VHH antibodies, HSP target protein and alexa-fluoro labelled streptavidin on a flow-through microsieve platform (Chapter 4). Flow-through assays may be advantageous over traditional flow-over assays due to increased contact of antigens in solution and bound antibodies. By passing through the surface apart from diffusion also physical mass flow parameters come into play.

Interestingly, the dimeric nature of the HSP protein seemed to result in the formation of aggregates on the sieves in sandwich assays combining HSP dimers with VHH antibodies coupled by quaterneric streptavidin. Assays involving multivalent recognition pairs can easily lead to aggregate formation similar to the well-known agglutination reaction used for bloodtyping. Detection of this aggregate sandwich pair was studied with the help of a DLS (dynamic light scattering) method [32]. Interestingly, DLS could measure aggregation down to 10 ng/ml suggesting that the reaction is potentially very sensitive and might be used to an advantage as an alternative way of measuring low titers of *M.tb.* antigens. To improve the method, replacing streptavidin by avidin-coated fluorescent/polystyrene beads or microspheres may represent a way to enhance the size and visibility of aggregates [33]. The aggregated beads will be more easily detectable and be retained on the sieves. Quantification of such complexes could be an issue however due to the time and environmental dependence of the formation of random and chaotic 3D complexes.

In the second strategy, the detection was based on a lateral flow immunoassay (LFIA). Two complementary VHH llama antibodies (with and without biotin tag) were pre-mixed with the HSP target protein along with a neutravidin-coated carbon NP in a single step detection procedure. The assay detected a lower limit of 0.25 $\mu$ g/ml of purified recombinant HSP antigen (Chapter 5). The LFIA set up was highly specific for *M.tb.* as it could discriminate *M.tb.* from atypical *Mycobacterium* (like *Mycobacterium smegmatis/M.smeg.*). This is highly relevant as the traditional immunodiagnostic tests often employed in the field – like *Mantoux test* – yield many false positives due to cross-reaction between antigens shared within different *Mycobacterium sp.* bacteria [31]. LFIA is an established and mature technology, where minimal operator-dependent steps and interpretations are required, thus making it an easy to handle assay [25]. It also has the flexibility to be integrated with on-board optical, reader and information systems. More importantly the assay offers high sensitivity, specificity, speed and stability at a relative low cost [30].

## 8.5 A NW FET-based assay of TB HSP antigen

NW-based sensors gained attention during the last decade due to their outstanding semiconductor properties as well as large surface to volume ratio that seemed to enable ultra-sensitive reversible assays utilizing electrical detection of the charge properties of an analyte bound to a surface [34-37]. It was the main original aim of this thesis to exploit these properties of NWs towards the development of a detection platform for TB. In this study - streptavidin coated NWs were functionalized with biotinylated VHH antibodies against the 16 kDa HSP antigen protein to form the biosensing layer of the sensor. NW-based detection is a direct detection method capable of sensing charges of biomolecules within the Debye layer. As a result it is not dependent on any labelling for signal production, but does require close proximity of the target molecule to the NW and changes in charge distribution at the surface. For connecting the NW with the readout electronics, a compact biosensing module equipped with automated microfluidics for controlled injection of the ligand was developed as well. The microfluidics potentially allows the user to control assay speed and throughput by means of flow speed, mixing, multiplexing and parallel assay designs. The functionality of

the sensing module with the NW chip was characterized by flow injection analysis of pH solutions, flow rate induced sensitivity changes and receptor-ligand binding in real time. The lowest concentration of HSP that appeared to be detected was 100 ng/ml, but further dilutions HSP and controls were not tested due to a lack of functional nanowire chips available to the project. This also prevented a further study of additional aspects such as specific functionalization with different probes of nanowires that are part of an array, allowing for better internal calibration of the signals. Other elements that needed testing were use of shorter cross linkers for anchoring VHH antibody at reduced salt concentrations of the running buffer to overcome the Debye length ionic screening effects that strongly influence the sensitivity of the system.

SiNW-FET-based biosensors may have potential in TB detection, but apart from this project - little research has been performed so far towards such an application. The results obtained in this PhD project, make clear that such SiNW-based devices will require a lot of further optimization. The challenges are to (i) obtain electronically functional nanowires reliably, (ii) to functionalize them with antibodies without increasing the distance to the wire too much, and (iii) to realize sufficient multiplexing to allow an analysis yielding robust data. Although several groups have shown better results with SiNW [37, 60, 61], there are still several issues such as device-to-device variation due to which results are not reproducible. Also, electrical drift and Debye screening and complex handling procedures are major drawbacks of the technique. Hence, the development of such SiNW-based tools is handicapped by the lack of proper nanofabrication and surface functionalization techniques. Finally, a point of concern for the development of microfluidic biosensing systems of TB is also their difficult compatibility to the kind of biological samples derived from TB patients. Sputum samples are viscous and irregular and may obstruct the microchannel and subsequent electrical measurements in various ways.

## **8.6 Development of label-free one step detection of TB host biomarkers using cellular membrane receptors**

Apart from producing specific biomarkers itself, *M.tb.* also induces host-derived biomarkers that circulate through the body in sputum, blood, urine, etc. These biomarkers are cellular messengers/hormones that are recognized by a range of cellular receptors. Host derived biomarkers released and circulating in response to an infection by TB are interferon gamma (IFN- $\gamma$ ), fork-head box P3 (FOXP3), interleukins (IL-1RA, IL-8, IL-18, IL-12), IP-10 and mast cell protease (MCP-1, MCP-2, MCP-3) [38-43]. Of these, IL-8 has a significant role in pathogenesis of TB and is specifically recognized by the G protein-coupled receptors CXCR1 and CXCR2. GPCR activations can be monitored by various assays but cell impedance, measuring changes in cell shape in response to a ligand, is particularly interesting as it requires no labeling, is highly sensitive and fast. For the related  $G_{\alpha i}$  dependent chemokine receptor CXCR3 it was already established that this technique worked well [44].

Cell-based biosensing platforms are developing fast and finding their place in diagnosing complex disease conditions. The basic principle of such cell-based assays depends upon the activation of specific cellular signalling cascades upon activation by specific ligands [45]. A broad range of such cell-based assays have been reported [45]. In order to apply such principles to the detection of *M.tb.* induced host biomarkers a microfluidics supported cell impedance measurement set up was built (Chapter 7). With the implementation of microfluidics, practical point-of-care needs such as high throughput, low amount and concentration of samples and lower costs may be achievable. Microfluidics based systems also allow user control over the assay in terms of flow rate, mixing and multiplexing along with parallel assay designs. This is true for both antibody and cell based assays. For proof of concept with cell based assays – a mammalian cell line expressing the Neurokinin 1 (NK1) pain receptor (which is a GPCR expressed in lungs) was utilized and Substance P (SP) was used as its ligand. It was found that SP could successfully trigger an impedance response upon activation of the NK1 receptor.

The SP activates the  $G_{\alpha_{12/13}}$  pathway and causes blebbing (local constrictions) of the membrane [46]. In general and depending on the sub-classes of G-proteins – four categories of GPCRs are recognized which are  $G_{\alpha_s}$ ,  $G_{\alpha_i/o}$ ,  $G_{\alpha_q/11}$  and  $G_{\alpha_{12/13}}$  [47]. Although the  $G_{\alpha_{12/13}}$  appears to be the predominant pathway, emerging data suggest that the other pathways also affect cell movement and shape [48]. Many studies so far have demonstrated impedance-based assays based with different GPCRs [49-53]. Interestingly GPCRs which do not utilize the  $G_{\alpha_{12/13}}$  pathway upon activation can be manipulated with chimeric G-proteins to redirect the response towards the  $G_{\alpha_{12/13}}$  pathway [54]. Apart from GPCRs, it has been reported that also other (nuclear) receptors like for interleukins and interferon also induce morphological changes in cells [59]. Thus many opportunities exist to develop new impedance-based diagnostic tools targeting the circulating ligands of these receptors.

Although not demonstrated within this thesis, IDE receptor arrays in a single flow cell can introduce a possibility of multiplexing and automation with HTS capabilities. Reverse transfection was shown to be a feasible technique to create local spots of cells on IDEs with specific receptors based on spotted plasmid DNA carrying the receptor gene. That technique will allow the creation of receptor cell arrays on different micro-IDEs. The possibility of arrays potentially provides the system with much better internal controls than microwell based systems. Such controls are essential for robust diagnostics. A downside of a fluidic system with repeated injection of samples over the same cells is the formation of memory in those cells. For this reason any diagnostic application of a fluidic system will probably work with disposable single use cartridges. In summary, impedance-based fluidic assays reporting receptor specific morphological changes can potentially provide an interesting new addition to the diagnostics repertoire.

## 8.7 Conclusions and Future Perspectives

In this thesis, LFIA, coated microsieves, nanowire FETs and cell impedance were developed and/or tested as potential diagnostic platforms for the sensitive and one step detection of TB. Some of the most important findings of this work include:

1. Successful characterization of the epitopes of 16kDa heat shock protein in relation to a large set of VHH llama antibodies. This intracellular protein may be upconcentrated from patient sputum by pre-concentrating the bacteria before lysing them. This procedure may potentially lead to more sensitive detection of tuberculosis. Interestingly, the HSP protein is a major protein especially in the latent phase. An immunoassay based on that protein might therefore potentially enable earlier diagnosis.
2. The polyDADMAC coated microsieve assisted up-concentration of *M.tb.* cells from samples such as sputum might be very useful in obtaining sufficient bacterial counts for any desired detection assay.
3. The LFIA based assay may present a promising platform for providing an affordable, fast and simple detection assay. We failed to establish reproducible results, possibly due to the deterioration of the protein sample.
4. Prototypes of the compact, modular, microfluidic biosensing platform with both NW-FET and IDE microelectrodes developed in this thesis are relevant first examples for a development of on-chip high throughput assays where simultaneous detection of multiple targets is possible. Assays equipped with microfluidics allow a more precise control over the volumes, read outs and timing of the assay, thus reducing time and reducing overall cost of the assay without compromising on the sensitivity.
5. The cell based impedance sensor of chapter 7 is the first demonstration of microfluidic cell impedance measurements. The experiments showed exquisite sensitivities and reversibility of the responses which both were new. Both reverse transient and stable transfected cells showed sensitive impedance responses. This marks a great potential of these types of fluidic and multiplexed assays for GPCR research and possibly diagnostics.

Cumulatively, the research demonstrated in the thesis will be useful in understanding the complexities and possibilities towards the development of effective biosensing platforms for TB detection. The main areas for improvements, building on the current advances are:

1. The development of a one step *M.tb.* cell concentration and lysis protocol from samples such as sputum where the viscosity of the sample obtained from the patients is too high. With the current available liquification techniques only half of the total cell present in the sputum could be extracted thus reducing the cell count for the desired assay.

2. The prototype biosensing module developed in this thesis, lacks the possibility to tackle thermal control and suffers from a poorly understood drift. Another shortfall of the module was its inability to perform simultaneous AC measurement on two parallel electrodes due to interferences originating from neighbouring electrodes. This was only an issue while doing AC measurement, as during DC measurement interference from neighbouring electrodes was not observed. These issues could be tackled in a next design of the module where sequential addressing of the electrodes could be implemented as in the case of existing microtiter plate format. Also electric drift compensation methods could be adapted in the chip layout by arranging a row-column format so that electrical contacts are better distributed at the sensing area.
3. The flowcell used in the prototype biosensing module did not allow a higher flowrate than typically one flowcell dead volume per minute. This slows down the step of delivering the samples through long tubing but this issue can easily be tackled in future designs by creating a wider and/or higher flowchannels.

An ideal diagnostic test for tuberculosis would be an assay that enables accurate diagnosis within the time of clinical consultation. So, far most of the approaches that emerged over the past few decades all have their own disadvantages and this work also did not bring the ideal outcome.

In final words, it can be stated that developing a highly effective biosensing platform remains a dream to achieve, and thus a topic for further research. This thesis may provide material for the interested researcher and developer to further work on one of these platforms to achieve a potent and sensitive detection assay for TB. Although the focus of the present thesis was TB, the scope of the evaluated diagnostic platforms is not limited to TB alone.

## References

1. Pavlou AK, Magan N, Jones JM, Brown J, Klatser P, *et al.*; *Biosens Bioelectron*, **2004**, *20*, 538
2. Turner APF, Magan N; *Nat Rev Microbiol*, **2004**, *2*, 161
3. Freeman R, Goodacre R, Sisson PR, Magee JG, Ward AC, *et al.*; *J Med Microbiol*, **1994**, *40*, 170
4. Lee TMH; *Sensors*, **2008**, *8*, 5535
5. Rachkov A, Patskovsky S, Soldatkin A, Meunier M; *Talanta*, **2011**, *85*, 2094
6. Hsieh SC, Chang CC, Lu CC, Wei CF, Lin CS, *et al.*; *Nanoscale Res Lett*, **2012**, *7*, 180
7. Prabhakar N, Arora K, Arya SK, Solanki PR, Iwamoto M, *et al.*; *Analyst*, **2008**, *133*, 1587
8. Duman M, Piskin E; *Biosens Bioelectron*, **2010**, *26*, 908.
9. Huang JG, Hung CCK, Lai HC, Lee CK, Lin SM, *et al.*; *Conference proceedings of IEEE Engg Med*, **2004**, *26*, 2553
10. Duman M, Ilayan, Demirel G, Khan, Pi, *et al.*; *Sensor Lett*, **2009**, *7*, 535
11. Trilling AK, de Ronde H, Noteboom L, van Houwelingen A, Roelse M, *et al.*, *PLoS One*, **2011**, *6*, e26754
12. Chinnappa NB; *Thorax*, **2011**, *66*, 590
13. Thanyani ST, Roberts V, Siko DGR, Vrey P, Verschoor JA; *J Immunol Method*, **2008**, *332*, 61
14. Hamasur B, Bruchfeld J, Haile M, Pawlowski A, Bjorvatn B, *et al.*; *J Microbiol Method*, **2001**, *45*, 41
15. Pariwono AM, Lim CS, Lo ST, Amrie Y, Mughtar A; *International Conference on Biomedical and Pharmaceutical Engineering*, **2006**, *1*, 372
16. Mcnerney R, Wondafrash BA, Amena K, Tesfaye A, Mccash EM, Murray NJ; *BMC Infect Dis*, **2010**, *10*, 161
18. Ren JL, He FJ, Yi SL, Cui XY; *Biosens Bioelectron*, **2008**, *24*, 403
19. He F, Zhao J, Zhang L, Su X; *Talanta*, **2003**, *59*, 935
20. Pang P, Cai Q, Yao S, Grimes CA; *Talanta*, **2008**, *76*, 360
21. Chun AL; *Nat Nano*, **2009**, *4*, 698
22. Lee H, Sun E, Ham D, Weissleder R; *Nat Med*, **2008**, *14*, 869
23. Global Tuberculosis Report; WHO, **2012**
24. Toussaint CH, Pritchard EK; *Postgrad Med J*, **1944**, *20*, 143
25. Kaewphinit T, Santiwatanakul S, Promptmas C, Chansiri K; *Sensors*, **2010**, *10*, 1846
26. Srivastava SK, Ruigrok VJ, Thompson NJ, Trilling AK, Heck AJ, *et al.*; *PLoS One*, **2013**, *8*, e64040
27. Muyldermans S; *Ann Rev Biochem*, **2013**, *82*, 775
28. Zuo X, Xiao Y, Plaxco KW; *J Am Chem Soc*, **2009**, *131*, 6944
29. Du C, Zhang A, Bai H, Li L; *ACS Macro Lett*, **2012**, *2*, 27
30. O'Farrell B; *Evolution in Lateral Flow-Based Immunoassay Systems*, **2009**, Springer, p35
31. Somoskovi A, Hotaling JE, Fitzgerald M *et al.*; *J Clin Microbiol*, **2000**, *38*, 2743
32. Li Y, Lubchenko V and Vekilov P G; *Rev Sci Instrum.*, **2011**, *82*(5): 053106
33. Blazer L I, Roman D L, Muxlow M R and Neubig R R; *Curr Protoc Cytom.*, **2010**, *13*.1115.
34. Gao A, Lu N, Dai P, Li T, Pei H, *et al.*; *Nano Lett*, **2011**, *11*, 3974
35. Wang WU, Chen C, Lin KH, Fang Y, Lieber CM; *Proc Natl Acad Sci*, **2005**, *102*, 3208
36. Cui Y, Wei Q, Park H, Lieber CM; *Science*, **2001**, *293*, 1289
37. Patolsky F, Lieber CM; *Mat Today*, **2005**, *8*, 20
38. Ameixa C, Friedland JS; *Infect Immun*, **2002**, *70*, 4743
39. Lin YG, Gong JH, Zhang M, Xue WF, Barnes PF; *Infect Immun*, **1998**, *66*, 2319
40. Ruhwald M, Bjerregaard-Andersen M, Rabna P, Eugen-Olsen J, Ravn P; *BMC Res Notes*, **2009**, *2*, 19
41. Sutherland JS, Hill PC, Adetifa IM, de Jong BC, Donkor S, *et al.*; *PLoS One*, **2011**, *6*, e25230
42. Wu B, Huang C, Kato-Maeda M, Hopewell PC, Daley CL, *et al.*; *J Immunol*, **2007**, *178*,

3688

43. Zhang Y, Broser M, Cohen H, Bodkin M, Law K, *et al.*; *J Clin Inv*, **1995**, 95, 586
44. Watts AO, Scholten DJ, Heitman LH, Vischer HF, Leurs R; *Biochem Biophys Res Commun*, **2012**, 419, 412
45. Ding L, Du D, Zhang XJ, Ju HX; *Curr Med Chem*, **2008**, 15, 3160
46. Meshki J, Douglas SD, Lai JP, Schwartz L, Kilpatrick LE, *et al.*; *J Biol Chem*, **2009**, 9280
47. Hermans E; *Pharmacol Therap*, **2003**, 99, 25
48. Perez V, Bouschet T, Fernandez C, Bockaert J, Journot L; *Eur J Neurosci*, **2005**, 21, 26
49. Peters MF, Scott CW; *J Biomol Screen*, **2009**, 14, 246
50. Scandroglio P, Brusa R, Lozza G, Mancini I, Petro R, *et al.*; *J Biomol Screen*, **2010**, 15, 1238
51. Halai R, Croker DE, Suen JY, Fairlie DP, Cooper MA; *Biosensors*, **2012**, 2, 273
52. Yu N, Atienza JM, Bernard J, Blanc S, Zhu J, *et al.*; *Anal Chem*, **2006**, 78, 35
53. Krawczyk C, Penninger JM; *J Leukocyte Biol*, **2001**, 69, 317
54. Vazquez-Prado J, Miyazaki H, Castellone MD, Teramoto H, Gutkind JS; *J Biol Chem*, **2004**, 279, 54283
55. Tsara V, Serasli E, Christaki P; *Hippokratia*, **2009**, 13, 20
56. Steingart KR, Ramsay A, Dowdy DW, Pai M; *Indian J Med Res.*, **2012**, 135(5), 695
57. Singh S, and Katoch V M; *Indian J Med Res.*, **2011**, 134(5), 583
58. Surendiran A, Sandhiya S, Pradhan S C and Adithan C; *Indian J Med Res.*, **2009**, 130(12), 689
59. Netea M G, Lewis E C, Azam T, Joosten L A B, *et al.*; *PNAS*, **2008**, 105(9), 3515.
60. Hu J, Odom TW, Lieber CM; *Acc Chem Res*, **1999**, 32, 435
61. Jiangtao H, Min O, Peidong Y, Charles ML; *Nature*, **1999**, 399, 48

# Appendix A

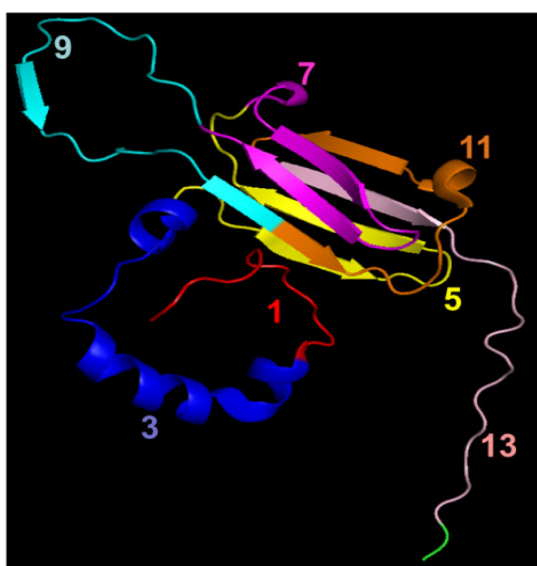
## Supporting Information: Chapter 3

### Table

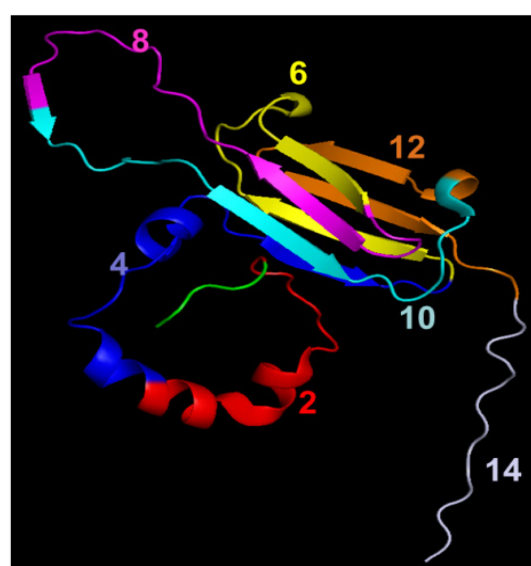
**Table S1.** Comparison between the actual and estimated molecular weights of the standard proteins along with the deviation percentage while calibrating the SEC column.

Protein	Mw (kD)	Ve (mL)	Est. MW	Deviation (%)
Blue Dextran 2000	2000	8.38	1736.89	13.16
Ferritin	440	10.72	538.94	-22.49
Catalase	232	12.7	200.21	13.70
Aldolase	158	13.22	154.37	2.30
Albumin	67	14.33	88.61	-32.25
Ovalbumin	43	15.43	51.11	-18.86
Chymotrypsinogen A	25	17.42	18.89	24.44
Ribonuclease A	13.7	18.19	12.85	6.20

### Figures



Odd Epitopes mapped



Even Epitopes mapped

**Figure S1:** Arrangement of odd and even epitopes on the 16kDa heat shock protein from *M.Tb*.

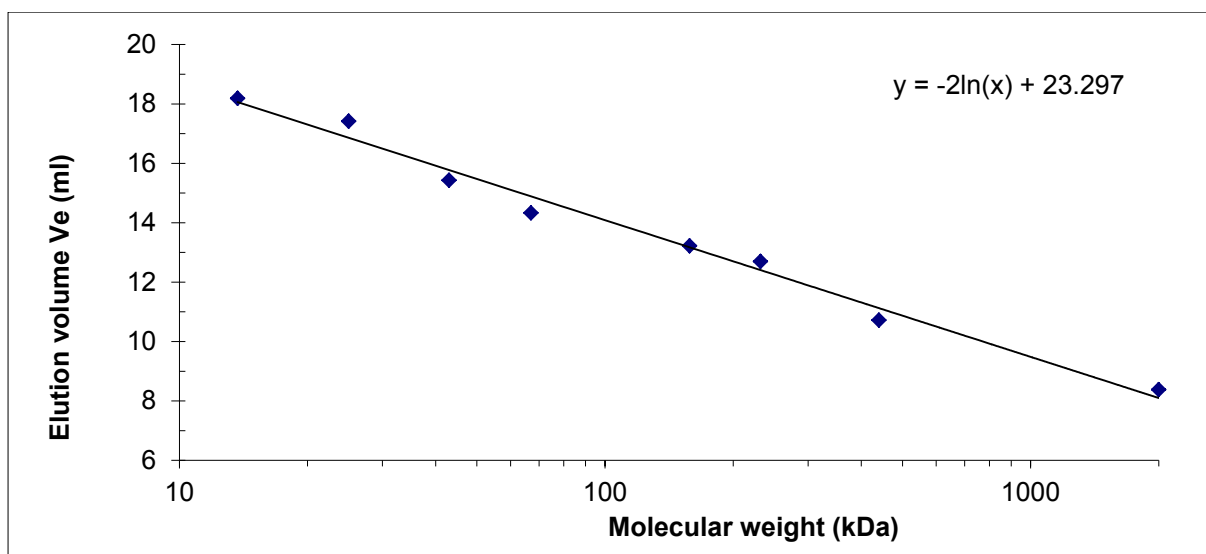


**Figure S2:** Plot for calibration of Superdex 200 10/300 GL SEC column with known standards.

# Summary

Tuberculosis (TB), caused by the bacteria *Mycobacterium tuberculosis* (*M. Tb.*), is a contagious disease, affecting mainly the human respiratory system. It causes millions of deaths worldwide every year. With the emergence of multiple drug resistant (MDR) strains, TB imposes a revived and stimulated health threat to humanity on a global scale. It causes diseases to patients coming from every age group and from all the continents. Usually patients with low immunity status are the main target for getting infected with TB and hence, it is making the situation difficult in sub-Saharan Africa where almost one-third of the TB population is also suffering with either an active or passive human immunodeficiency virus (HIV) infection.

One of the major obstacles in the management of TB is an early detection of the cases. Unfortunately, the popular techniques today lack the desired amenities to apply them in resource-poor areas. Moreover, most of the current techniques demand laboratory and logistic back up which further hinder their scopes. In this PhD project amongst others unique properties of nanowire-based biosensing techniques were investigated to see if fast, affordable and more sensitive detection methods for TB diagnosis can be obtained.

Chapter 1 gives an introduction on the topic along with outlining the needs for the present PhD project. In order to do so, the chapter first outlines the seriousness and emergency caused by TB as a disease along with some initiatives taken on a global scale, like that by the World Health Organization (WHO), to eliminate TB. The introduction will lay the background for the necessity of the introduction of novel techniques in order to tackle TB while recognizing the inadequacies of the current techniques. The desired characteristics of an ideal TB detection platform were also discussed and the potential of nanotechnology towards development of new biosensing platforms for TB detection was accounted for. The concept of silicon nanowires and microchips in detection of TB was also introduced.

However, in order to streamline the research towards developing novel nanotechnology-based biosensing platform, it is essential to make a concise review of the current techniques in TB detection. Therefore, chapter 2 gives a detailed review of the current biosensing modalities present in the field of TB detection along with enlisting their pros and cons.

The heat resistant 16 kDa heat shock protein (HSP) had been repeatedly recognized as an important factor in the pathogenesis of TB. However, considerable discrepancy and debate exists over its structural format and about its antigenic components. For example, it is still debated if it exists as a dimer, tetramer, nonamer or dodecamer in its native form. Thus to understand such mysteries lying with HSP, sandwich ELISA and SPR experiments were designed where 12 different VHH Llama antibodies were used and their binding kinetics were assayed against 14 overlapping epitopes (each epitope 20 amino acid long). It was

found that 8 out of 9 VHH antibodies recognized 7 out of 14 epitopes.. The most effective binding was shown by both the B-F10 and A-23 antibodies. While the B-F10 could be used as secondary antibody, both B-F10 and A-23 can be used as anchoring antibodies. Finally, a homodimer model was suggested to describe the structure of the HSP, when it is isolated using harsh conditions like urea lysis.

One of the key challenges in TB detection is the rather low sensitivity of most prevalent techniques. In chapter 4, an effort has been made to improve the sensitivity of *M. Tb.* detection. In order to do so, a two-step approach was undertaken. First, the concentration of *M. Tb.* bacteria in biological samples was increased/densified by concentrating the bacteria on a PolyDADMAC coated microsieve followed by a lysis step using standard procedures in order to extract the cellular internal proteins. In a next step, another set of microsieves were surface functionalized utilizing biotin-streptavidin coupling chemistry to attach the antibody VHH A-23 on the microsieve for capturing the HSP dimer. When HSP dimer has been captured on the surface of the microsieves, they were sandwiched using a biotinylated secondary antibody i.e. VHH F-10, followed by detection using a fluorescence labelled streptavidin. The results revealed protein aggregates on the microsieve which were confirmed and measured on their sizes with the help of Dynamic Light Scattering. This new approach may offer a new detection method and could improve the sensitivity level with respect to prevalent techniques.

In chapter 5, a lateral flow immunoassay (LFIA) technique is reported to improve the sensitivity of detection in TB while demonstrating the capture of HSP dimer in a sandwich assay. In order to do so, nitrocellulose membranes were cut into strips and fixed on a plastic backing. The LFIA strips were sprayed with anti-VSV capture antibody as a test line where the pre-mixed antibody-antigen complex coupled with carbon nanoparticles (CNPs) could bind. CNPs were used in the assay as black labels to visualize the results. The technique demonstrated detection capabilities at a range of 0.25 µg/ml which is comparable in efficiency to other popular techniques while potentially being easier to implement.

In chapter 6, a compact modular biosensing system was developed utilizing nanowire field effect transistor (FET)-based devices hosted under a re-sealable glass microfluidic flow cell. The sensing module was equipped with an option to perform both AC impedance as well as DC conductivity measurements. To demonstrate the usefulness of the set-up, DC conductivity responses to sequential injections of different iso-ionic pH solutions and AC impedance responses to sequential binding of proteins (streptavidin, antibody, protein ligand) to the surface were done in real time. Though there were certain limitations such as drift and inability to perform simultaneous measurement on more than one electrode (due to electrical interferences) the system showed considerable promise and can be used in high throughput screening (HTS) assays.

In chapter 7, the compact modular biosensing system developed in chapter 6 was utilized by replacing the nanowire FET chips with interdigitated electrodes (IDE) to perform AC impedance electrochemical measurement towards interrogation of ligand specific

reversible activation of live mammalian (HEK293) cells expressing specific G protein-coupled receptors (GPCRs). A comparative study was also performed where stable GPCR transfection was compared with GPCR expressed via reverse transfection in HEK293 cell lines. The focus was to validate and provide a proof of concept to show that GPCR expressing mammalian cell with AC impedance measurement could be applied towards the detection of endogenous TB biomarkers produced within the cells. In relation to TB, biomarkers such as interferon gamma (IFN- $\gamma$ ), fork-head box P3 (FOXP3), interleukins (IL-1RA, IL-8, IL-18, IL-12), IP-10 and mast cell protease (MCP-1, MCP-2, MCP-3) are shown to be interesting. The GPCR used in the study was Neurokinin receptor 1 (NK1) with its specific ligand i.e. Substance P (SP). Upon activation of NK1 receptor, the  $G\alpha_{12/13}$  pathway is activated, causing the cell to undergo a morphological change (shrinking of membrane cortex) termed as *blebbing*. Due to this blebbing, a decrease in the overall impedance of the system was observed. Sensitive measurements at a flow speed of 10  $\mu\text{l}/\text{min}$  were done up to a concentration of 1 pM of SP using impedance measurements at 10 mV and 15 kHz, which was many folds more sensitive than the existing techniques. Though the response profiles obtained for stable as well as reverse transfected cell lines were a little different, the overall signal obtained with various ligand doses were generally reproducible and thus facilitating the possibilities to perform parallel measurements on IDE arrays with distinct receptors per IDE in a single flow channel. The present system could directly be applicable for other GPCR's which utilize the  $G\alpha_{12/13}$  pathway upon activation but for GPCRs which do not naturally follow the  $G\alpha_{12/13}$  pathway, chimeric versions could be produced and utilized. These findings open up further possibilities to use impedance measurements as a truly generic platform for GPCR research.

Finally, chapter 8 concludes the thesis with general discussion while outlining the scopes for further research.



# Samenvatting

Tuberculose (TBC), veroorzaakt door de bacterie *Mycobacterium tuberculosis* (*M.tb.*), is een besmettelijke ziekte, die vooral het ademhalingsstelsel aantast en wereldwijd jaarlijks tot miljoenen doden leidt. Met de opkomst van multi-drug resistente (MDR) stammen, is het aantal TBC gevallen weer toegenomen en vormt deze een groeiende bedreiging voor de gezondheid van mensen in elke leeftijdsgroep en op vrijwel alle continenten. De belangrijkste groep die besmet raakt met TBC zijn patiënten met een lage weerstand. In Sub-Saharisch Afrika is de situatie het meest ernstig, en lijdt bijna een derde van de door TBC getroffen mensen ook nog eens aan een actieve of passieve human immunodeficiency virus (HIV) infectie.

Een van de grootste obstakels voor de beheersing van TBC is een vroege opsporing van de besmetting. Helaas ontbreken in arme gebieden veelal de gewenste faciliteiten evenals getraind personeel om de hedendaagse technieken toe te passen. In dit promotieonderzoek worden nieuwe, innovatieve “biosensing” methoden bestudeerd of ontwikkeld om snelle, betaalbare en gevoelige diagnostiek van TBC mogelijk te maken.

Hoofdstuk 1 bevat een inleiding over het onderwerp en beargumenteert de motivatie achter dit promotieonderzoek. Hiertoe wordt eerst de ernst van TBC als ziekte geschetst en de rol van initiatieven, zoals van de World Health Organization (WHO), om TBC te elimineren. Hieruit volgt een noodzaak om nieuwe technieken te ontwikkelen, door tekortkomingen van huidige technieken om tuberculose aan te pakken te identificeren. Hierbij worden de gewenste eigenschappen waaraan een TBC opsporingsplatform geschikt dient te zijn voor ontwikkelingslanden besproken, alsmede het potentieel van nanotechnologie om daarin een bijdrage te kunnen leveren. De mogelijke bijdrage van silicium nanodraad- en microchip-gebaseerde oplossingen in de opsporing van tuberculose wordt hierbij aangegeven.

Om het onderzoek naar de ontwikkeling van nieuwe, op nanotechnologie gebaseerde, ‘biosensing’ platforms goed te positioneren, is het essentieel om een beknopt overzicht van de huidige technieken te geven. Hoofdstuk 2 geeft derhalve een meer gedetailleerd overzicht van ‘biosensing’ oplossingen voor de opsporing van TBC die de afgelopen jaren gepubliceerd zijn met een inschatting van de voor- en nadelen van de voorgestelde technieken.

In de pathogenese van TBC wordt het 16 kDa heat shock eiwit (HSP) aangemerkt als een belangrijke indicator. Tot nog toe niet volledig begrepen is de exacte quaternaire conformatie van dit multimere eiwit evenals de positie van de belangrijkste epitopen. Er zijn publicaties die HSP typeren als een dimeer, tetrameer, nonameer of dodecameer. Om deze puzzle van HSP eerst te begrijpen, zijn sandwich ELISA- en SPR-experimenten uitgevoerd, waarin de bindingskinetiek van twaalf verschillende VHH-lama antilichamen werd getest t.o.v. veertien overlappende epitopen (elk epitooop 20 aminozuren lang). Het bleek dat acht

van de negen gebruikte VHH-antilichamen bonden aan zeven van de veertien epitopen. De meest effectieve binding werd geregistreerd voor het B-F10 en A-23 antilichaam. B-F10 kon het meest effectief gebruikt worden als detectie-antilichaam, terwijl zowel B-F10 als A-23 gebruikt konden worden als anker-antilichaam. Op grond van experimenten na urea lysis en renaturatie werd een homodimeer model voorgesteld om de structuur van de HSP te beschrijven.

Eén van de belangrijkste beperkingen in de opsporing van TBC is de lage gevoeligheid van de huidige technieken. In hoofdstuk 4, is een poging gedaan om de gevoeligheid voor *M.tb* opsporing te verbeteren. Hiertoe werd een tweestapsbenadering gekozen. Voor de eerste concentratiestap, werd een techniek ontwikkeld om de concentratie van *M.tb*. bacteriën in monsters van patienten te verhogen door het vangen/concentreren van de bacteriën op een met poly-DADMAC gefunctionaliseerde microzeef. De bacteriën kunnen hierna gemakkelijk worden gelyseerd met behulp van standaardprocedures om interne cellulaire eiwitten, zoals HSP, vrij te maken. In een tweede detectiestap werd het oppervlak van een tweede type microzeven gefunctionaliseerd met antilichaam VHH A-23 voor het binden van te detecteren HSP-dimeren. Eventueel HSP-dimeer op het oppervlak van de microzeven werd vervolgens gekoppeld met gebiotinyleerd VHH F-10 detectie-antilichaam, waarna fluorescente detectie mogelijk werd gemaakt met behulp van een streptavidine marker voorzien van een fluorescent label. De resultaten gaven tevens opmerkelijke fluorescente eiwitaggregaten te zien welke waren gevangen of gevormd op de microzeef. Met Dynamische Licht Verstrooiing (DLS) werd dit beeld bevestigd en kon een schatting van de grootte van deze aggregaten worden gedaan. Toepassing van elementen van de gevonden resultaten en gebruikte methodes kunnen mogelijk de gevoeligheid van de huidige methodes aanzienlijk verbeteren.

In hoofdstuk 5 wordt een laterale flow immunoassay (LFIA) techniek voor de detectie van *M.tb*. beschreven. Daarbij wordt gebruikgemaakt van een sandwich assay met lama antilichamen gericht tegen de HSP-dimeer. Hierbij werden nitrocellulose membranen in stroken gesneden en op een cellulose basis vastgehecht. De LFIA strips werden besproeid met een testlijn van een anti-VSV anker-antilichaam. Daaraan kan een voorgemengd complex van twee detectie-antilichamen (met VSV of biotine tag), een HSP monster en koolstofnanodeeltjes (CNPs) bedekt met neutravidine binden. CNP's werden in de test gebruikt om het signaal te versterken, met als bijkomend voordeel dat CNP's heel eenvoudig met een relatief goedkope scanner gekwantificeerd kunnen worden. Met de techniek kon in een 25  $\mu$ l sample 0.25  $\mu$ g/ml HSP gedetecteerd worden, wat vergelijkbaar is met gangbare technieken, maar die vaak complexer zijn om uit te voeren.

In hoofdstuk 6 is een compact modulair biosensor-systeem ontwikkeld waarbij gebruik gemaakt werd van een nanodraad-field-effect transistor (FET) principe. De sensor werd toegankelijk gemaakt voor het sequentieel screenen van een monster door het op te sluiten in een hersluitbare glazen microfluidische flowcel. De sensor module is verder uitgerust met de mogelijkheid om zowel AC impedantie, als DC geleidbaarheidsmetingen uit te voeren. Om de bruikbaarheid van de opstelling aan te tonen werden twee type metingen

gedaan, één waarbij de DC geleidbaarheid reageerde op opeenvolgende injecties van ionische oplossingen die verschilden in hun pH waarden (hetgeen verklaarbaar is door verschillen in de protonering van het oppervlak van de sensor) en één waarbij de AC impedantie reageerde op een opeenvolgende binding van eiwitten (streptavidine, antilichaam, en HSP eiwit ligand) aan het oppervlak. Beide veranderingen in de lading aan het oppervlak van de nanodraad konden in *real time* gevolgd worden. Hoewel er bepaalde beperkingen waren zoals drift van het signaal en de onmogelijkheid om gelijktijdige metingen uit te voeren aan meer dan één nanodraadjie is aangetoond dat dit meetsysteem bruikbaar kan zijn voor gebruik in high throughput screening (HTS) methoden.

Het compacte modulaire biosensor-systeem, dat beschreven is in hoofdstuk 6, werd in hoofdstuk 7 gebruikt voor AC impedantie-metingen aan cellen, welke speciaal gegroeid zijn op 'interdigitated' (kam-vormige) electrodes. Het betreft hier humane HEK293 cellen, die specifieke G-proteïne gekoppelde receptoren (GPCRs) tot expressie hebben gebracht. Stabiel getransfekteerde cellen werden hierbij vergeleken met cellen die op de electrodes zelf getransfekteerd werden m.b.v. de zogenaamde 'omgekeerde transfectie' methode. De focus van dit hoofdstuk was een proof of concept en aan te tonen dat GPCR expressie in zoogdiercellen met AC impedantie metingen kunnen worden gedetecteerd, waardoor mogelijk ook detectie van endogene TB biomarkers gerealiseerd kan worden. Met betrekking tot TB, zijn biomarkers zoals interferon gamma (IFN- $\gamma$ ), fork-head box P3 (FOXP3), interleukinen (IL-1RA, IL-8, IL-18, IL-12), IP-10 en mestcel protease (MCP-1, MCP-2, MCP-3) mogelijk interessant. De GPCR welke in deze studie is gebruikt is de Neurokinine receptor 1 (NK1) in combinatie met het specifieke peptide ligand 'Substance P' (SP). Na de activering van de NK1 receptor, wordt de  $G\alpha_{12/13}$  pathway/route geactiveerd, waardoor de cel een morfologische verandering ondergaat (insnoeringen/blebbing). Door deze insnoeringen, vermindert het contactoppervlak van de cellen met de electrodes en daalt de impedantie van het systeem. Metingen werden uitgevoerd bij een stroomsnelheid van 10  $\mu\text{l}/\text{min}$  en signalen bij een concentratie van 1 pM SP konden nog worden gedetecteerd, wat aanzienlijk gevoeliger is dan tot nog toe gerapporteerd voor vergelijkbare technieken op veel grotere IDEs. Hoewel de reactieprofielen verkregen voor stabiele en reverse getransfekteerde cellijnen enigszins verschilden, waren de verkregen signalen over het geheel genomen reproduceerbaar en aantoonbaar concentratie-afhankelijk. De reverse transfectie methode biedt mogelijkheden voor het doen van parallelle metingen op verschillende electrodes en met cellen met verschillende receptoren per IDE allen in dezelfde flowcel. Het huidige systeem kan mogelijk rechtstreeks worden toegepast voor andere GPCRs, die eveneens gebruik maken van de  $G\alpha_{12/13}$  route, maar mogelijk ook voor GPCRs die niet de natuurlijke  $G\alpha_{12/13}$  route volgen. Deze vindingen maken het mogelijk om de hier gedane impedantie-metingen aan cellen verder te ontwikkelen tot een generiek platform.

Hoofdstuk 8 van het proefschrift sluit af met een algemene discussie waarbij een overzicht van de mogelijkheden voor verder onderzoek wordt gegeven.



## Overview of Completed Training Activities

### Discipline specific activities

Micro-Nano conference'09	Delft, Netherlands	2009
IPOP Bio-Nano Symposium	Wageningen, Netherlands	2010
14 <sup>th</sup> International Conference on Miniaturized systems for Chemistry and Life Sciences.	Groningen, Netherlands	2010
Post Graduate Program in Bio-Nanotechnology & Medical Applications	Noida, India.	2010 –2011
EMBO Practical Course Methods in Chemical Biology	Heidelberg, Germany	2011- 2011
3 <sup>rd</sup> International Advance course on Proteomics	Wageningen, Netherlands	2011
GPCR Day 2011	Vlaardingen, Netherlands	2011

### General Courses

Philosophy and Ethics of Food Science and Technology	VLAG	2011
Advanced Course Guide to Scientific artwork	WUR Library	2011
Adobe InDesign	WUR Library	2011
Techniques for writing and presenting a scientific paper	WGS	2012
NI Day 2012 for Labview	Utrecht, Netherlands	2012
NI Day 2013 for Labview	Utrecht, Netherlands	2013
Scientific Publishing	WGS	2013

### Optionals

Preparing PhD research proposal	PRI, Wageningen	2009
Weekly work discussion meetings	PRI, Wageningen	2009-2013
Weekly Bioscience Cluster meetings	PRI, Wageningen	2009-2013
Colloquium meetings	ORC, Wageningen	2009-2013
PhD study trip 2011 to Scotland and Northern UK	ORC, Wageningen	2011
PhD trip 2013 + Organisation	ORC, Wageningen	2013



# *Acknowledgement*

Like everyone, my 4 years of PhD was like a roller coaster ride, but with constant support from my supervisors, family and friends I landed safely on ground. Today as I look back a famous saying by Winston Churchill echoes in my head –

*“Success is walking from failure to failure with no loss of enthusiasm.”*

I had been a strong, determined person throughout my life but I must say that the motivation and guidance given by my Co-promoter and daily supervisor **Dr. Maarten Jongsma** has been the key player in bringing me closer to my goal. If anything contained in this thesis is deemed meritorious, it most assuredly can be attributed to his lessons and fruitful suggestion; I alone take credit for the less than meritorious content. Maarten your suggestions and faith in me kept me going even during the dark period when I was stuck and helped me come out with flying colours. I feel privileged for having an opportunity to work under your guidance and supervision. You taught me the essence of Dwayne Michael Carter words “Repetition is the father of learning, I repeat, repetition is the father of learning.” I would always be deeply in debt to you for believing in me and supporting me throughout my tenure as a PhD student in Wageningen.

My sincere gratitude also goes to my promotor **Prof. Dr. Cees van Rijn** for his guidance and encouragement during this period, without which the completion of this work would not have been possible. Discussions with him were stimulating and always showed me the right path, around which I was roaming. I thank you Cees for the continuous support you gave in my PhD study and research, Your patience, motivation, enthusiasm, and immense knowledge helped me a lot at the time of research and writing of this thesis.

I gratefully acknowledge **Prof. Dr. Ernst Sudholter** and **Dr. Louis deSmet** for several insightful discussions we had during our STW meeting and especially for their timely help with surface chemistry related issues. I would also like to thanks **Dr. Aart van Amerongen** and **Dr. Geertruida A. Posthuma-Trumpie** for their useful suggestions, help and support during the LFA study, which was rather a new technique for me. They helped me a lot in understanding the basics and applications of the technique. Discussions with **Dr. Jules Beekwilders** and his suggestions were always fruitful and his friendly nature will always be admired. I would also like to thanks **Dr Hien Duy Tong** and the company **Nanosens B.V.** for designing, fabricating and providing the interdigitated electrodes chips on which the cell-based sensor work was done.

I extend my sincere thanks to the members of my PhD Committee for their valuable time and suggestions on the preliminary version of my thesis. Their feedback acted as an enhancement in the overall presentation of this multi-disciplinary work.

As this was a multi-disciplinary project and thus without help of the experts from different fields I cannot even imagine to reach here. I would start with Rajesh Ramaneti who played an important role at the final stage by giving fruitful suggestions, assistance and inputs regarding the electronic measurements involved. Rajesh, you helped me a lot in establishing the set-up for measurements, which enhanced the speed of my work. I would thank my colleague Anke, who worked with me on llama antibodies along with assistance and discussing various practical issues involved. I wish you success in all your endeavours. I would also like to thank Elwin from Micronit for preparing the customized flowcell and the Nanowire/IDE chip holding cascade for my biosensing module. I am also very grateful to Margriet, you gave me constant support from my first day at PRI and it was a pleasure to discuss science with you. You taught me a lot of skills involved in day-to-day molecular biology and animal cell culture experiments. Besides, it was also very sweet of you to translate for me the letters in Dutch that I received from IND. I wish you all the best for your future. I would always be grateful to Maurice for the help and support he extended but moreover I would also remember him for the jokes and funny moments we had to lighten the burden of work. I am also thankful to Jacob and Ai for their extended help and support during the microsieve experiments at the ORC lab. I would also like to extend my sincere thanks to Hans Meijer for his help and support towards the manufacturing of the print circuit board along with the required cable connections.

To all my problems with the measurement setup Harrie Verhoeven has a solution. I had been saying this ever since I started working with electrical biosensing setup. Thanks for being there; you were like a boon in my PhD tenure. I would like to thank Nikolay, Tamara, Adele and Katja for your useful suggestions and inputs in my work. I am also very thankful to Dr. Willem Haasnoot and Vincent Ruigrok thanks for helping me with surface plasmon resonance experiments. I also thankfully appreciate Dr. Richard Antony and Hans from Royal Tropical Institute, Amsterdam for providing me with the *Mycobacterium* lysates, without your help I would not have been able to do this.

I would also like to thank all the ORC staff members for their support during my PhD. Special thanks to Jannie, Elly, Aleida and Anita for their assistance with the official and financial matters.

Thank to all my PhD and Postdoc colleagues both in PRI and laboratory of organic chemistry: Anke, Aldana, Ting, Yury, Irene, Ana, Maria, Anna, Neli, Marcella, Bart, Sourav, Ai Willem, Nagesh, Jaime, Wouter, Tin, Alexandre, Sidhu, Radostina, Umesh, Nagendra, Satesh, Florine, Yao, Bas, Aline, Wilco, Sweecha, Jorin, Tjerk, Rick, Christie for all the great times that we shared during my stay. Thanks also goes to the visiting students of the student room at PRI Bram, Mart, Christina, Thomas, Venessa, Maria, Inga, Anieke and Fernanda and the great friends of mine in student room with whom I had the awesome Barcelona trip and barbeques at my place. I would also like to thank Sourav for providing his assistance and inputs towards raising funds and organisation of the PhD trip 2013. Thanks also to Nagendra, Wilco and Jorin for their cooperation during the organisation of the PhD trip. This trip was very fruitful and memorable and the funny and exciting moment we all had together there in

Munich and Basel will always be cherished. Also thanks to all my colleagues at PRI, for providing the friendly working environment during my thesis work. I have spent a wonderful time with you all.

Special thanks to Sourav aka Doctor for his **“POSITIVE CRITICISM and TAUNTS”** which always sparked a fire of motivation and envious at the same time to excel in the project and get good publications. I would especially remember this sentence from him **“Guru, ek aur paper chap diya, tumlog kya kar rahe ho?”** i.e. “Dude, got one more paper publish, what you guys are doing?” I would also like to thank him for translating the summary of my thesis in Dutch along with correcting and proof reading my thesis. Sourav you were always a patient listener to all my problems and a good advisor. Your support helped me sail through many storms. I will always miss the fun we had together when you were in Wageningen.

A good support system is very crucial for surviving and staying sane during your PhD and what could be better than loving and caring friends who are always around. This reminds me of Charles R. Swindoll words-

*“I cannot even imagine where I would be today were it not for that handful of friends who have given me a heart full of joy. Let’s face it, friends made life a lot more fun.”*

Saumi and Surendra, both of you are always been a good friend and your extended help was overwhelming. We always had good time together over dinners and cheesecakes to lighten up the spirit. Not to forget the barbeques we used to have with discussions over planning a trip together that we could unfortunately never materialize. Also I would like to thank Rajshri and Nagendra for being there always and I would never forget the great trip we had to Italy. Liyaqat, Nagendra, Jueeli, Rajeesh and Umesh we had some fun time together as neighbours while cooking together, playing games and enjoyed a lot on those small trips we made.

I thank you Yuri for being there with me at coffee breaks to lighten my head after intense lab work. I will always remember the basketball, pool and bowling games that we played together that we had. I will always appreciate your help when my leg was fractured and you picked and dropped me from work. You were always there for me even in the 12<sup>th</sup> hour of night I am blessed to have you as a friend.

I would also like to thanks Sharifa and Jasper for being a very helpful support system during the last phase of my stay in Wageningen. I also appreciate their help in moving, transferring and finally helping in cleaning and preparing my house to surrender it back to the social housing agency.

I can not imagine how difficult it would have been for us to survive in Netherlands without the homely feeling and support offered by the **DESI** gang, I was lucky to have good friends like Jonathan, Abhilasha, Tiggy, Jatin, Sid, Angelina, Akshay, Damini, Venkat, Murli, Anindya, Poushali, Choka, Krishna, Sameer, Aparna, Priyanka, Himanshu, Jueeli, Sourav, Umesh, Nagendra, Sateesh, Sidhu, Nagesh, Ankush, Awaan, Imran, Abhay, and Ram.

Moreover, I am deeply thankful and indebted to my lovely wife Shruti, who was always there to share the excitement sorrow and pain that I came across. She was one of the pillars on which my PhD thesis is standing. Shruti your everlasting encouragement, support and patience over the three years of my PhD, has made this thesis possible. I have many more things to say about you both but I guess silence speaks it better.....

As once Franz Schubert said-

*“Happy is the man who finds a true friend, and far happier is he who finds that true friend in his wife”*

Shruti, you gave me one of the best gifts possible to me on 5<sup>th</sup> February 2013, i.e. my son “**Shauryansh**”. A special thanks to Shauryansh who permitted me to write the last few part of my thesis at home ☺. Together you both made my life full with joy and made me more responsible. Nothing has brought me more peace and content in life than being a good husband and a good father.

Last but not least, I would like to express my deep gratefulness to my parents who are always there for me with their immense love, support, sacrifices and encouragements. It is their confidence and blessings, which supported me throughout this tenure. I would also thank my parents-in-laws for their encouragement in finishing my thesis.

Thanks all for being there in one-way or the other. I will always appreciate your role towards completing my doctoral study.

Saurabh Kumar Srivastava

# *List of Publications*

1. Trilling AK, de Ronde H, Noteboom L, van Houwelingen A, Roelse M, **Srivastava S.K.**, *et al.* (2011) A broad set of different llama antibodies specific for a 16 kDa heat shock protein of Mycobacterium tuberculosis. PLoS One 6: e26754.
2. Moh, T.S.Y, **Srivastava, S.K.**, Milosavljevic, S., Roelse, M., Pandraud, G., *et al.* (2012) Silicon nanowire FET arrays for real time detection of chemical activation of cells. MEMS 2012 IEEE 25th International Conference.
3. **Srivastava, S.K.**, Ruigrok, V.J.B, Thompson, N.J., Trilling, A.K., Heck, A.J.R., *et al.* (2013) 16 kDa heat shock protein from heat-inactivated Mycobacterium tuberculosis is a homodimer – suitability for diagnostic applications with specific llama VHH monoclonals. Plos one 8(5): e64040.
4. **Srivastava, S.K.**, Ramaneti, R., Vrouwe, E., *et al.* A generic microfluidic biosensor of G protein-coupled receptor activation – impedance measurements of reversible morphological changes of reverse transfected HEK293 cells on microelectrodes. (Manuscript submitted for publication).
5. **Srivastava, S.K.**, van Rijn, C.J.M. and Jongsma, M.A., Biosensor based detection of tuberculosis biomarkers. (Manuscript submitted for publication).
6. **Srivastava, S.K.**, Ramaneti, R., Vrouwe, E., *et al.* A generic microfluidic biosensing module for nanowire-based FET measurements. (Manuscript in preparation).
7. **Srivastava, S.K.**, Nguyen, A.T., Baggerman, J., *et al.* Up-concentration and fluorescence-based detection of Mycobacterium tuberculosis bacteria and proteins with microsieves. (Manuscript in preparation)



## *About the Author*

Saurabh was born on 1<sup>st</sup> of May, 1982 in Ballia, Uttar Pradesh India. He received his bachelor's degree in Biotechnology with specialization in Genetic Engineering from Allahabad Agricultural Institute-Deemed University, Allahabad, India. After his bachelor's degree he has worked at the Department of Biotechnology, in Allahabad Agricultural Institute-Deemed University, India as an Assistant Professor for a period of two years after which he went on to pursue an Erasmus Mundus dual master's degree program. He obtained his first Masters's degree in Nanoscience from Delft University of Technology, Delft, The Netherlands while the second Masters degree in Molecular Bioengineering from Dresden University of Technology, Dresden, Germany. From November 2009 onwards, he became a PhD student in Laboratory of Organic Chemistry at the Wageningen University and research centre, Wageningen, The Netherlands (WUR), under the supervision of Prof. Dr. Cees van Rijn and Dr. Maarten Jongsma. His main research interest focuses on the development of nanowire and interdigitated electrodes based biosensor devices for point-of-care diagnostic applications. He also has research experience in recombinant DNA and cloning techniques, characterization and bio-functionalization of thin films for the immobilization of biosensing species on single and/or hybrid surfaces.



The research described in this thesis was financially supported by Dutch Technology Foundation STW (Project no. 10255).

Design & Layout: Saurabh Kumar Srivastava

Printed by Wöhrmann Print Service, Zutphen, The Netherlands